Supplemental Information

Chemometric Sensing of Stereoisomeric Compound Mixtures with a Redox-responsive Optical Probe

Jeffrey S. S. K. Formen, Diandra S. Hassan and Christian Wolf*
Department of Chemistry, Georgetown University, 37th and O St., Washington DC 20057, USA.
Email: cw27@georgetown.edu

Contents **Page**

1. General information

All chemicals were used as purchased and reactions were carried out without special precautions to exclude water or air. Probe **1** was purchased from Sigma Aldrich. (*R*,*S*)-**2** and (*S*,*R*)-**2** were purchased from Combi-Blocks and (*R*,*R*)-**2**, (*S*,*S*)-**2** were purchased from Santa-Cruz Biotechnology. (*R*,*S*)-**2**, purity: 97% [α]/D -4.2°, concentration = 0.6 in ethanol, (*S*,*R*)-**2**, purity: 98% [α]/D +6.3°, concentration = 0.5 in ethanol, (*S*,*S*)-**2**, purity: 99% [α]/D -122 (+/- 3°), concentration = 0.87 in ethanol, (*R*,*R*)-**2**, purity: 99% [α]/D +124 (+/- 3°), concentration = 0.87 in ethanol. All stereoisomers of **3** and **4** were purchased from Combi Blocks. For consistency, the absolute configuration at the chiral amino group is always listed before the one at the chiral alcohol group, i.e. (*R,S*)-**2** has *R*-configuration at the amine and *S*-configuration at the alcohol position. ^{1}H and ^{13}C NMR spectra were obtained at 400 and 100 MHz, respectively. Chemical shifts are reported in ppm relative to the solvent peaks. CD spectra were collected on a Jasco-710 calibrated with a Ni(II) tartrate complex using a standard sensitivity of 100 mdeg, a data pitch of 0.5 nm, and a bandwidth of 0.5 nm in a continuous scanning mode with a scanning speed of 200 nm/min and a response of 1.0 s (1 cm path length). The data were baseline corrected and smoothed using a binomial equation. UV spectra were collected with an average scanning time of 0.5 s, a data interval of 0.5 nm and a scan rate of 60 nm/s.

2. Initial amino alcohol screening

The chiral analyte (16.7 mM), Et_3N (16.7 mM) and 2,3-dichloro-1,4-naphthoquinone (16.7 mM) were mixed in 1.5 mL of DMSO and the reaction was stirred for 30 minutes. A colorimetric change from yellow to orange was observed. CD analysis was performed after dilution with DMSO to 0.33 mM. The product was subsequently reduced by the addition of 0.5 mL of $NaBH_4$ in MeOH (33.3 mM) resulting in another color change from orange to light yellow. CD analysis of the reduced compounds was performed after 5 minutes in DMSO:MeOH (3:1) at 0.26 mM.

Scheme S1. Reaction of 2,3-dichloro-1,4-naphthoquinone with chiral amino alcohols

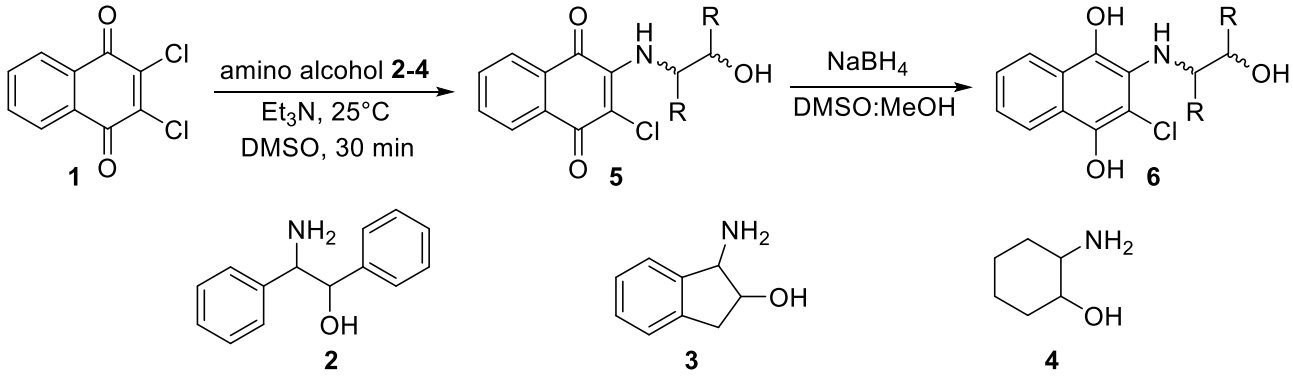

Figure S1. CD spectra of the reaction product between the stereoisomers of **2** and 2,3-dichloro-1,4-naphthoquinone.

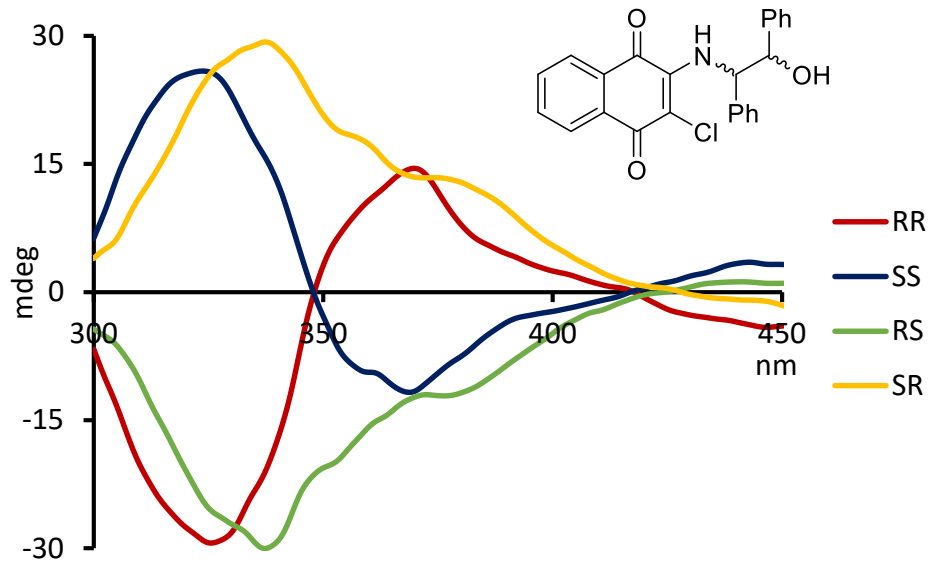

CD measurements were taken at 0.33 mM in DMSO

Figure S2. CD spectra of the reduced state of the reaction product between the stereoisomers of **2** and 2,3-dichloro-1,4-naphthoquinone.

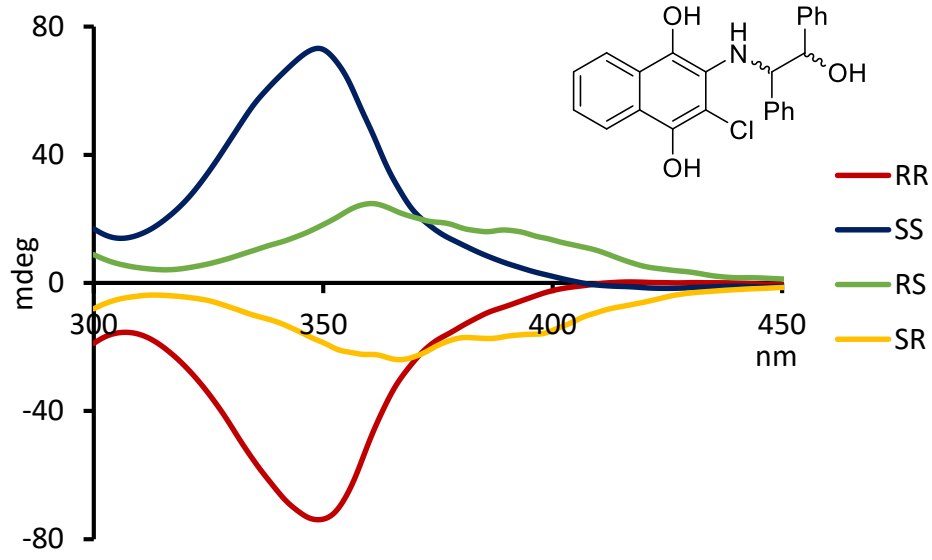

CD measurements were taken at 0.26 mM in 3:1 DMSO:MeOH

Figure S3. CD spectra of the reaction product between the stereoisomers of **3** and 2,3-dichloro-1,4-naphthoquinone.

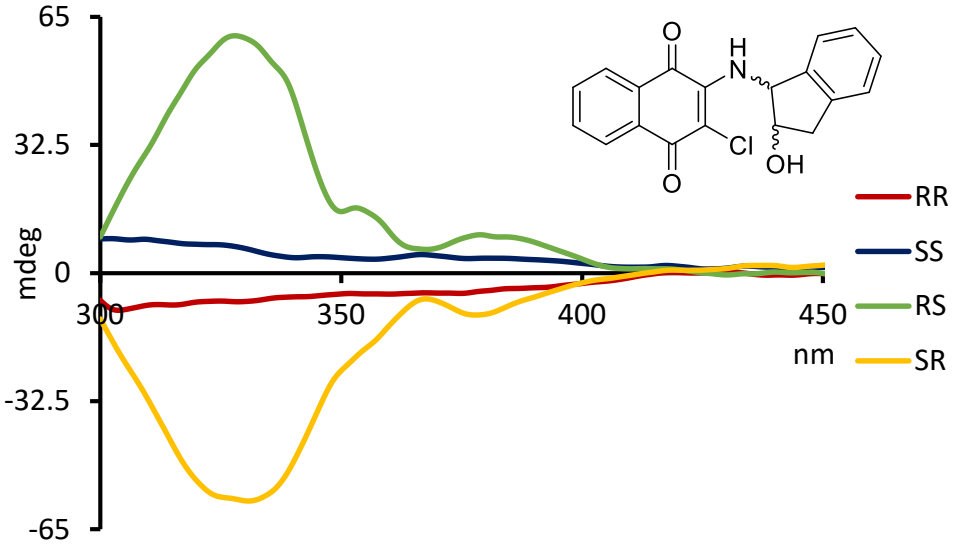

CD measurements were taken at 0.33 mM in DMSO

Figure S4. CD spectra of the reduced state of the reaction product between the stereoisomers of **3** and 2,3-dichloro-1,4-naphthoquinone.

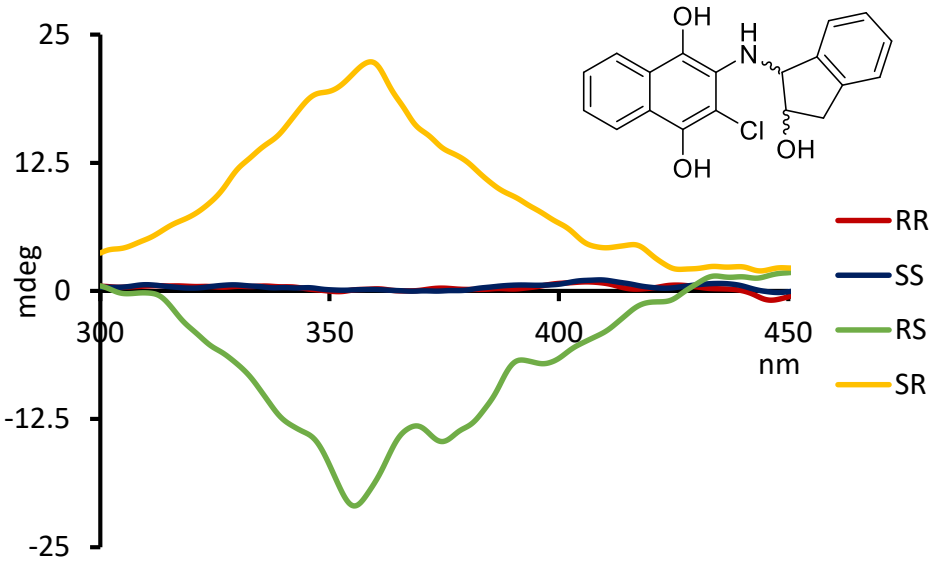

CD measurements were taken at 0.26 mM in 3:1 DMSO:MeOH

Figure S5. CD spectra of the reaction product between the stereoisomers of **4** and 2,3-dichloro-1,4-naphthoquinone.

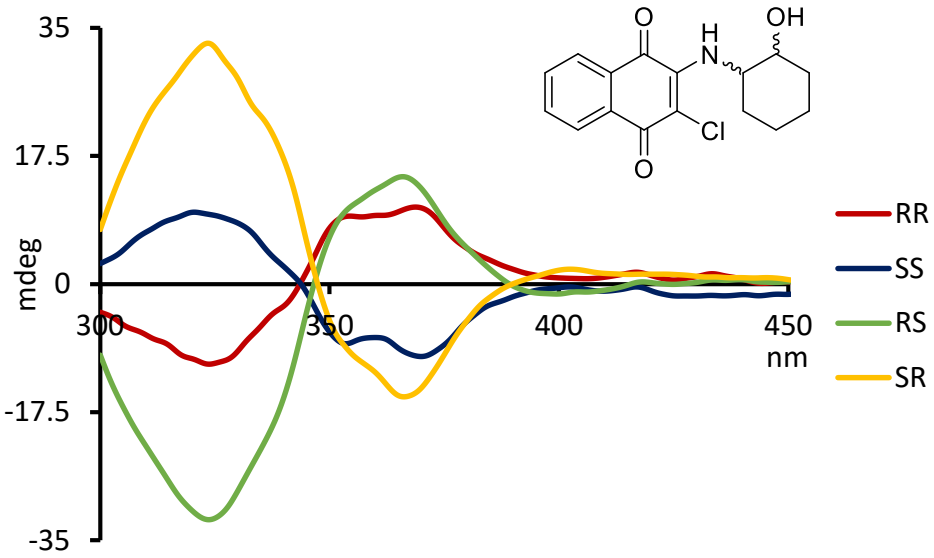

CD measurements were taken at 0.33 mM in DMSO

Figure S6. CD spectra of the reduced state of the reaction product between the stereoisomers of **4** and 2,3-dichloro-1,4-naphthoquinone.

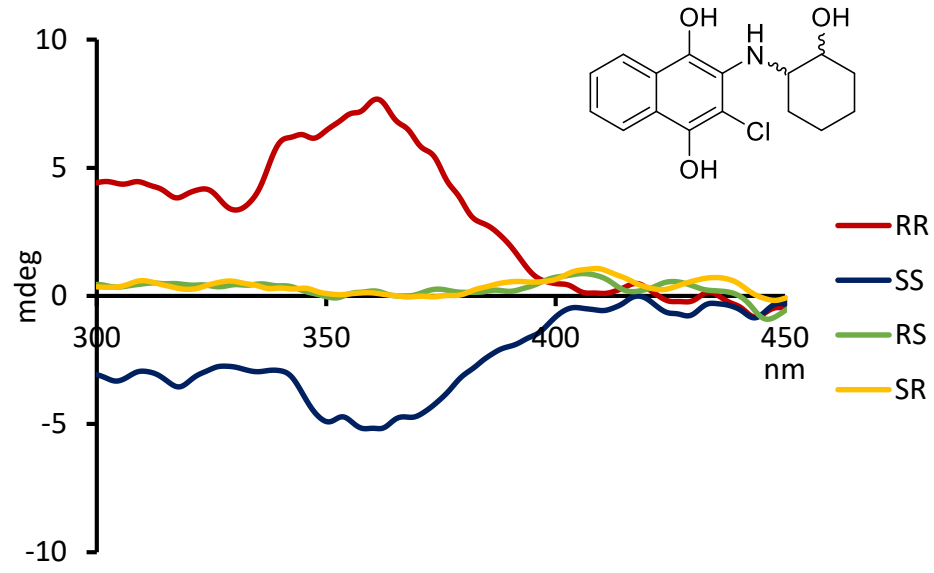

CD measurements were taken at 0.26 mM in 3:1 DMSO:MeOH

3. Comprehensive chirality sensing of 2-amino-1,2-diphenylethanol

3.1. Initial UV-Vis analysis

Separate solutions of the (*R*,*R*)-, (*S*,*S*)-, (*R*,*S*)-, and (*S*,*R*)-isomers of **2** (30.0 mM) were prepared in DMSO. Stock solutions (30.0 mM) of Et_3N and of 2,3-dichloro-1,4-naphthoquinone were also prepared. Four samples with varying *dr* (100:0 *R,R*:*R,S*, 75:25 *S,S*:*R,S*, 25:75 *R,R*:*S,R*, 0:100 *S,S*:*S,R*) at identical concentration (30.0 mM) were prepared. To each sample, 1 eq. of the Et_3N stock solution and 1 eq. of the 2,3-dichloro-1,4-naphthoquinone stock solution were added. The mixtures were stirred for 30 minutes and diluted to 0.225 mM with DMSO prior to UV analysis.

Figure S7. Change in the UV absorbance upon reaction of 2,3-dichloro-1,4-naphthoquinone and samples of **2** in varying *dr*.

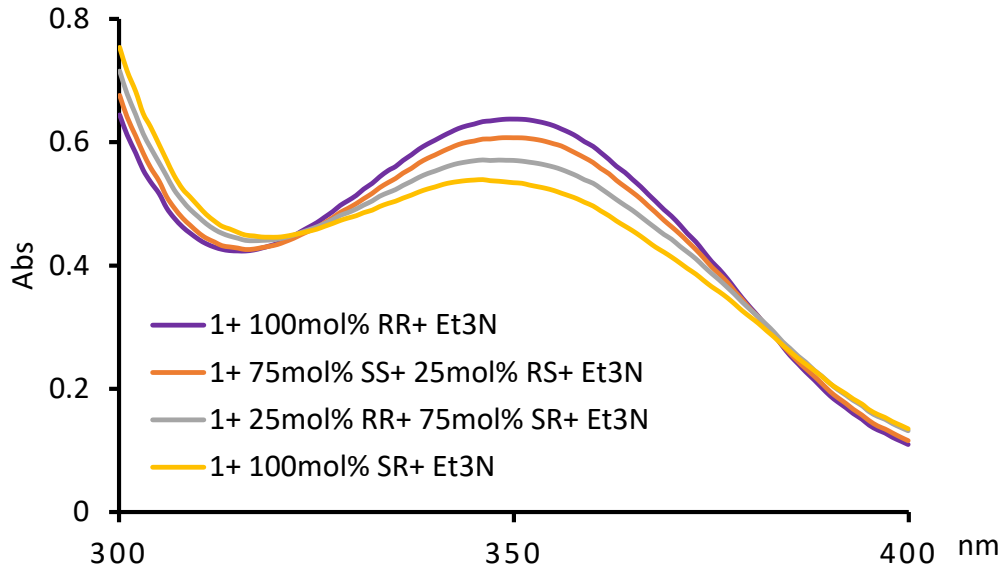

UV measurements were taken at 0.225 mM in DMSO

The signal intensity at 350 nm increases as the relative amount of the homochiral diastereomer (i.e. (*R*,*R*)-**2** and (*S*,*S*)-**2**) versus the heterochiral diastereomer (i.e. (*R*,*S*)-**2** and (*S*,*R*)-**2**) increases. Thus, the change in UV absorbance in the oxidized state can be used to determine the diastereomeric ratio of the sample.

UV spectra of the reaction product between **1** and enantiopure stereoisomers were collected to verify that the absorbance is identical for enantiomers at the same concentration (Figure S8).

Figure S8. UV spectra of the reaction products between enantiopure samples of **2** with 2,3-dichloro-1,4-naphthoquinone.

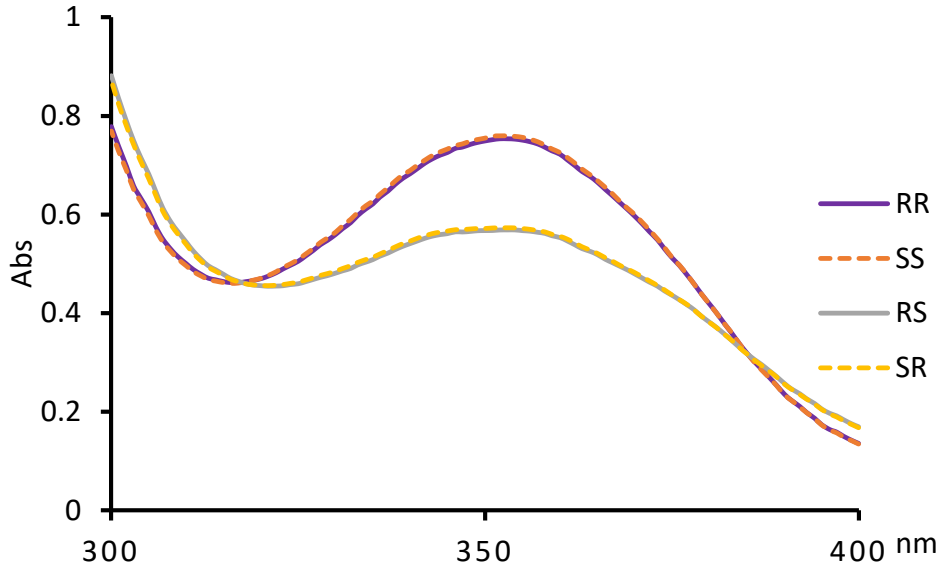

UV measurements were taken at 0.23 mM in DMSO

3.2. Concentration analysis using UV-Vis spectroscopy

We found that the overall concentration (all stereoisomers together) of **2** can be determined from the reduced state of the reaction product between **2** and 2,3-dichloro-1,4-naphthoquinone. Separate solutions of the (*R*,*R*)-, (*S*,*S*)-, (*R*,*S*)-, and (*S*,*R*)-isomers of **2** (50.0 mM) were prepared in DMSO. Stock solutions (50.0 mM) of Et_3N and of 2,3-dichloro-1,4-naphthoquinone were also prepared. To each vial, varying amounts of **2** were added (0.30, 0.40, 0.50 mL), followed by 0.5 mL of the Et_3N stock solution and 0.50 mL of the 2,3-dichloro-1,4-naphthoquinone stock solution. After 30 minutes of stirring, 0.50 mL of $NaBH_4$ in MeOH (100.0 mM) was added. The mixtures were diluted with 3:1 DMSO:MeOH prior to UV analysis. The final concentrations (in order of decreasing UV signal intensities) were: a) 0.23 mM (**1**, Et_3N and **2**); b) as above but [**2**] was 0.18 mM; c) [**2**] was 0.14 mM.

Figure S9. Change in UV absorbance upon reaction of **2** with 2,3-dichloro-1,4-naphthoquinone and subsequent reduction.

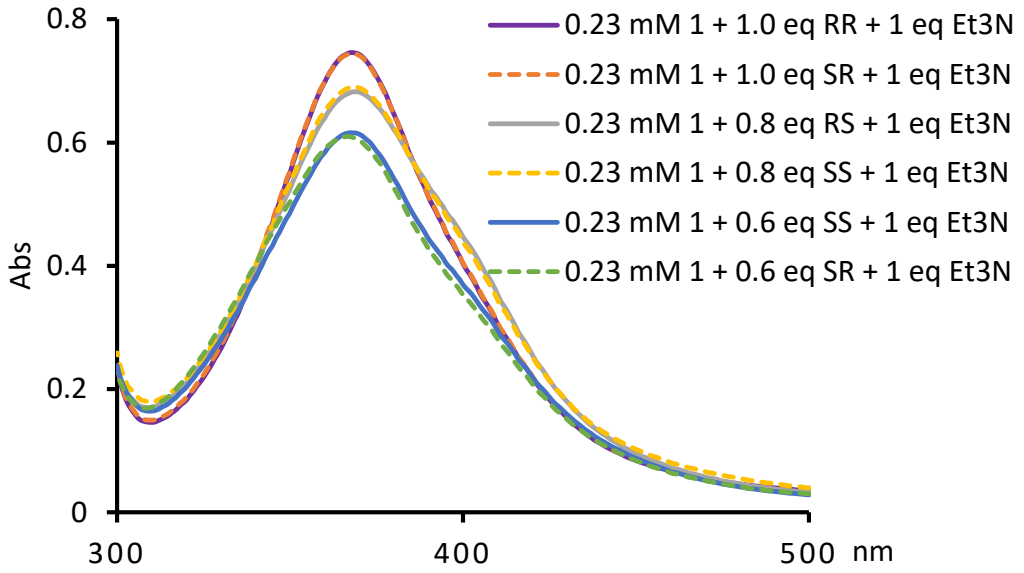

The results in Figure S9 prove that in the reduced state the absorbance is identical for all stereoisomers at a given concentration. The UV absorbance steadily increases as the concentration increases. Thus, the change in UV absorbance in the reduced state can be used to determine the overall concentration of the sample.

3.3. Enantiomeric ratio analysis using CD spectroscopy

We found that the enantiomeric ratio of the stereoisomers of **2** can be determined by using both the oxidized and reduced state of the reaction product obtained with 2,3-dichloro-1,4-naphthoquinone. The chiral analyte (16.7 mM), Et_3N (16.7 mM) and 2,3-dichloro-1,4-naphthoquinone (16.7 mM) were mixed in 1.5 mL of DMSO. The reaction was stirred for 30 minutes and diluted to 0.33 mM with DMSO prior to CD analysis. The quinone product was subsequently reduced with 0.5 mL of $NaBH_4$ in MeOH (33.3 mM). CD analysis of the reduced compounds was performed after 5 minutes in DMSO:MeOH (3:1).

Figure S10. CD spectra of homochiral enantiomer products

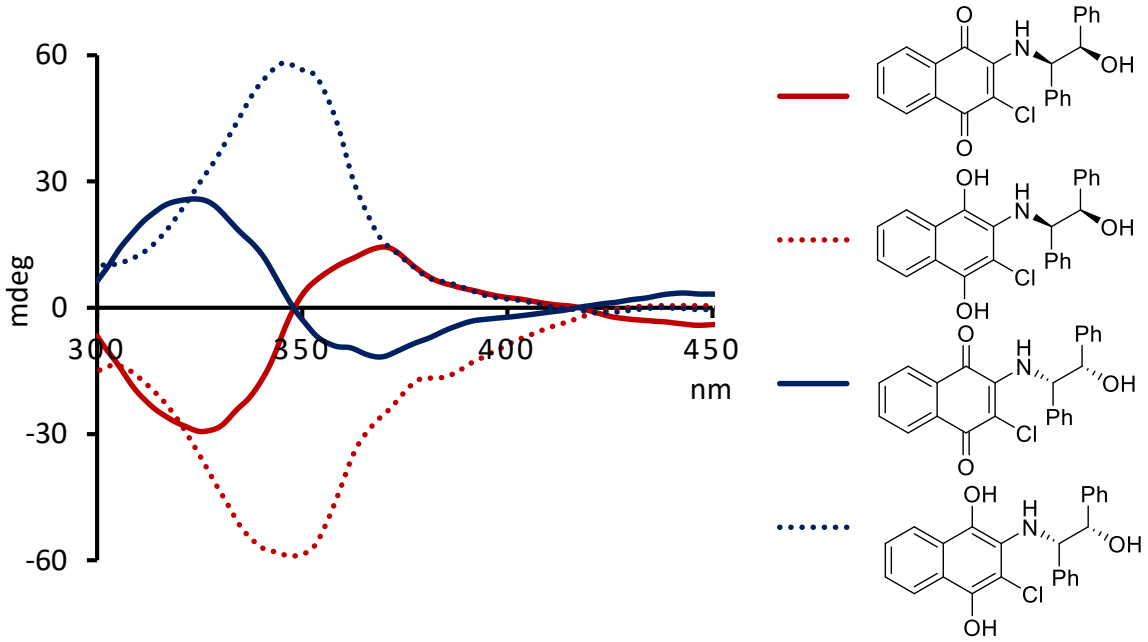

CD measurements were taken at 0.33 mM in DMSO

Figure S11. CD spectra of heterochiral enantiomer products

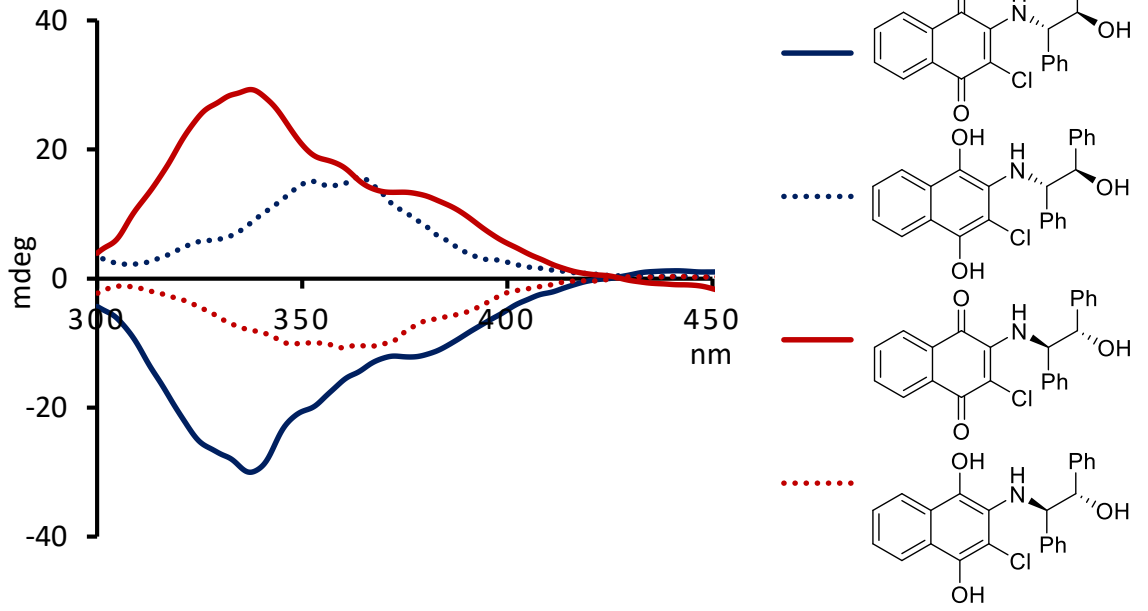

CD measurements were taken at 0.26 mM in 3:1 DMSO:MeOH

4. NMR studies

4.1. Characterization of (*S*,*R*)-2-chloro-3-((2-hydroxy-1,2-diphenylethyl)amino)-1,4-naphtoquinone

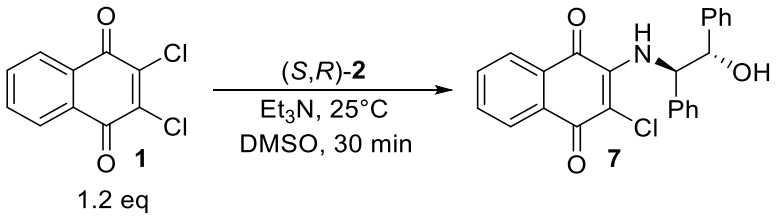

A solution of (*S*,*R*)-**2** (42.7 mg, 0.2 mmol), Et_3N (20.2 mg, 0.2 mmol) and 2,3-dichloro-1,4-naphthoquinone (54.5 mg, 0.24 mmol) was stirred in 1.5 mL of DMSO for 30 minutes. The mixture was washed with water and extracted with dichloromethane. The combined organic layers were dried over Na_2SO_4 and concentrated *in vacuo*. Purification by flash chromatography on silica gel (20% ethyl acetate in hexanes) afforded 70.3 mg (0.17 mmol, 87%) of a red solid. ^{1}H NMR (400 MHz, CD_3CN): δ= 8.02-7.98 (m, 2H), 7.76 (m, 1H), 7.69 (m, 1H) 7.27-7.19 (m, 6H), 7.15-7.11 (m, 2H), 7.10-7.07 (m, 3H), 5.85 (dd, *J*= 9.2, 4.6 Hz, 1H), 5.24 (dd, *J*= 4.6 Hz, 4.5 Hz, 1H), 3.93 (d, *J*= 4.6 Hz, 1H). ^{13}C NMR (100 MHz, CD_3CN): δ= 181.4, 177.4, 145.1, 141.5, 139.8, 135.9, 133.8, 133.3, 131.0, 129.0, 128.8, 128.7, 128.5, 128.3, 127.6, 127.5, 127.5, 127.1, 76.5, 63.6. HRMS (ESI-TOF) *m*/*z*: $[M+H]^+$ calcd for $C_{24}H_{18}ClNO_3$ 404.1048, found 404.1049.

Figure S12. ^{1}H NMR spectrum of **7**

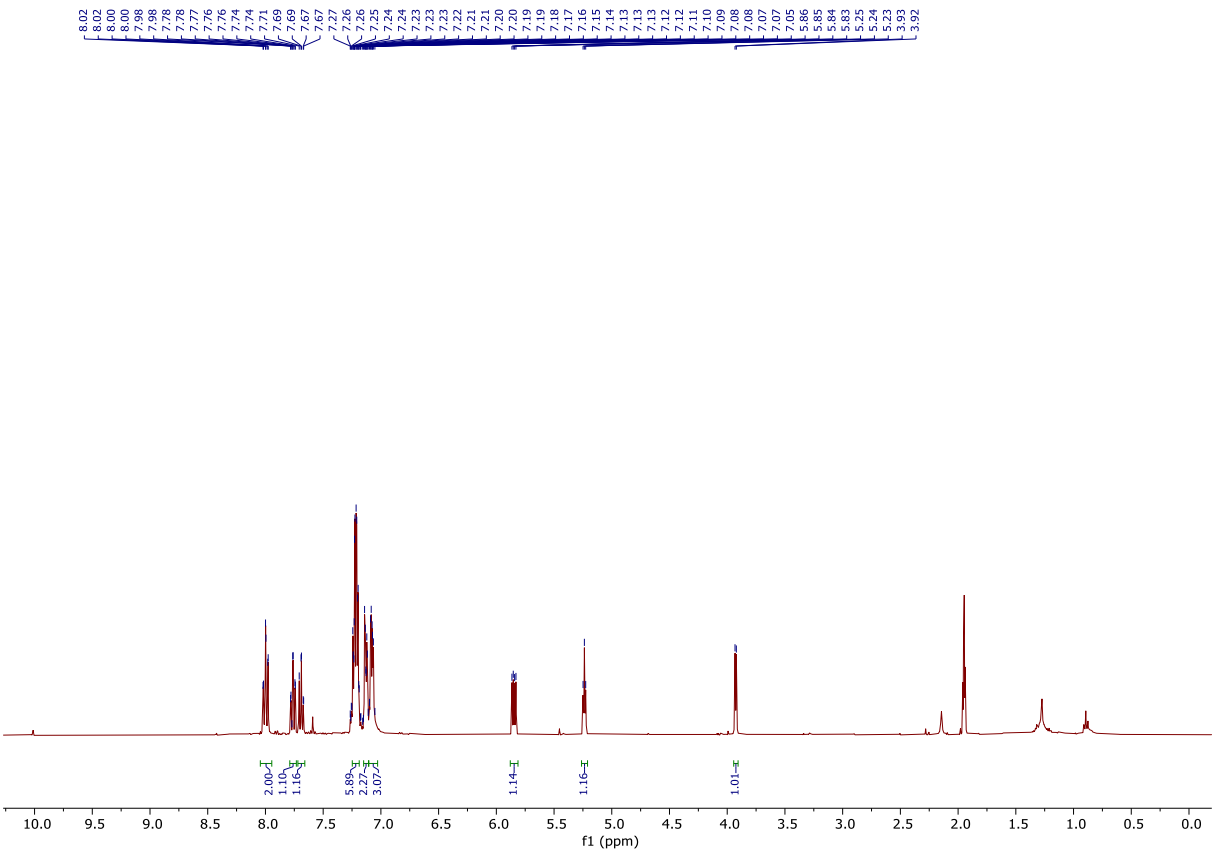

Figure S13. ^{13}C NMR spectrum of **7**

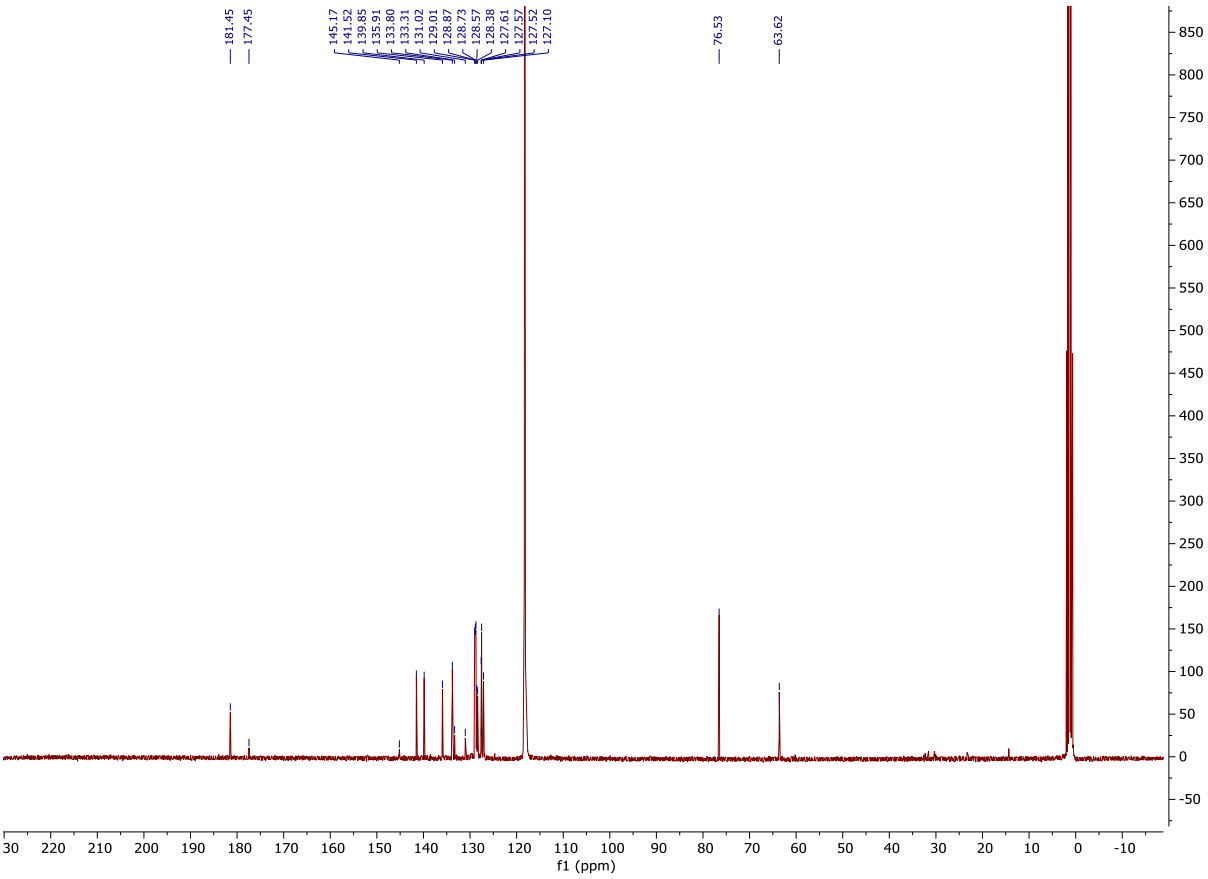

The CD spectrum of the isolated species obtained in the presence of 1 eq. of Et_3N proved to be identical to the Cotton effect observed during *in situ* CD sensing (Figure S14).

Figure S14. CD spectra of the crude reaction product of *S*,*R*-**1** and 2,3-dichloronaphthoquinone obtained during *in situ* sensing and the isolated reaction product in the presence of Et_3N.

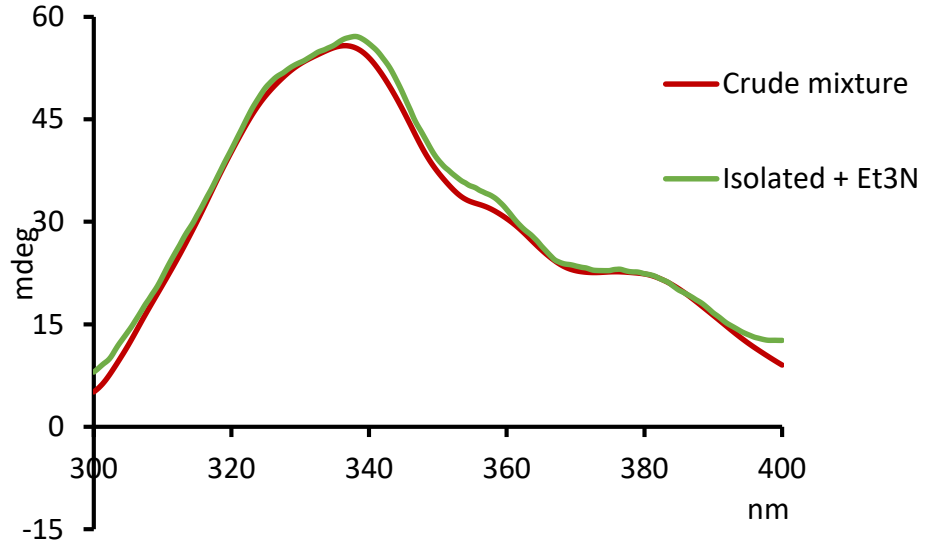

4.2. Characterization of (*R*,*R*)-2-chloro-3-((2-hydroxy-1,2-diphenylethyl)amino)-1,4-naphtoquinone

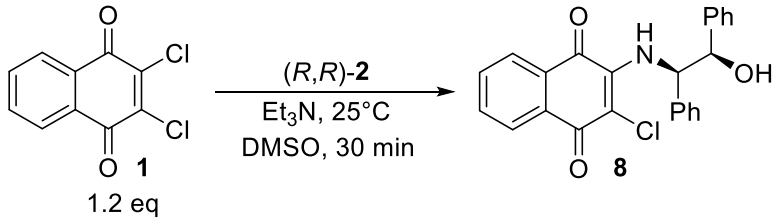

A solution of (*R*,*R*)-**2** (42.7 mg, 0.20 mmol), Et_3N (20.2 mg, 0.20 mmol) and 2,3-dichloro-1,4-naphthoquinone (54.5 mg, 0.24 mmol) was stirred in 1.5 mL of DMSO for 30 minutes. The mixture was washed with water and extracted with dichloromethane. The combined organic layers were dried over Na_2SO_4 and concentrated *in vacuo*. Purification by flash chromatography on silica gel (20% ethyl acetate in hexanes) afforded 73.5 mg (0.18 mmol, 91%) of a red solid. ^{1}H NMR (400 MHz, CD_3CN): δ= 8.00-7.94 (m, 2H), 7.74 (m, 1H), 7.67 (m, 1H), 7.59 (bs, 1H), 7.5-7.47 (m, 2H), 7.43-7.32 (m, 7H), 7.25-7.21 (m, 1H), 5.85 (dd, *J*= 9.1, 2.8 Hz, 1H), 5.10 (dd, *J*= 3.4 Hz, 3.4 Hz, 1H), 3.92 (d, *J*= 4.2 Hz, 1H). ^{13}C NMR (100 MHz, CD_3CN): δ= 180.3, 176.3, 144.6, 141.9, 141.3, 134.9, 132.8, 132.3, 129.9, 128.4, 128.2, 127.5, 127.4, 127.1, 126.9, 126.6, 126.1, 125.9, 75.9, 63.4. HRMS (ESI-TOF) *m*/*z*: $[M+H]^+$ calcd for $C_{24}H_{18}ClNO_3$ 404.1048, found 404.1040.

Figure S15. ^{1}H NMR spectrum of **8**

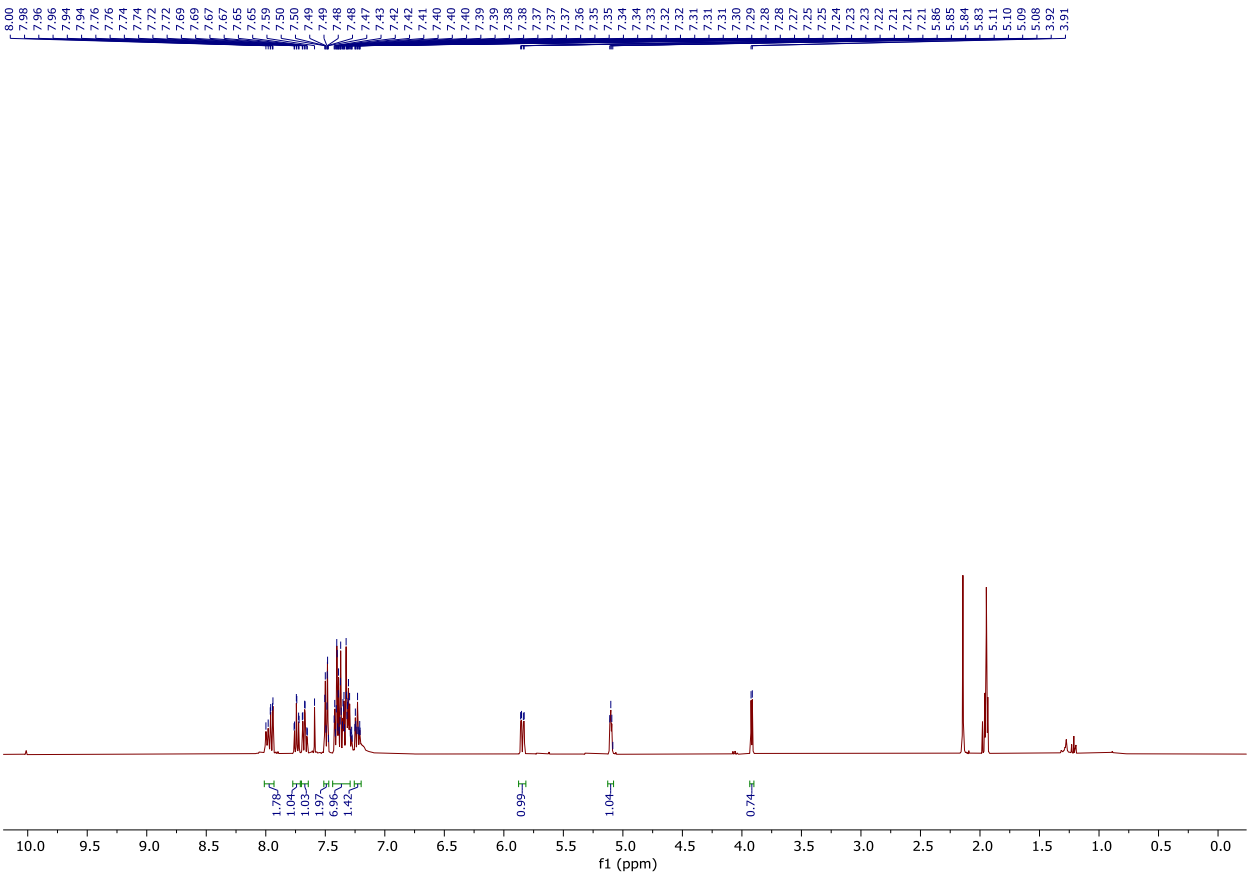

Figure S16. ^{13}C NMR spectrum of **8**

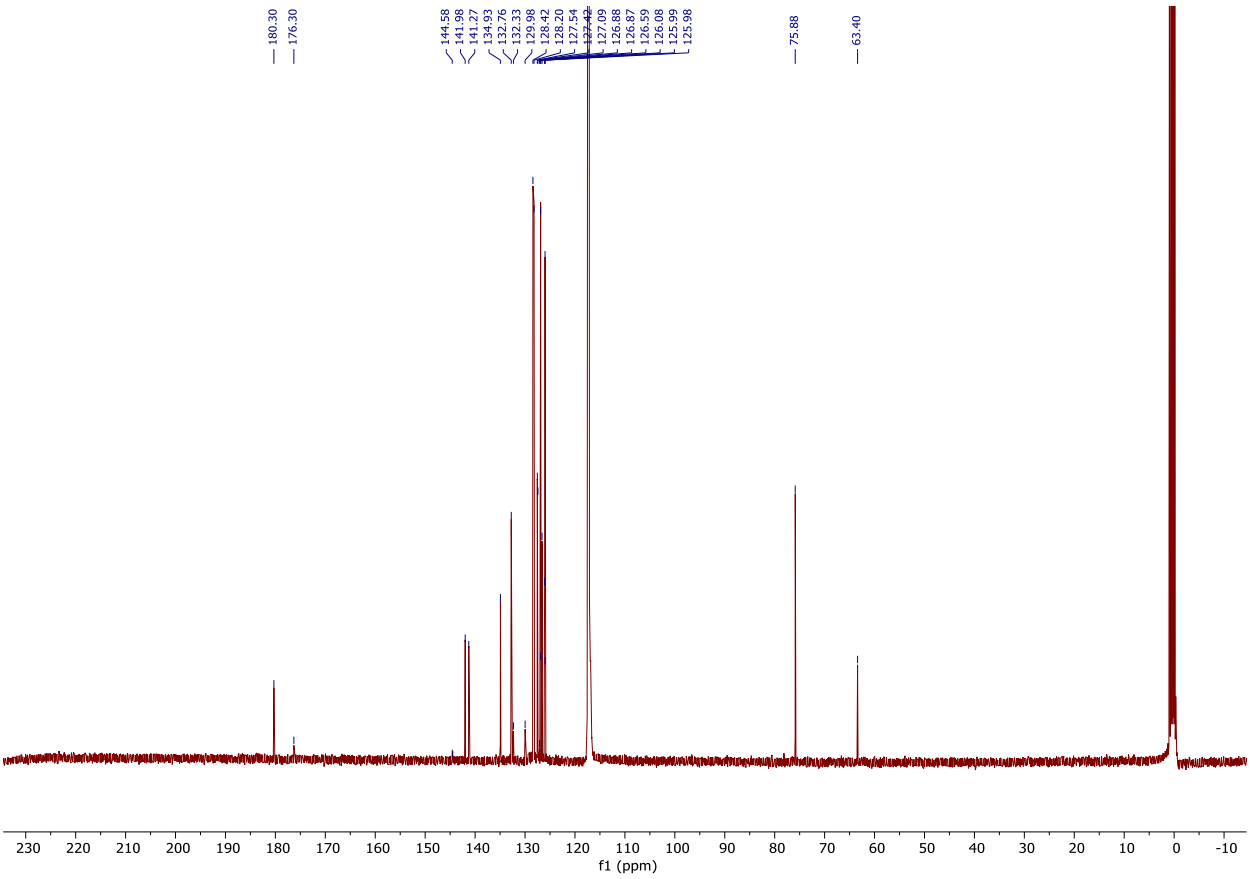

4.3. Characterization of (*S*,*R*)-2-chloro-3-((2-hydroxy-1,2-diphenylethyl)amino)naphthalene -1,4-diol

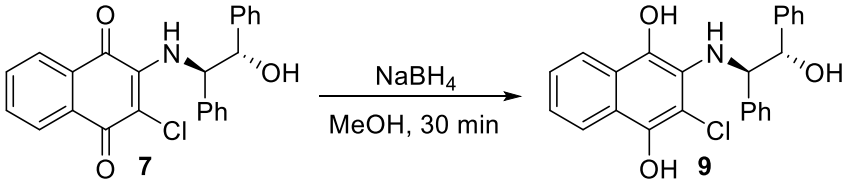

A solution of **7** (60 mg, 0.2 mmol) and $NaBH_4$ (15.1 mg, 0.4 mmol) were mixed in 5 mL of CD_3OD under nitrogen. The mixture was allowed to stir for 5 minutes at room temperature, prior to ^1H NMR analysis. Hydronaphthoquinone **9** is sufficiently stable for ^1H NMR analysis but oxidizes too quickly for ^{13}C NMR analysis. ^1H NMR (400 MHz, CD_3OD): δ= 8.05-8.00 (m, 2H), 7.40 (bs, 1H), 7.30 (t, *J*= 7.41 Hz, 1H), 7.22 (t, *J*= 7.51 Hz, 1H), 7.12-7.01 (m, 10H), 5.08 (d, *J* = 3.65 Hz, 1H), 4.98 (d, *J*= 3.71 Hz, 1H).

Figure S17. ^{1}H NMR spectrum of **9**

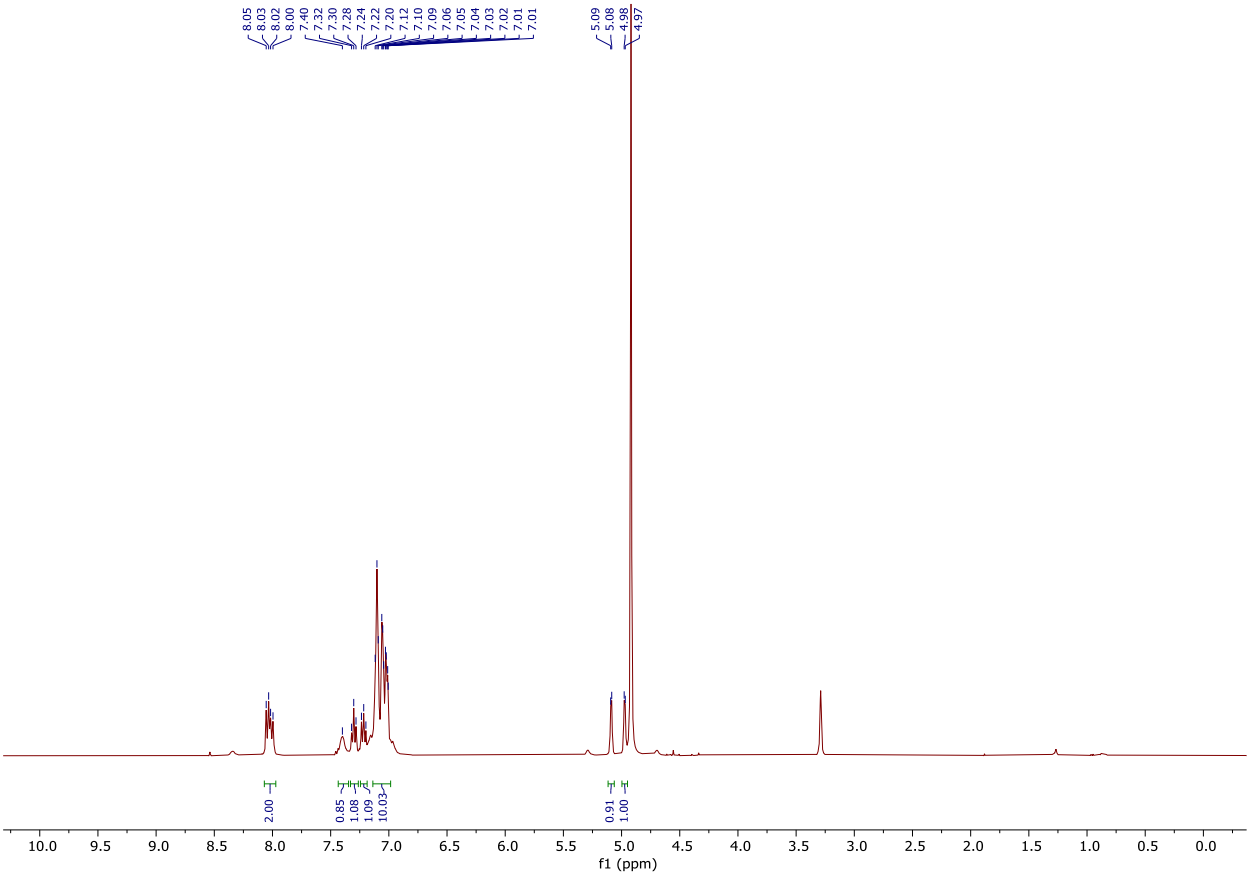

4.4. Characterization of (*R*,*R*)-2-chloro-3-((2-hydroxy-1,2-diphenylethyl)amino)naphthalene -1,4-diol

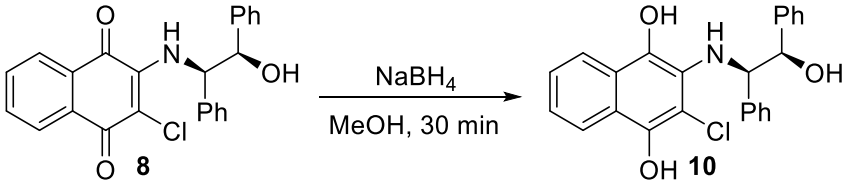

A solution of **8** (60 mg, 0.2 mmol) and $NaBH_4$ (15.1 mg, 0.4 mmol) were mixed in 5 mL of CD_3OD under nitrogen. The mixture was allowed to stir for 5 minutes at room temperature, prior to ^{1}H NMR analysis. Hydronaphthoquinone **10** is sufficiently stable for ^{1}H NMR analysis, but oxidizes too quickly for ^{13}C NMR analysis. ^{1}H NMR (400 MHz, CD_3OD): δ= 8.01-7.98 (m, 2H), 7.34-7.30 (m, 1H), 7.25-7.21 (m, 3H), 7.15-7.03 (m, 9H), 5.00 (d, J = 8.3 Hz, 1H), 4.63 (d, J = 8.3 Hz, 1H).

Figure S18. ^{1}H NMR spectrum of **10**

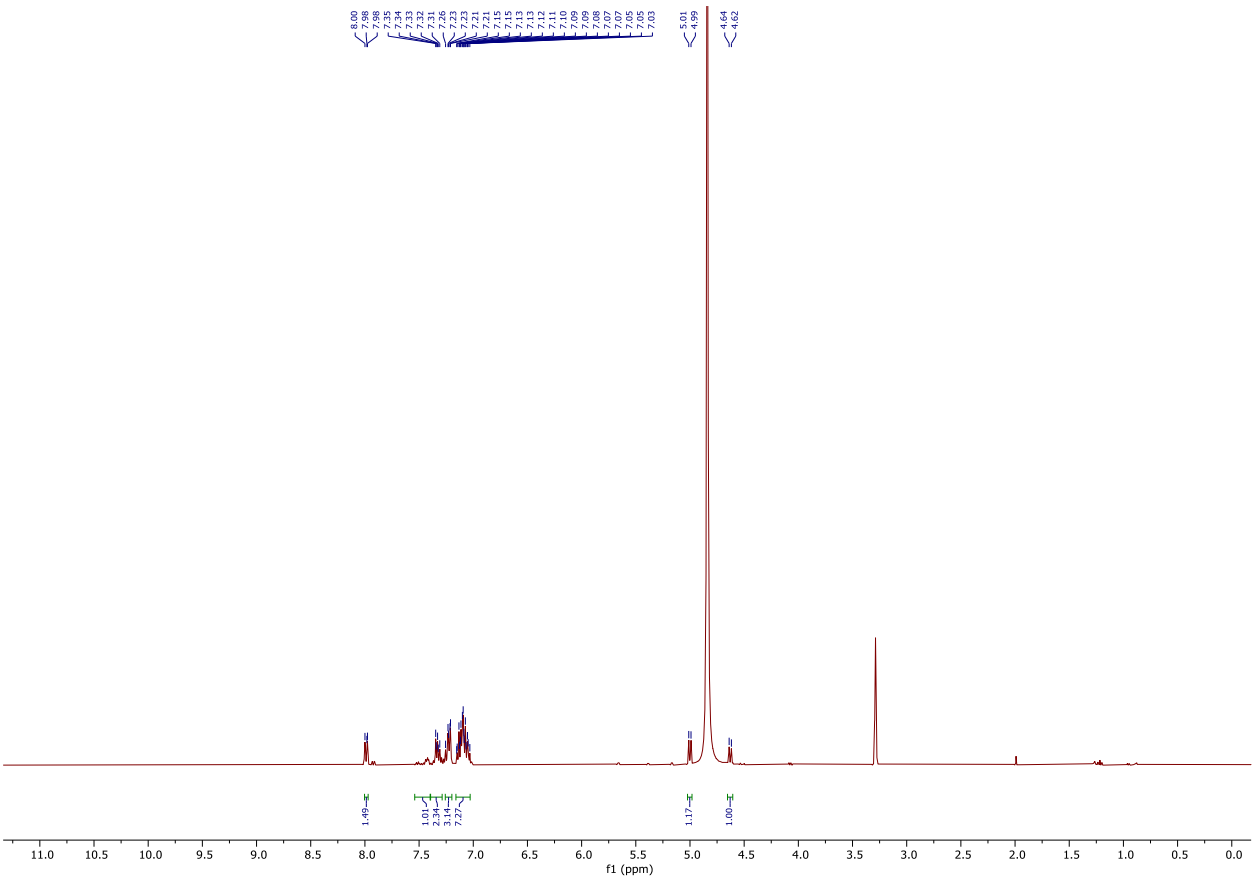

5. Crystallographic analysis

Figure S19. (*S*,*R*)-2-Chloro-3-((2-hydroxy-1,2-diphenylethyl)amino)naphthoquinone crystal structure

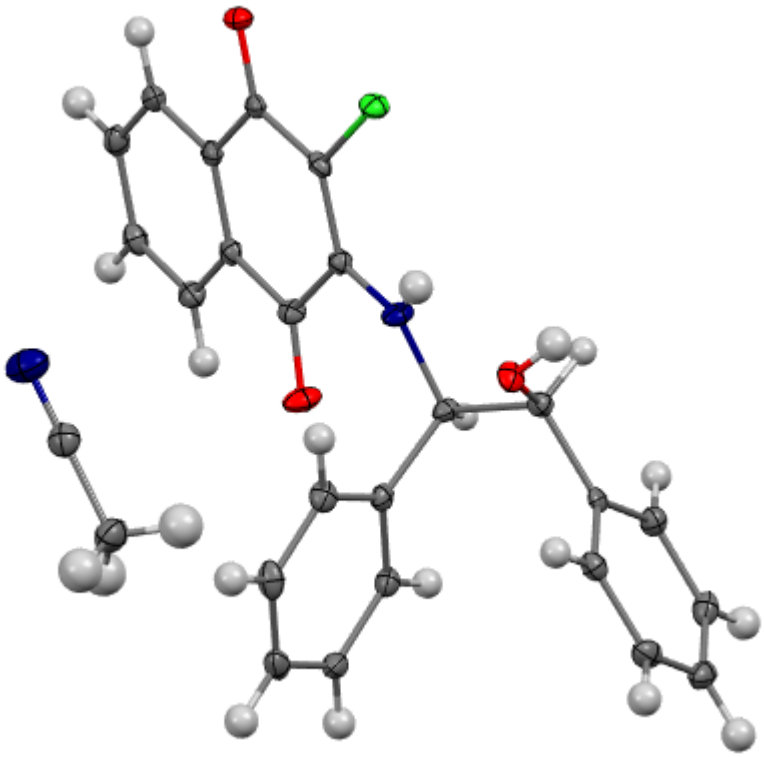

A single crystal was obtained by slow evaporation of a solution of the (*S*,*R*)-2-chloro-3-((2-hydroxy-1,2-diphenylethyl)amino)naphthoquinone in acetonitrile. Single crystal X-ray analysis was performed at 100K using a Siemens platform diffractometer with graphite monochromated Mo-Kα radiation (λ = 0.71073 Å). Data were integrated and corrected using the APEX 3 program. The structures were solved by direct methods and refined with fullmatrix least-square analysis using SHELXL-2018/3 software. Non-hydrogen atoms were refined with anisotropic displacement parameter. Crystal data: $C_{26}H_{21}ClN_2O_3$, M = 444.9, 0.426 x 0.088 x 0.066 mm^3, orthorhombic, space group $P2_12_12_1$, a = 5.8943(5), b = 13.4561(11), c = 27.524(2) Å, V = 2183.0(3) Å 3, Z = 4. The CCDC number for the crystal reported in this study is 2155745.

6. Epimerization study

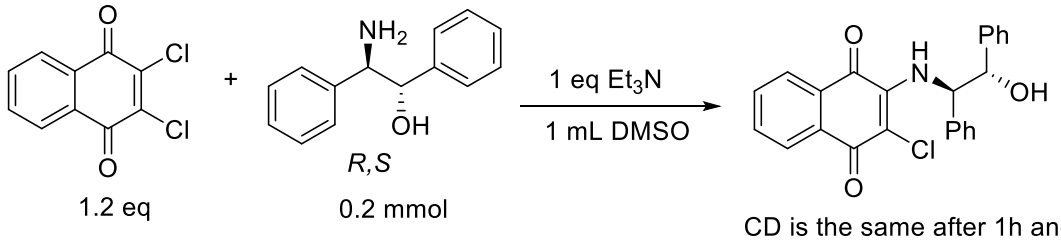

The chiral analyte (16.7 mM), Et_3N (16.7 mM) and 2,3-dichloro-1,4-naphthoquinone (16.7 mM) were mixed in 1.5 mL of DMSO. After 1 hour, an aliquot was taken and diluted to 0.33 mM with DMSO and subjected to CD analysis. The reaction was allowed to stir for an additional 23 hours after which another aliquot was taken and diluted to 0.33 mM followed by CD analysis. The CD spectra was identical to the one taken after 1 hour showing no degradation, epimerization, and racemization of the product.

Figure S20. Epimerization study with an enantiopure sample of **5**.

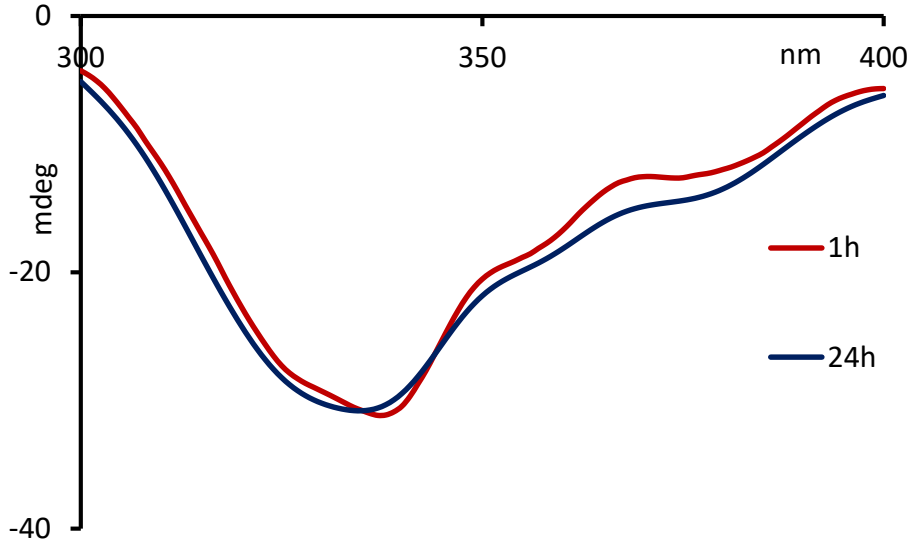

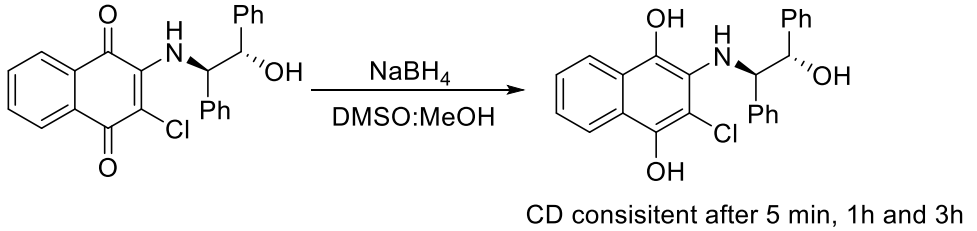

The chiral analyte (16.7 mM), Et_3N (16.7 mM) and 2,3-dichloro-1,4-naphthoquinone (16.7 mM) were mixed in 1.5 mL of DMSO. After 1 hour, the quinone was reduced with 0.5 mL of $NaBH_4$ in MeOH (33.3 mM). CD analysis of the reduced species was performed after 5 minutes at 0.26

mM in DMSO:MeOH (3:1). To ensure the compound stayed reduced, 0.5 mL of $NaBH_4$ in MeOH (50.1 mM) was added every 30 minutes. After 3 hours, CD analysis of the reduced species was performed at 0.26 mM in DMSO:MeOH (3:1). The CD spectra was identical to the one taken after 5 minutes showing no degradation, epimerization, and racemization of the product.

Figure S21. Epimerization study with an enantiopure sample of **6**.

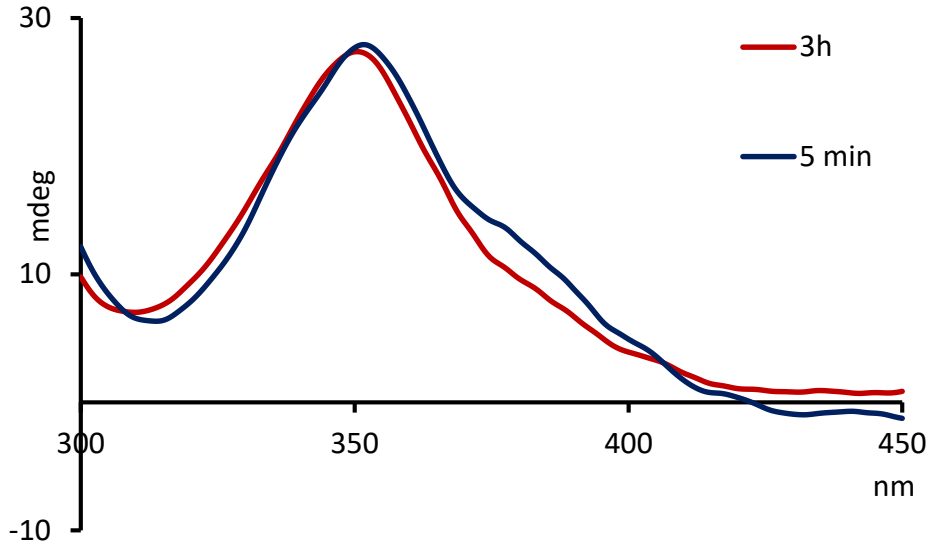

7. Chemometric sensing of quaternary mixtures

Fifteen samples of 2-amino-1,2-diphenylethanol at varying concentrations and stereoisomeric compositions in DMSO were prepared and subjected to simultaneous analysis using probe **1**. For each sample, 15.0 μL aliquots were combined with 2.0 mL of DMSO and 5 single point UV measurements taken at 351 nm and averaged. Upon addition of excess of $NaBH_4$ (0.5 mL of a 50 mM stock solution in MeOH) another 5 single point UV measurements were taken at 370 nm and averaged. Finally, aliquots of 40.0 μL from each sample were combined with 2.0 mL of DMSO and 3 CD spectra were collected and averaged. Upon addition of excess of $NaBH_4$ (0.5 mL of a 50 mM stock solution in MeOH) another 3 CD spectra were collected and averaged. The results from the linear regression analysis of the total concentration, the UV absorptions and the CD spectra of the oxidized state and the reduced states were used to quantify the individual stereoisomer concentration in mM using partial least squares (PLS). Scikit learn library, a free Python library for machine learning, was used for all pre-processing (scaling) and data analysis using PLS.

7.1. Sample spectra

Figure S22. CD analysis of a mixture containing 20.0 mM of *(R,R)*-**2**, 5.0 mM of (*R*,*S*)-**2**, 22.0 mM of (*S*,*S*)-**2**, and 3.0 mM of (*S*,*R*)-**2** (Oxidized state).

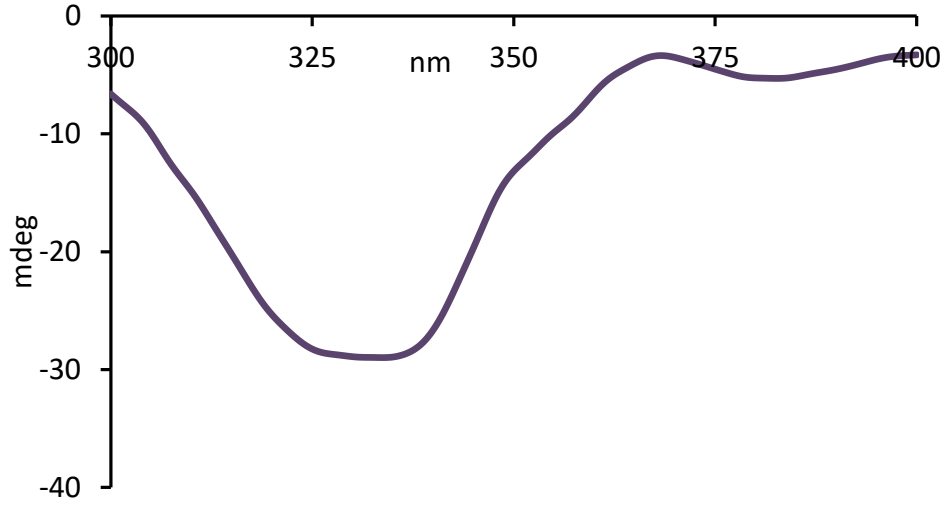

Figure S23. CD analysis of a mixture containing 4.0 mM of *(R,R)*-**2**, 16.0 mM of (*R*,*S*)-**2**, 18.0 mM of (*S*,*S*)-**2**, and 2.0 mM of (*S*,*R*)-**2** (Oxidized state).

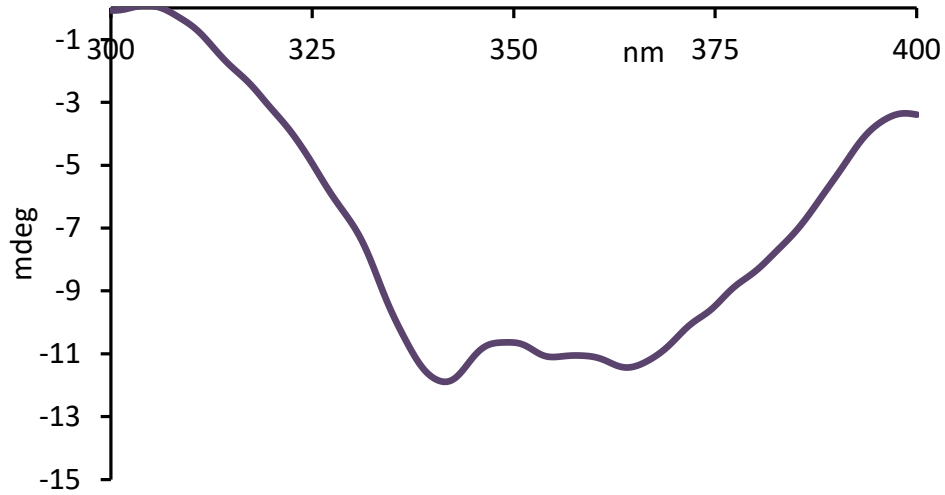

Figure S24. CD analysis of a mixture containing 19.0 mM of *(R,R)*-**2**, 4.0 mM of (*R*,*S*)-**2**, 10.0 mM of (*S*,*S*)-**2**, and 12.0 mM of (*S*,*R*)-**2** (Oxidized state).

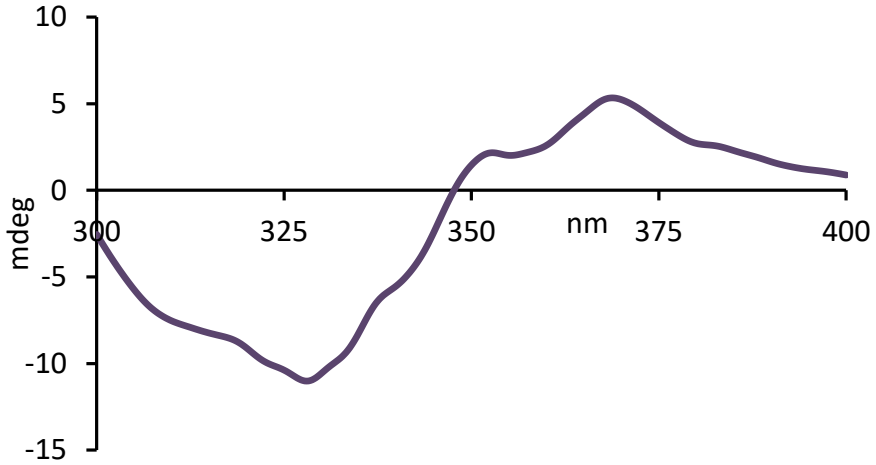

Figure S25. CD analysis of a mixture containing 13.0 mM of *(R,R)*-**2**, 2.0 mM of (*R*,*S*)-**2**, 7.0 mM of (*S*,*S*)-**2**, and 8.0 mM of (*S*,*R*)-**2** (Oxidized state).

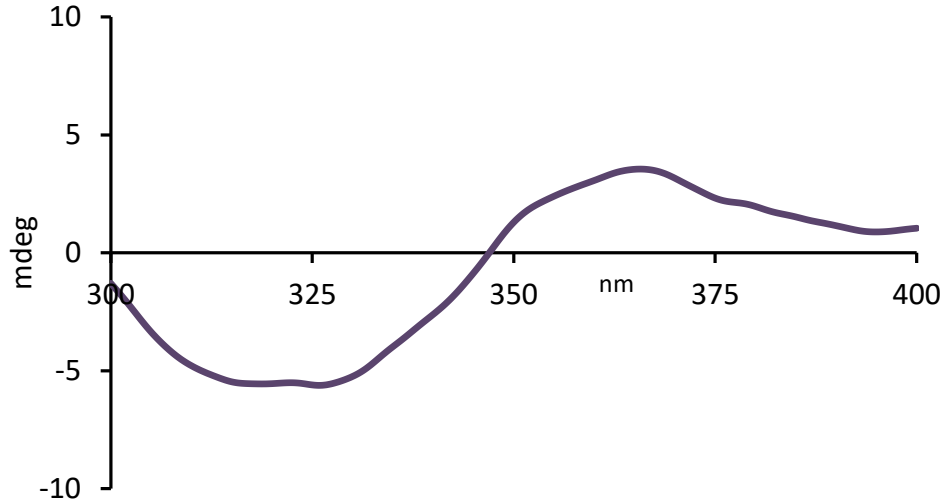

Figure S26. CD analysis of a mixture containing 10.0 mM of *(R,R)*-**2**, 7.0 mM of (*R*,*S*)-**2**, 15.0 mM of (*S*,*S*)-**2**, and 3.0 mM of (*S*,*R*)-**2** (Oxidized state).

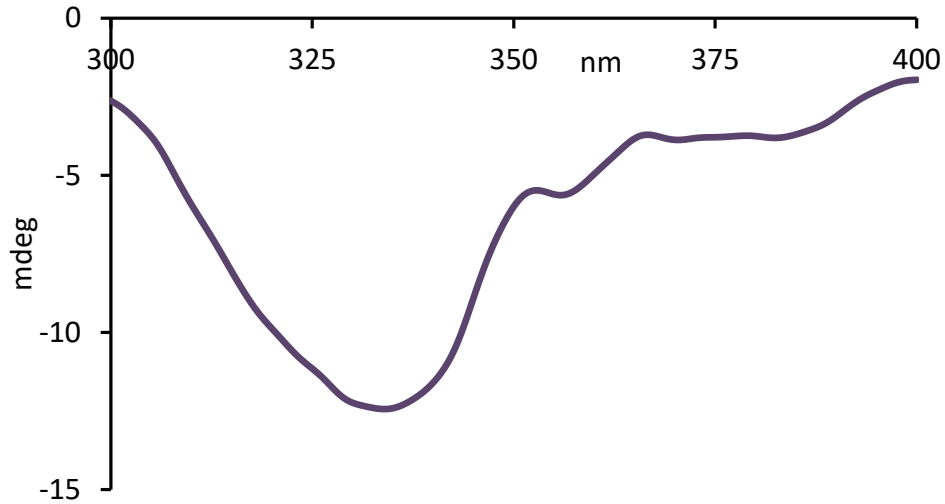

Figure 7 CD analysis of a mixture containing 15.0 mM of *(R,R)*-**2**, 5.0 mM of (*R*,*S*)-**2**, 1.0 mM of (*S*,*S*)-**2**, and 19.0 mM of (*S*,*R*)-**2** (Oxidized state).

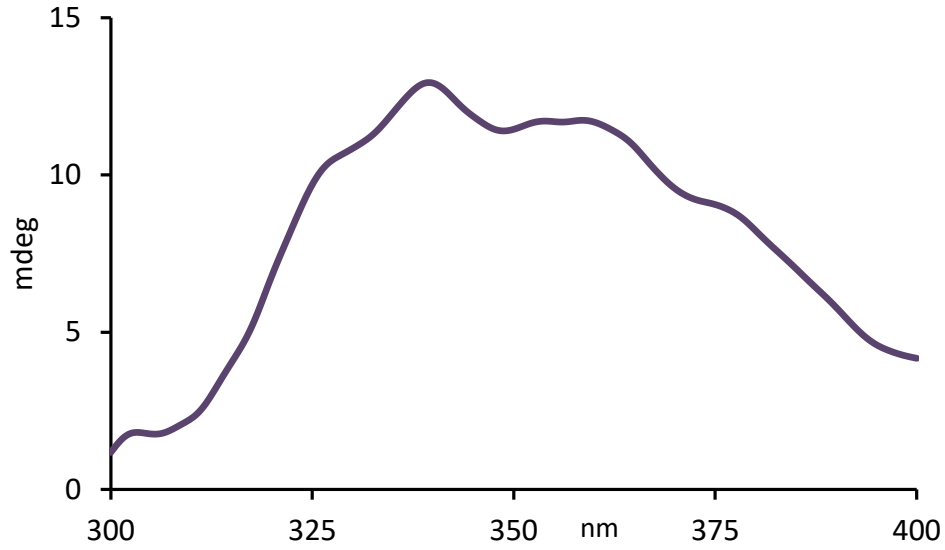

Figure S28. CD analysis of a mixture containing 3.0 mM of *(R,R)*-**2**, 22.0 mM of (*R*,*S*)-**2**, 7.0 mM of (*S*,*S*)-**2**, and 18.0 mM of (*S*,*R*)-**2** (Oxidized state).

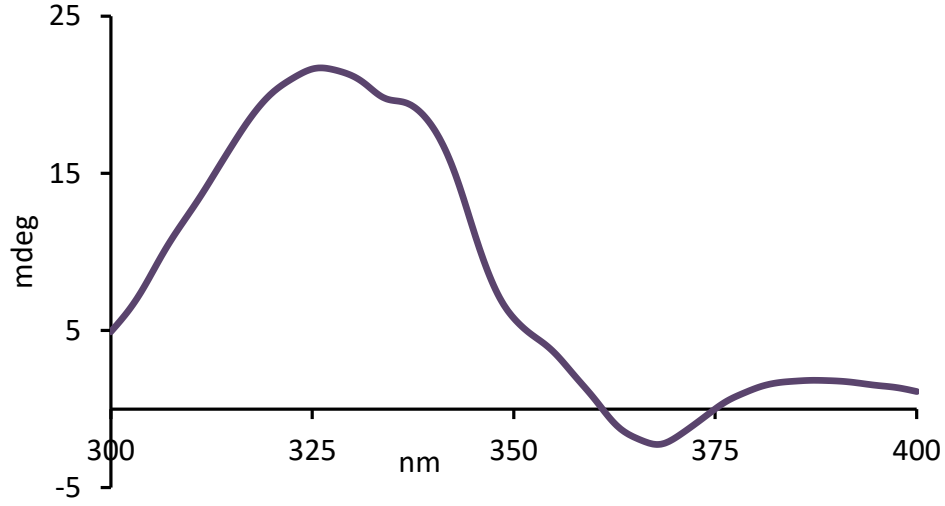

Figure S29. CD analysis of a mixture containing 2.0 mM of *(R,R)*-**2**, 23.0 mM of (*R*,*S*)-**2**, 24.0 mM of (*S*,*S*)-**2**, and 1.0 mM of (*S*,*R*)-**2** (Oxidized state).

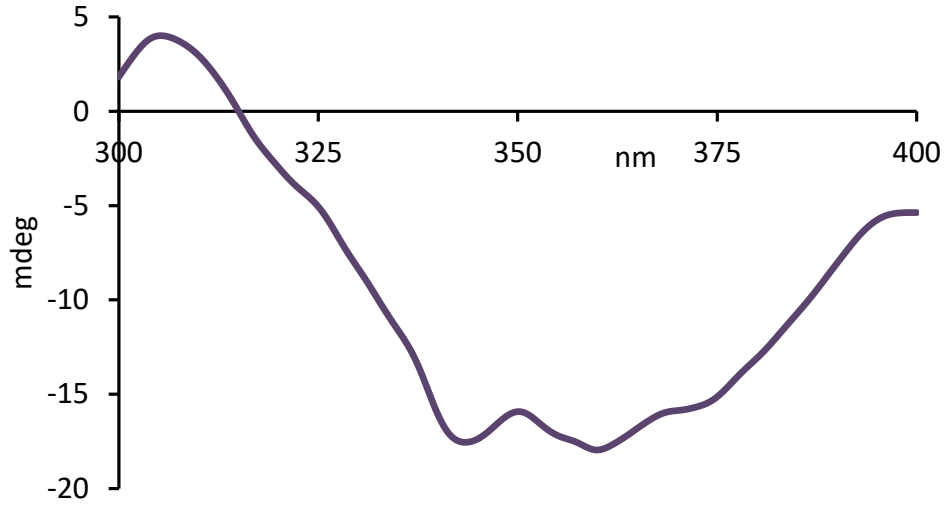

Figure S30. CD analysis of a mixture containing 10.0 mM of *(R,R)*-**2**, 13.0 mM of (*R*,*S*)-**2**, 1.0 mM of (*S*,*S*)-**2**, and 21.0 mM of (*S*,*R*)-**2** (Oxidized state).

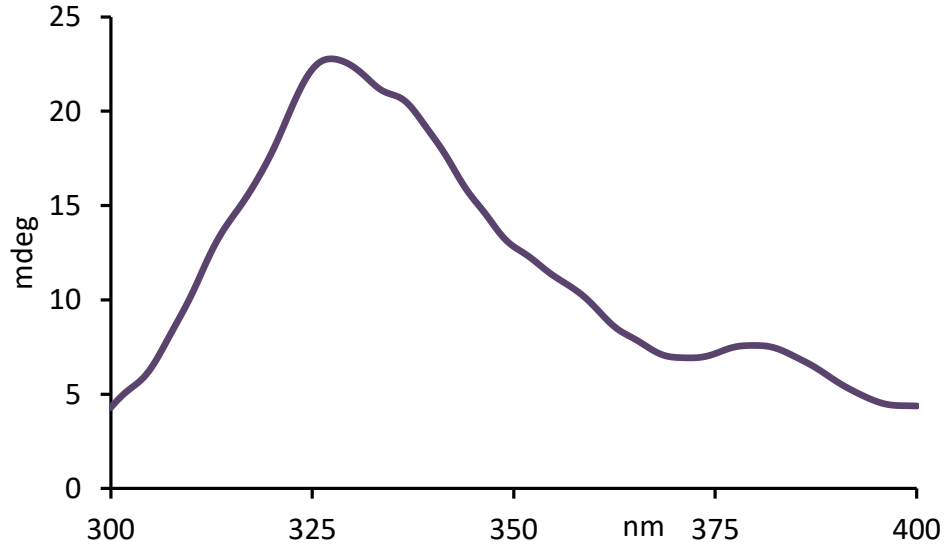

Figure S31. CD analysis of a mixture containing 15.0 mM of *(R,R)*-**2**, 5.0 mM of (*R*,*S*)-**2**, 12.0 mM of (*S*,*S*)-**2**, and 8.0 mM of (*S*,*R*)-**2** (Oxidized state).

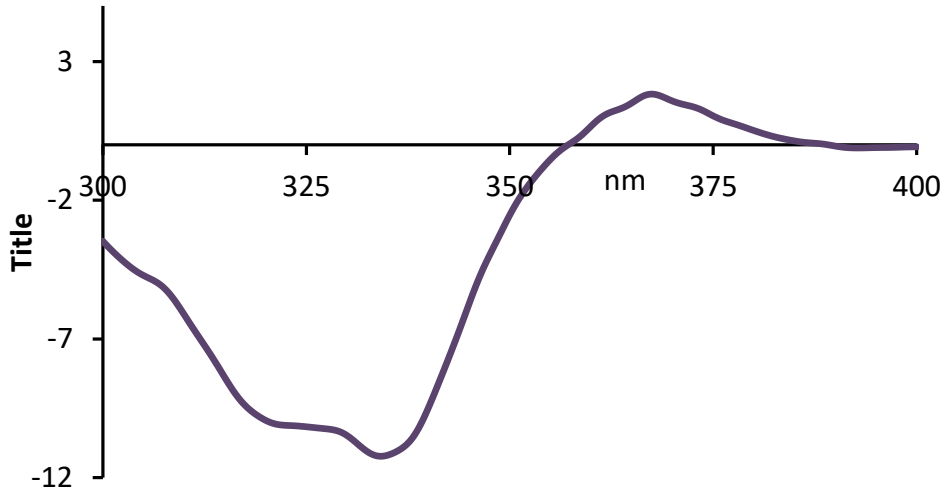

Figure S32. CD analysis of a mixture containing 14.0 mM of *(R,R)*-**2**, 6.0 mM of (*R*,*S*)-**2**, 9.0 mM of (*S*,*S*)-**2**, and 6.0 mM of (*S*,*R*)-**2** (Oxidized state).

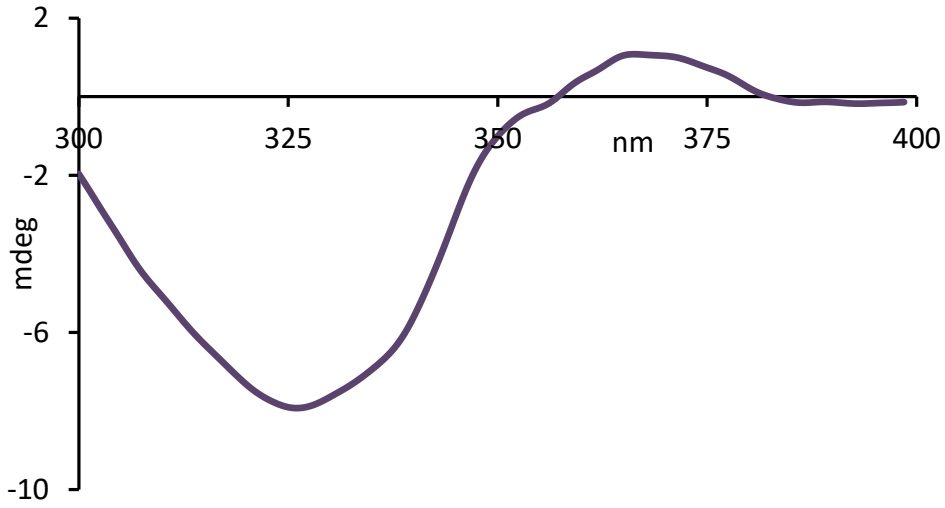

Figure S33. CD analysis of a mixture containing 15.0 mM of *(R,R)*-**2**, 5.0 mM of (*R*,*S*)-**2**, 15.0 mM of (*S*,*S*)-**2**, and 7.0 mM of (*S*,*R*)-**2** (Oxidized state).

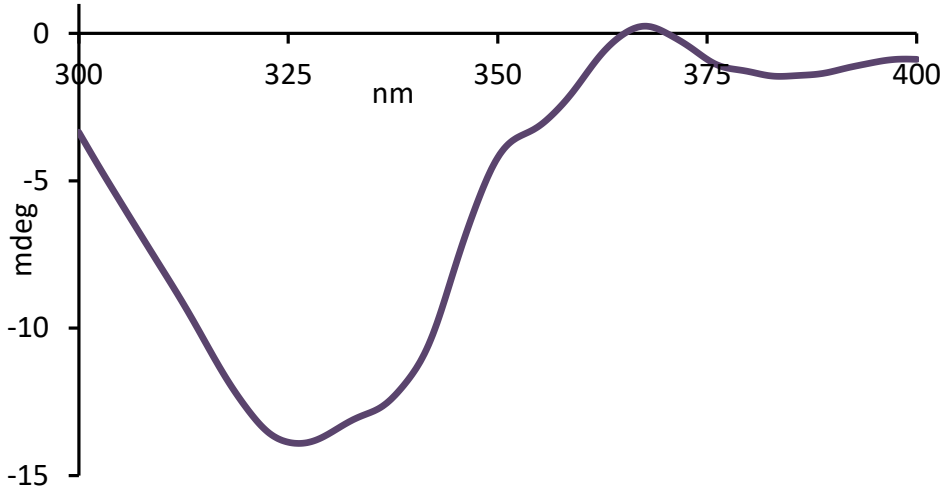

Figure S34. CD analysis of a mixture containing 10.0 mM of *(R,R)*-**2**, 14.0 mM of (*R*,*S*)-**2**, 12.0 mM of (*S*,*S*)-**2**, and 7.0 mM of (*S*,*R*)-**2** (Oxidized state).

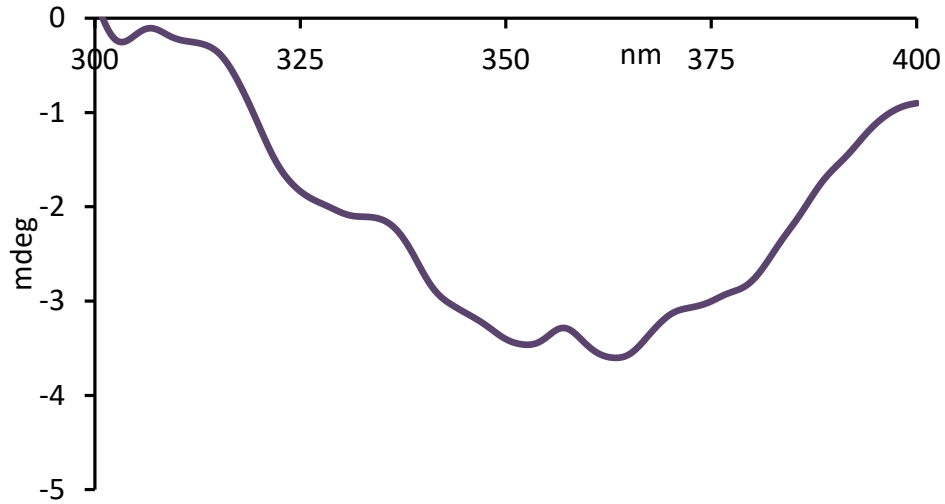

Figure S35. CD analysis of a mixture containing 12.0 mM of *(R,R)*-**2**, 13.0 mM of (*R*,*S*)-**2**, 7.0 mM of (*S*,*S*)-**2**, and 14.0 mM of (*S*,*R*)-**2** (Oxidized state).

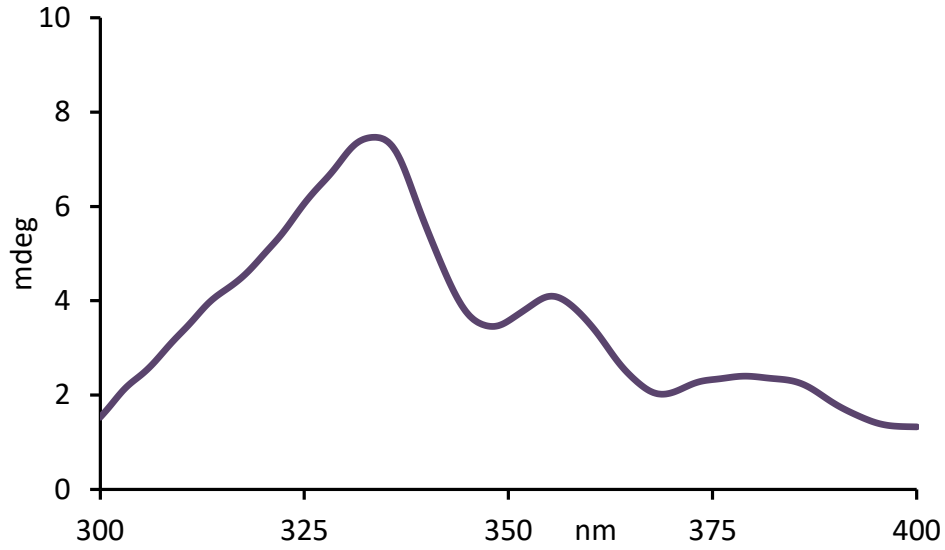

Figure S36. CD analysis of a mixture containing 9.0 mM of *(R,R)*-**2**, 5.0 mM of (*R*,*S*)-**2**, 8.0 mM of (*S*,*S*)-**2**, and 13.0 mM of (*S*,*R*)-**2** (Oxidized state).

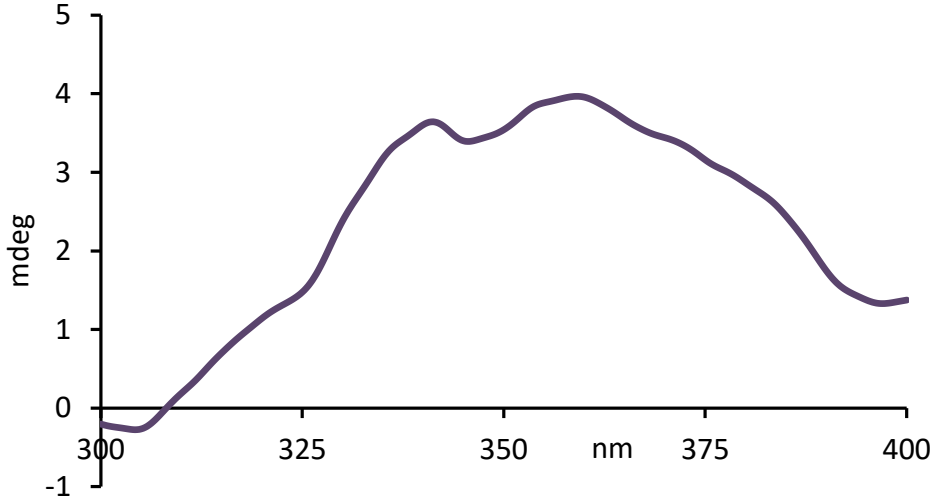

Figure S37. CD analysis of a mixture containing 20.0 mM of *(R,R)*-**2**, 5.0 mM of (*R*,*S*)-**2**, 22.0 mM of (*S*,*S*)-**2**, and 3.0 mM of (*S*,*R*)-**2** (Reduced state).

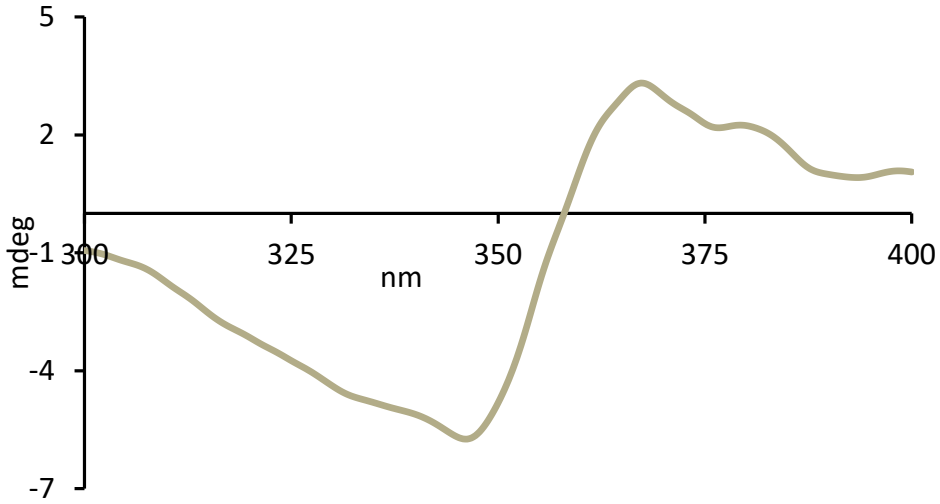

Figure S38. CD analysis of a mixture containing 4.0 mM of *(R,R)*-**2**, 16.0 mM of (*R*,*S*)-**2**, 18.0 mM of (*S*,*S*)-**2**, and 2.0 mM of (*S*,*R*)-**2** (Reduced state).

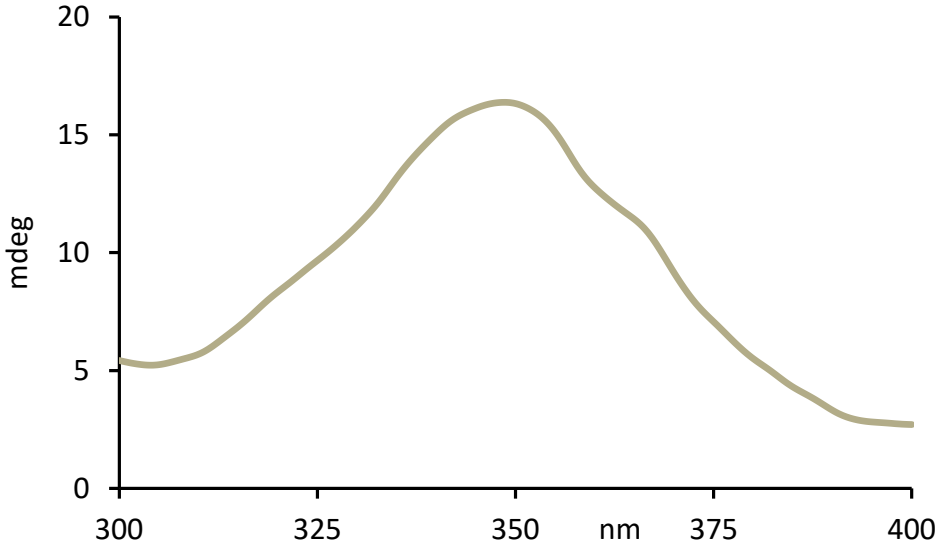

Figure S39. CD analysis of a mixture containing 19.0 mM of *(R,R)*-**2**, 4.0 mM of (*R*,*S*)-**2**, 10.0 mM of (*S*,*S*)-**2**, and 12.0 mM of (*S*,*R*)-**2** (Reduced state).

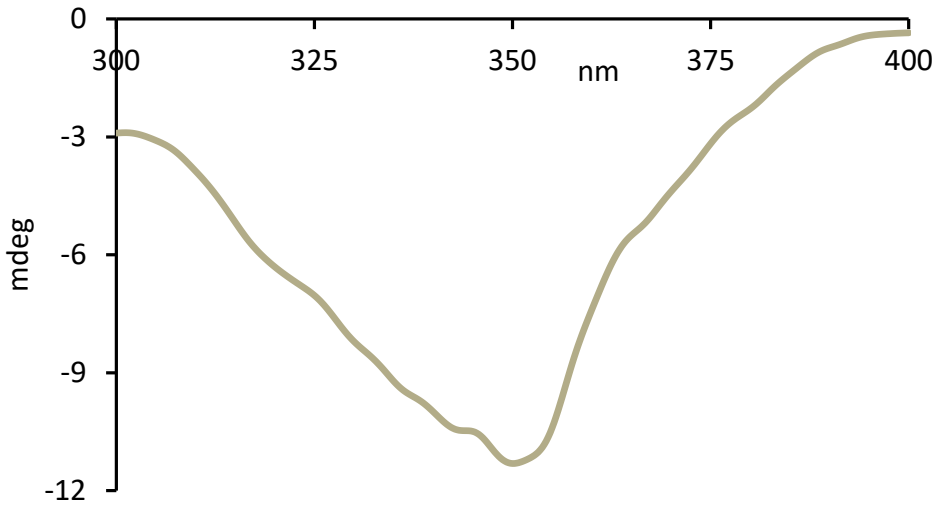

Figure S40. CD analysis of a mixture containing 13.0 mM of *(R,R)*-**2**, 2.0 mM of (*R*,*S*)-**2**, 7.0 mM of (*S*,*S*)-**2**, and 8.0 mM of (*S*,*R*)-**2** (Reduced state).

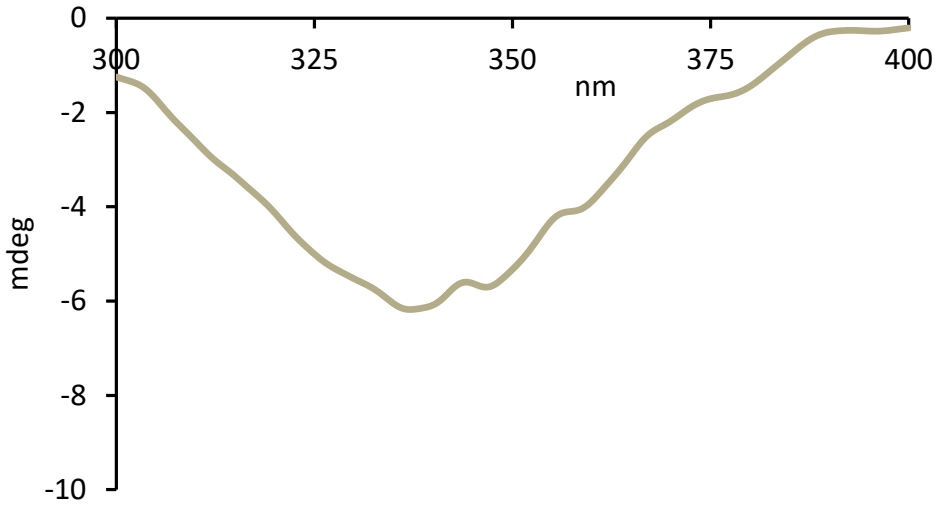

Figure S41. CD analysis of a mixture containing 10.0 mM of *(R,R)*-**2**, 7.0 mM of (*R*,*S*)-**2**, 15.0 mM of (*S*,*S*)-**2**, and 3.0 mM of (*S*,*R*)-**2** (Reduced state).

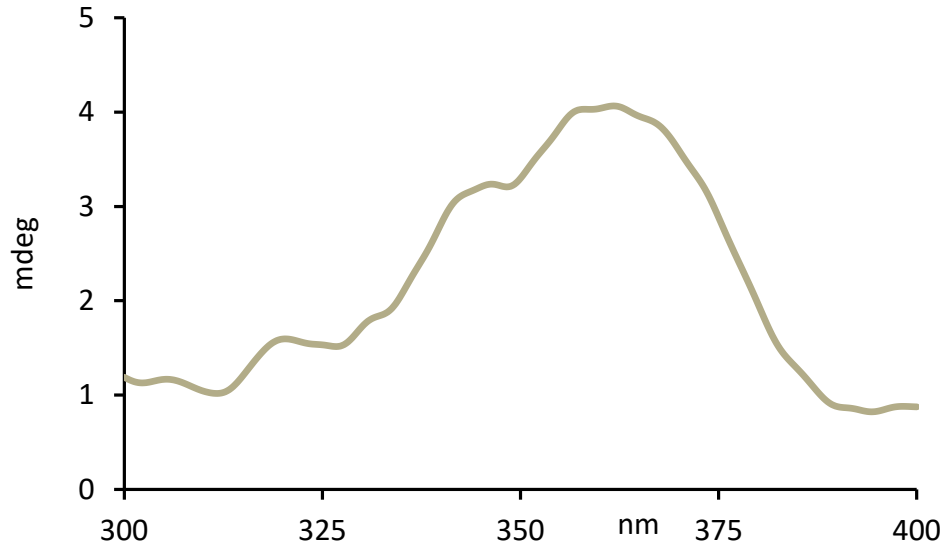

Figure S42. CD analysis of a mixture containing 15.0 mM of *(R,R)*-**2**, 5.0 mM of (*R*,*S*)-**2**, 1.0 mM of (*S*,*S*)-**2**, and 19.0 mM of (*S*,*R*)-**2** (Reduced state).

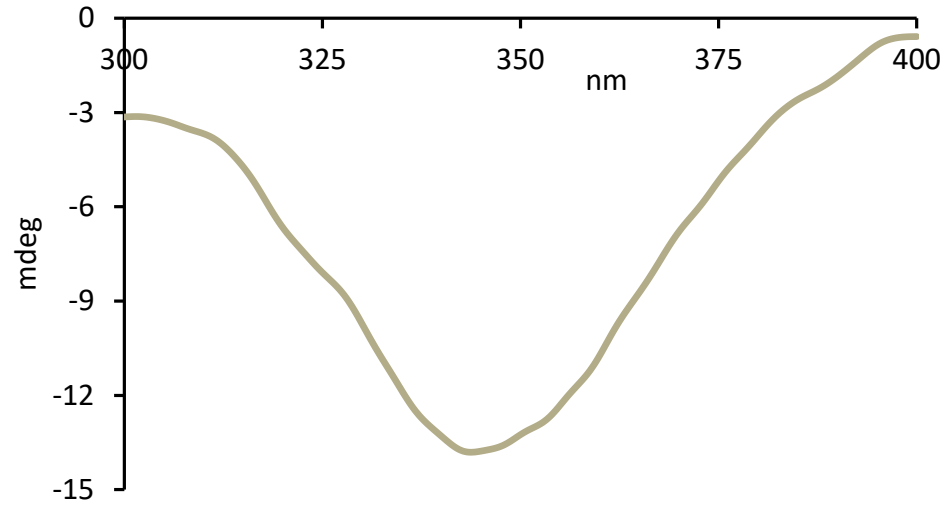

Figure S43. CD analysis of a mixture containing 3.0 mM of *(R,R)*-**2**, 22.0 mM of (*R*,*S*)-**2**, 7.0 mM of (*S*,*S*)-**2**, and 18.0 mM of (*S*,*R*)-**2** (Reduced state).

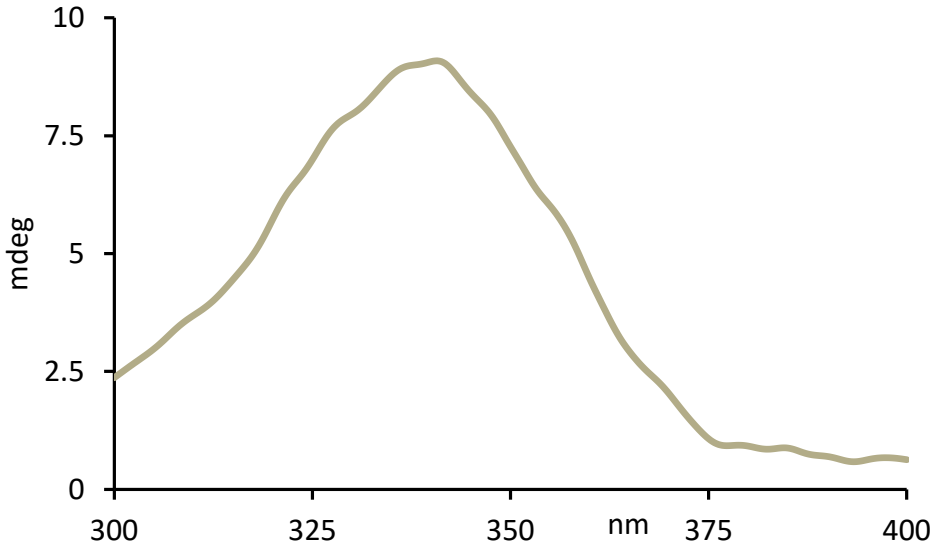

Figure S44. CD analysis of a mixture containing 2.0 mM of *(R,R)*-**2**, 23.0 mM of (*R*,*S*)-**2**, 24.0 mM of (*S*,*S*)-**2**, and 1.0 mM of (*S*,*R*)-**2** (Reduced state).

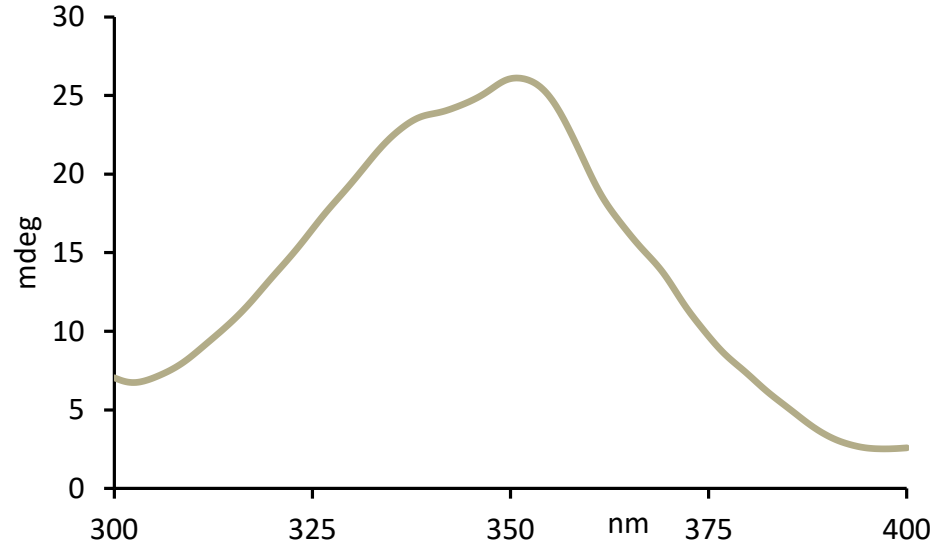

Figure S45. CD analysis of a mixture containing 10.0 mM of *(R,R)*-**2**, 13.0 mM of (*R*,*S*)-**2**, 1.0 mM of (*S*,*S*)-**2**, and 21.0 mM of (*S*,*R*)-**2** (Reduced state).

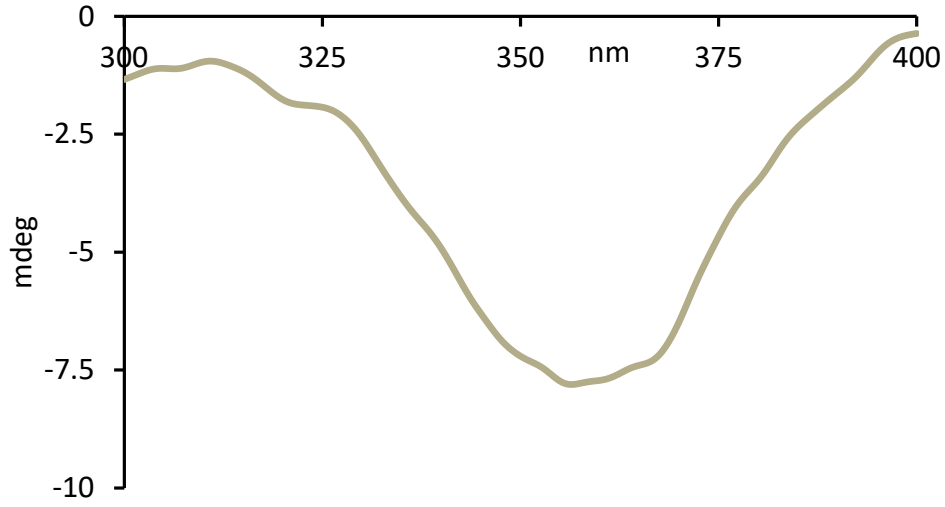

Figure S46. CD analysis of a mixture containing 15.0 mM of *(R,R)*-**2**, 5.0 mM of (*R*,*S*)-**2**, 12.0 mM of (*S*,*S*)-**2**, and 8.0 mM of (*S*,*R*)-**2** (Reduced state).

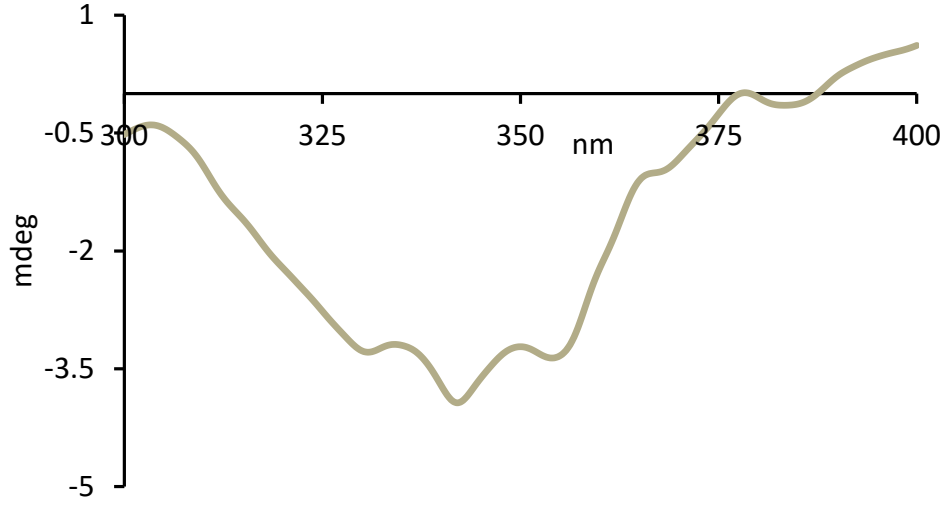

Figure S47. CD analysis of a mixture containing 14.0 mM of *(R,R)*-**2**, 6.0 mM of (*R*,*S*)-**2**, 9.0 mM of (*S*,*S*)-**2**, and 6.0 mM of (*S*,*R*)-**2** (Reduced state).

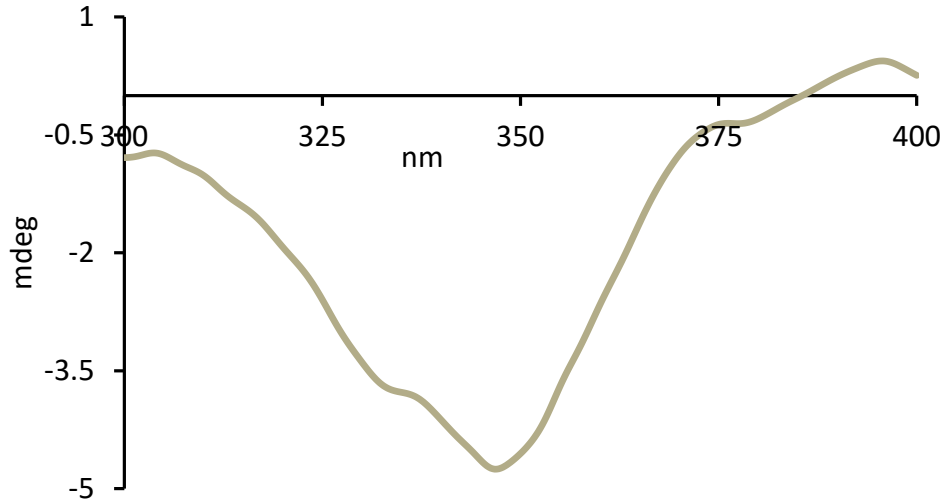

Figure S48. CD analysis of a mixture containing 15.0 mM of *(R,R)*-**2**, 5.0 mM of (*R*,*S*)-**2**, 15.0 mM of (*S*,*S*)-**2**, and 7.0 mM of (*S*,*R*)-**2** (Reduced state).

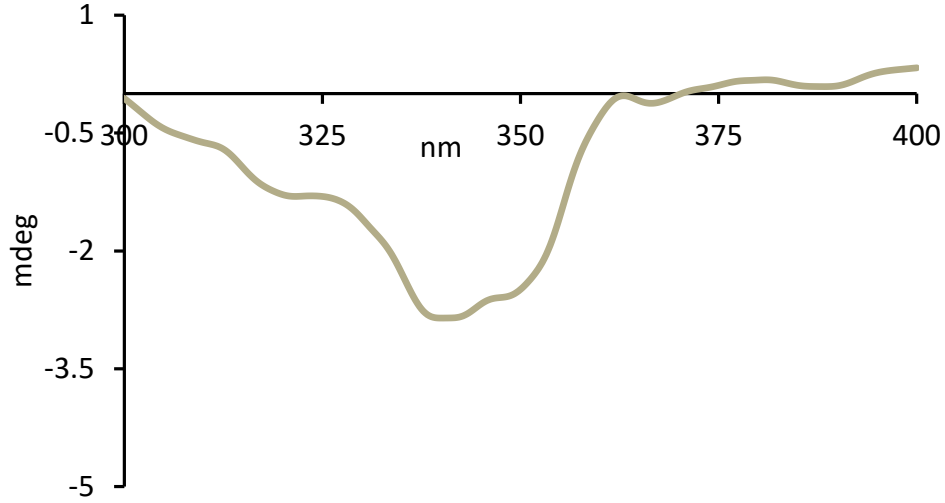

Figure S49. CD analysis of a mixture containing 10.0 mM of *(R,R)*-**2**, 14.0 mM of (*R*,*S*)-**2**, 12.0 mM of (*S*,*S*)-**2**, and 7.0 mM of (*S*,*R*)-**2** (Reduced state).

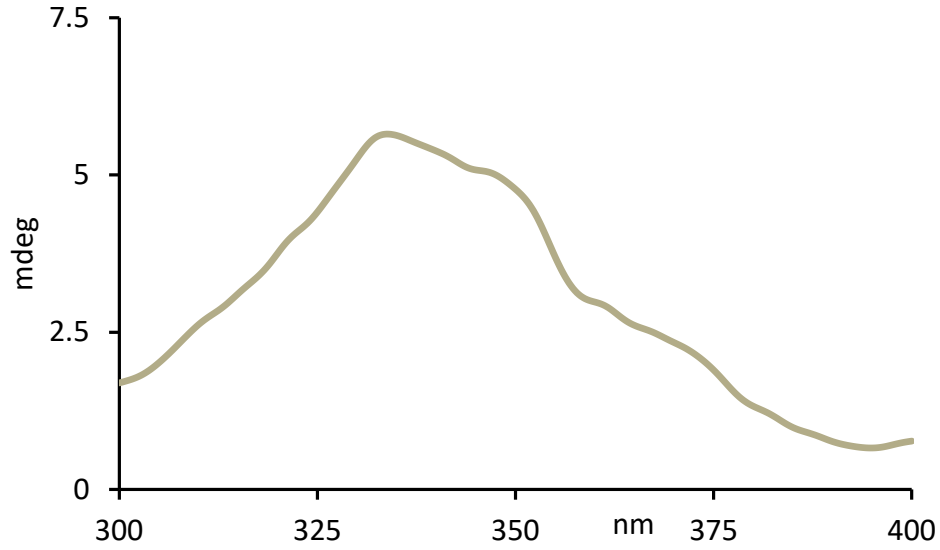

Figure S50. CD analysis of a mixture containing 12.0 mM of *(R,R)*-**2**, 13.0 mM of (*R*,*S*)-**2**, 7.0 mM of (*S*,*S*)-**2**, and 14.0 mM of (*S*,*R*)-**2** (Reduced state).

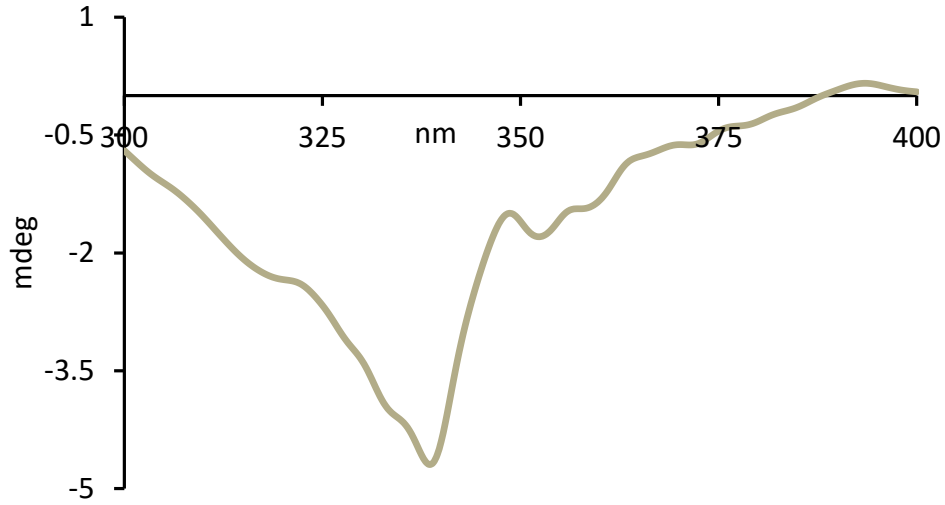

Figure S51. CD analysis of a mixture containing 9.0 mM of *(R,R)*-**2**, 5.0 mM of (*R*,*S*)-**2**, 8.0 mM of (*S*,*S*)-**2**, and 13.0 mM of (*S*,*R*)-**2** (Reduced state).

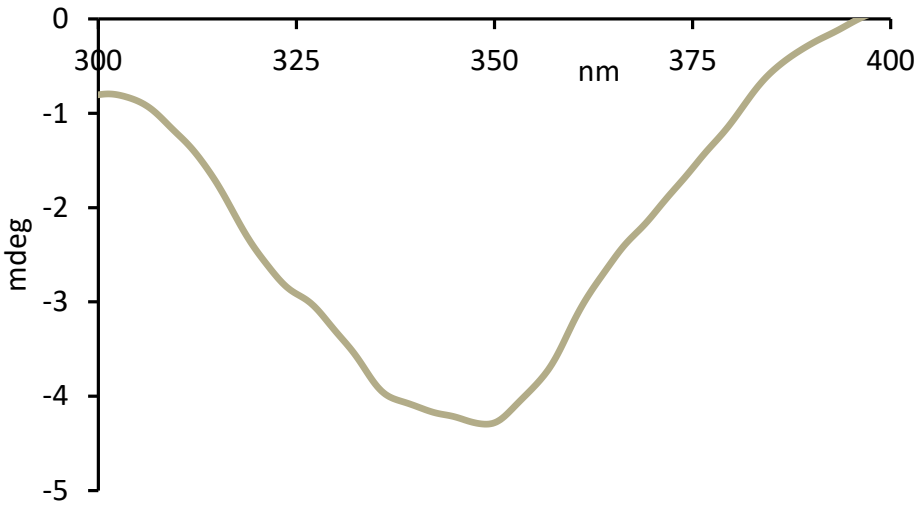

7.2. UV sensing results

Table S1. Average of 5 single UV measurements of the oxidized and reduced states.

Sample number	UV absorption of oxidized state at 351 nm	UV absorption of reduced state at 370 nm
1	0.670082	0.747750
2	0.632439	0.683235
3	0.653012	0.715480
4	0.615743	0.618777
5	0.611366	0.651050
6	0.632439	0.683245
7	0.626149	0.747689
8	0.670082	0.747691
9	0.653012	0.715472
10	0.632439	0.683235
11	0.624877	0.649948
12	0.636213	0.69670
13	0.652896	0.703388
14	0.661879	0.723428
15	0.597856	0.649942

7.3. Linear regression analysis of the total concentration

The amplitude of the UV maxima in the reduced state has a linear relationship with the total concentration. The total concentration can be calculated with the following equation:

Total concentration (M)= 0.154 x absorbance (reduced state at UV 370 nm) -0.06528

Table S2. Actual vs. Predicted concentration (mM) of the total concentration.

Sample number	Actual concentration (mM)	Predicted concentration (mM)
1	50.0	49.9
2	40.0	39.9
3	45.0	44.9
4	30.0	30.0
5	35.0	35.0
6	40.0	39.9
7	50.0	49.9
8	50.0	49.9
9	45.0	44.9
10	40.0	39.9
11	35.0	34.8
12	42.0	42.0
13	43.0	43.0
14	46.0	46.1
15	35.0	34.8

7.4. Linear regression analysis of diastereomeric excess

The diastereomeric excess was determined by multiple linear regression (MLR) using the total concentration (M) and the UV absorption of oxidized state at 351 nm as the independent variables. The *de* can be calculated with the following equation:

de= 1270.7186 x absorbance (oxidized state at UV 351 nm) – 4822.672 x total concentration (M) – 611.756

The results for are shown in the following table.

Table S3. Actual vs predicted diastereomeric excess

Sample number	Actual diastereomeric excess	Predicted diastereomeric excess
1	0.00	-0.79
2	0.00	-0.71
3	2.22	1.48
4	0.00	0.00
5	-2.86	-3.59
6	0.00	-0.72
7	0.00	0.00
8	0.00	-0.75
9	2.22	1.49
10	0.00	-0.71
11	14.29	14.40
12	-4.76	-5.92
13	11.63	10.32
14	8.70	8.95
15	-20.00	-19.93

7.5. Chemometric analysis of the individual stereoisomer concentrations

The results from the linear regression of the total concentration, the UV absorption of the oxidized state at 351 nm, and the CD spectra of the oxidized and the reduced states were used to quantify the individual stereoisomer concentration in mM using partial least squares (PLS). Scikit learn library, a free Python library for machine learning, was used for all pre-processing (scaling) and data analysis using PLS.

7.5.1. Partial Least Squares

Partial least squares (PLS) is a supervised learning method that decomposes both **X** (independent variable) and **Y** (dependent variable) matrices as a product of a common set of orthogonal factors and a set of specific loadings. It is often used in datasets with large multicollinearity which are observed in chemometrics and process control. Equation 1 and 2 show the underlying model of PLS:

$$X = TP^T + E \qquad \text{(equation 1)}$$

$$Y = UQ^T + F \qquad \text{(equation 2)}$$

Where X is the independent variable matrix, T is the X score matrix that contains the projections of X, P is the orthogonal loading matrix for X, Y is the dependent variable matrix, U is the Y score matrix that contains the projection of Y, Q is the orthogonal loading matrix for Y, and E and F are the error terms. Concentration from UV and UV absorption of oxidized state are only included as independent variables along with the CD spectra.

7.5.2. Cross-validation

In cross-validation, one or more samples are randomly left out and are used as “test set”, meanwhile the other samples are used as “training set.” This procedure is applied until all samples have been left out. Cross-validation shows how well the algorithm can perform on a new data set. For our data set, leave-one-out cross-validation, where one sample is left out each time is used because the number of training samples is relatively low. The cross-validation results are shown in Table S4. A heatmap showing accuracy of each stereoisomer quantification is shown in Table S5. The correlation graph and the bar graph are shown on Figures S49 and S50, respectively.

Table S4. Actual versus predicted concentrations.

Sample #		(*R*,*R*)-2 (mM)	(*S*,*S*)-2 (mM)	(*R*,*S*)-2 (mM)	(*S*,*R*)-2 (mM)
1	Actual	20.0	5.0	22.0	3.0
	Predicted	20.7	5.7	20.4	2.1
2	Actual	4.0	16.0	18.0	2.0
	Predicted	3.5	18.2	16.1	0.1
3	Actual	19.0	4.0	10.0	12.0
	Predicted	18.9	4.5	10.1	11.0
4	Actual	13.0	2.0	7.0	8.0
	Predicted	13.5	2.5	7.3	8.8
5	Actual	10.0	7.0	15.0	3.0
	Predicted	10.7	6.6	15.1	3.7
6	Actual	15.0	5.0	1.0	19.0
	Predicted	14.2	5.3	1.4	18.4
7	Actual	3.0	22.0	7.0	18.0
	Predicted	2.9	20.4	7.3	18.9
8	Actual	2.0	23.0	24.0	1.0
	Predicted	2.4	23.9	24.0	0.4
9	Actual	10.0	13.0	1.0	21.0
	Predicted	10.5	13.4	0.0	21.7
10	Actual	15.0	5.0	12.0	8.0
	Predicted	14.1	4.0	12.5	9.2
11	Actual	14.0	6.0	9.0	6.0
	Predicted	13.1	4.8	10.5	7.3
12	Actual	15.0	5.0	15.0	7.0
	Predicted	14.8	5.4	14.1	6.5
13	Actual	10.0	14.0	12.0	7.0
	Predicted	9.1	13.4	13.3	6.6
14	Actual	12.0	13.0	7.0	14.0
	Predicted	11.6	11.6	8.1	14.8
15	Actual	9.0	5.0	8.0	13.0
	Predicted	11.0	6.3	6.3	11.7

Table S5. Heatmap showing the accuracy of the quaternary mixture sample analysis.

Sample	*RR* (mM)	*SS* (mM)	*RS* (mM)	*SR* (mM)
1	20.7	5.7	20.4	2.1
2	3.5	18.2	16.1	0.1
3	18.9	4.5	10.1	11.0
4	13.5	2.5	7.3	8.0
5	10.7	6.6	15.1	3.7
6	14.2	5.3	1.4	18.4
7	2.9	20.4	7.3	18.9
8	2.4	23.9	24.0	0.4
9	10.5	13.4	0.0	21.7
10	14.1	4.0	12.5	9.2
11	13.1	4.8	10.5	7.3
12	14.8	5.4	14.1	6.5
13	9.1	13.4	13.3	6.6
14	11.6	11.6	8.1	14.8
15	11.0	6.3	6.3	11.7

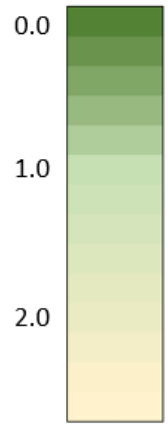

Figure S52. Correlation of predicted versus actual concentration for each stereoisomer in the 15 samples.

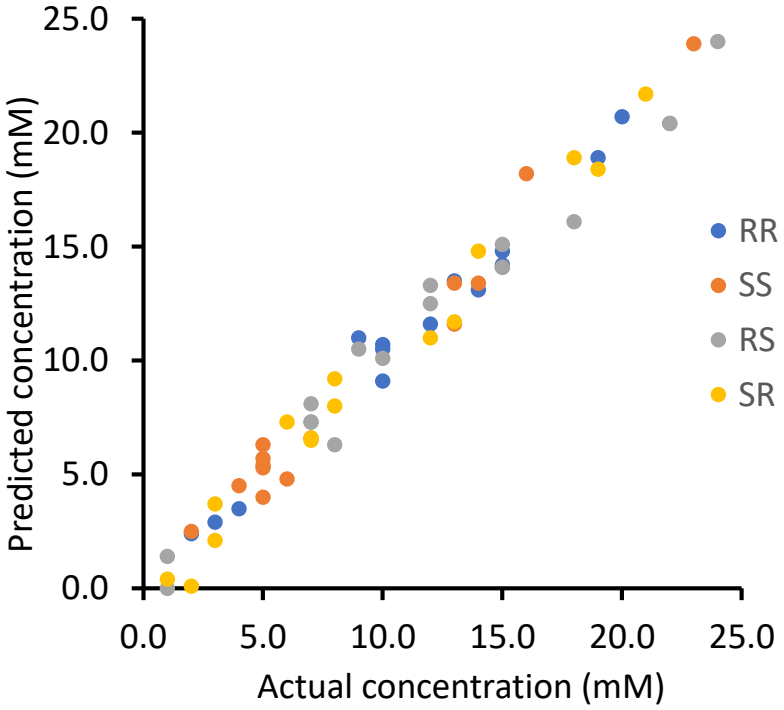

Figure S53. Bar graph visualization of the quaternary mixture analysis.

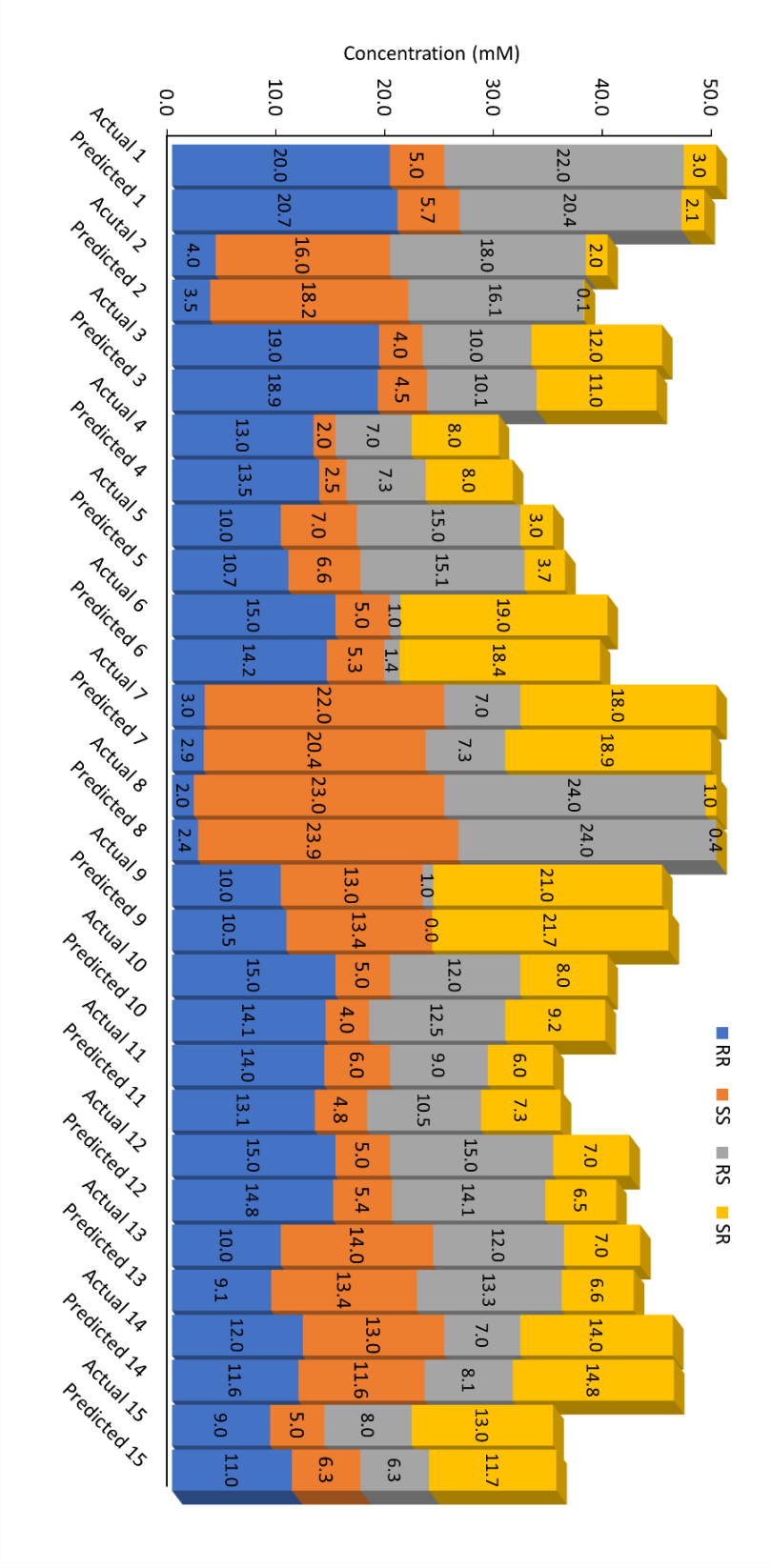

8. Chemometric analysis with samples containing only two or three stereoisomers

Thirty samples of 2-amino-1,2-diphenylethanol stereoisomers at varying concentrations and isomeric compositions in DMSO were prepared and subjected to simultaneous analysis using probe **1**. For each sample, aliquots of 15.0 μL were combined with 2.0 mL of DMSO and 5 single point UV measurements were taken at 351 nm and averaged. The diastereomeric ratio was calculated using UV measurements of the oxidized state as described below (Chapter 7.3.). Upon addition of excess of $NaBH_4$ (0.5 mL of a 50 mM stock solution in MeOH) another 5 single point UV measurements were taken at 370 nm and averaged. The overall concentration was calculated using UV measurements of the reduced state as described below (Chapter 7.4.). Finally, for each sample 40.0 μL aliquots were combined with 2.0 mL of DMSO and CD spectra of both the oxidized and reduced state after addition of excess of $NaBH_4$ (0.5 mL of a 50 mM stock solution in MeOH) were collected and used in tandem to determine the enantiomeric ratios as described in Chapter 6.0 and Chapter 6.4.

8.1. Sample spectra

Figure S54. CD analysis of a mixture containing 9.9 mM of *(R,R)*-**2**, 20.1 mM of (*R*,*S*)-**2**, 0.0 mM of (*S*,*S*)-**2**, and 0.0 mM of (*S*,*R*)-**2** (Oxidized state).

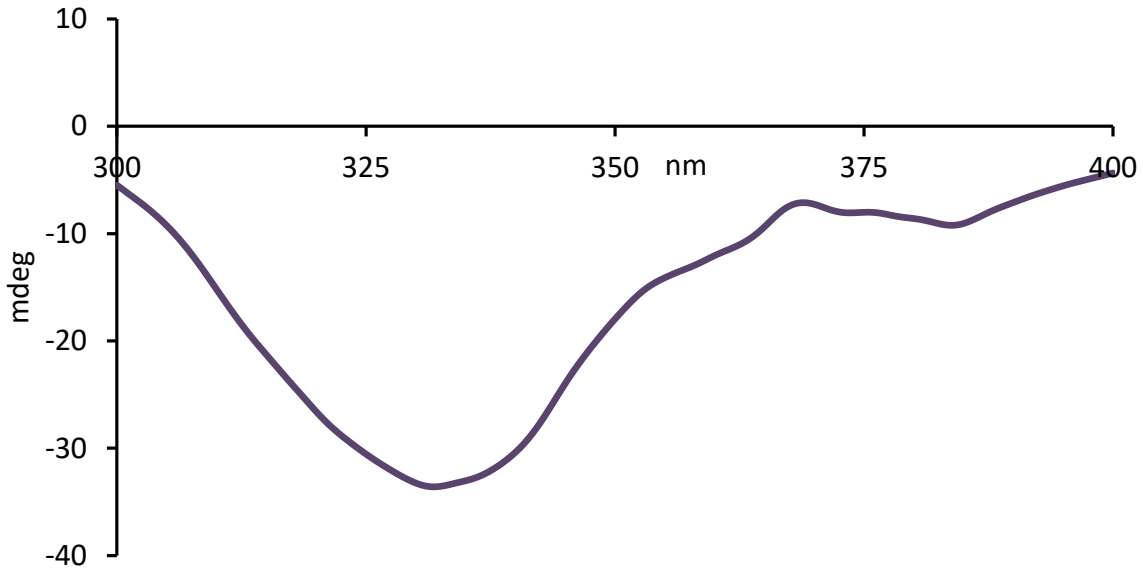

Figure S55. CD analysis of a mixture containing 33.5 mM of *(R,R)*-**2**, 0.0 mM of (*R*,*S*)-**2**, 16.5 mM of (*S*,*S*)-**2**, and 0.0 mM of (*S*,*R*)-**2** (Oxidized state).

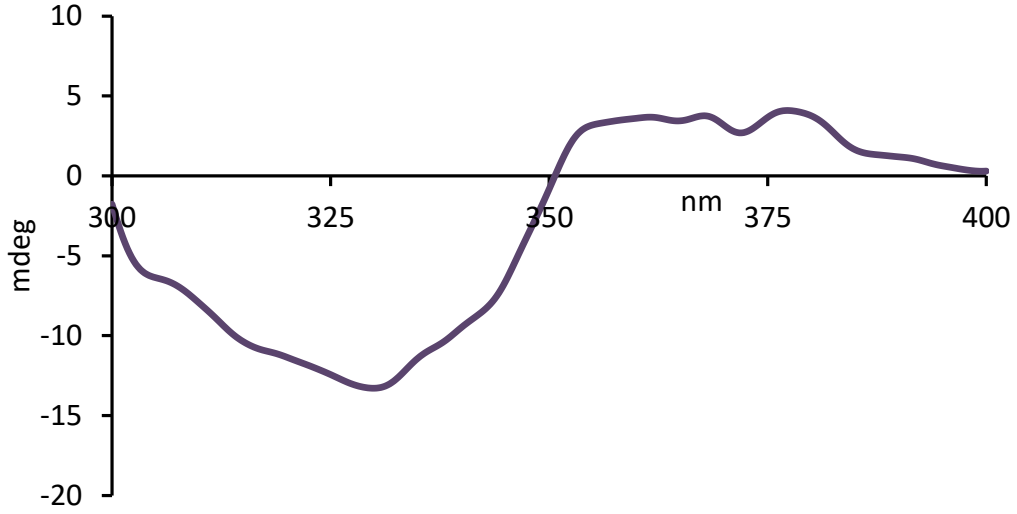

Figure S56. CD analysis of a mixture containing 9.9 mM of *(R,R)*-**2**, 0.0 mM of (*R*,*S*)-**2**, 20.1 mM of (*S*,*S*)-**2**, and 0.0 mM of (*S*,*R*)-**2** (Oxidized state).

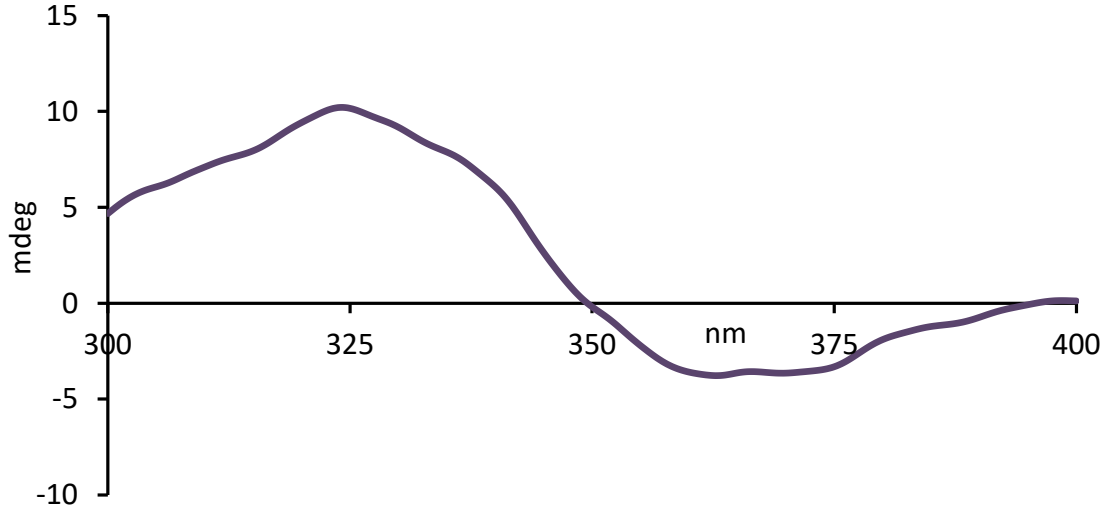

Figure S57. CD analysis of a mixture containing 26.8 mM of *(R,R)*-**2**, 0.0 mM of (*R*,*S*)-**2**, 0.0 mM of (*S*,*S*)-**2**, and 13.2 mM of (*S*,*R*)-**2** (Oxidized state).

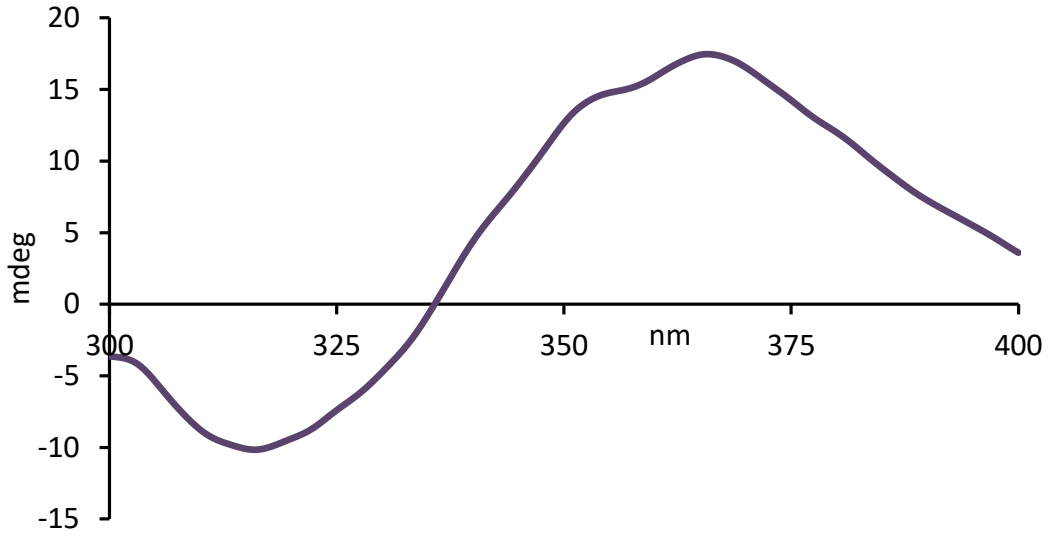

Figure S58. CD analysis of a mixture containing 13.2 mM of *(R,R)*-**2**, 0.0 mM of (*R*,*S*)-**2**, 0.0 mM of (*S*,*S*)-**2**, and 26.8 mM of (*S*,*R*)-**2** (Oxidized state).

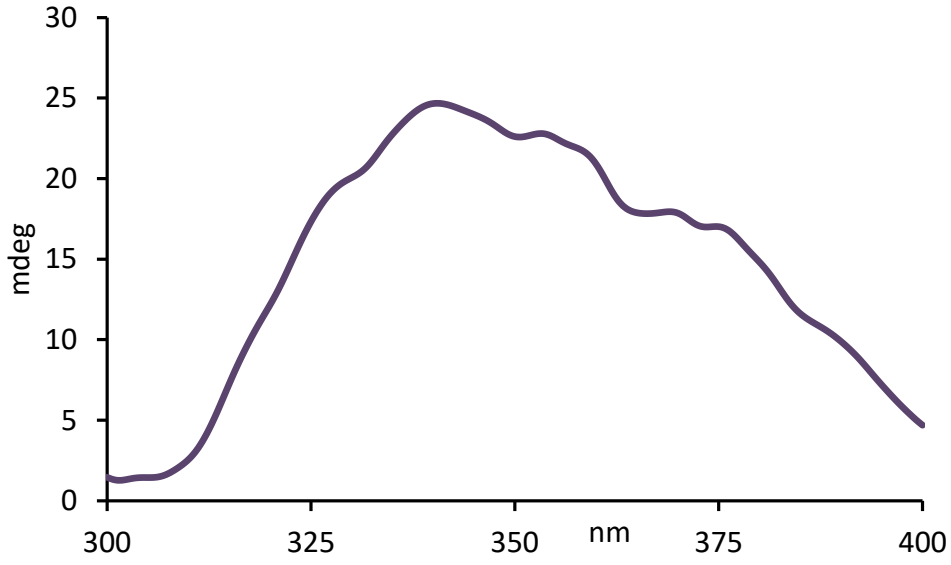

Figure S59. CD analysis of a mixture containing 0.0 mM of *(R,R)*-**2**, 0.0 mM of (*R*,*S*)-**2**, 20.1 mM of (*S*,*S*)-**2**, and 9.9 mM of (*S*,*R*)-**2** (Oxidized state).

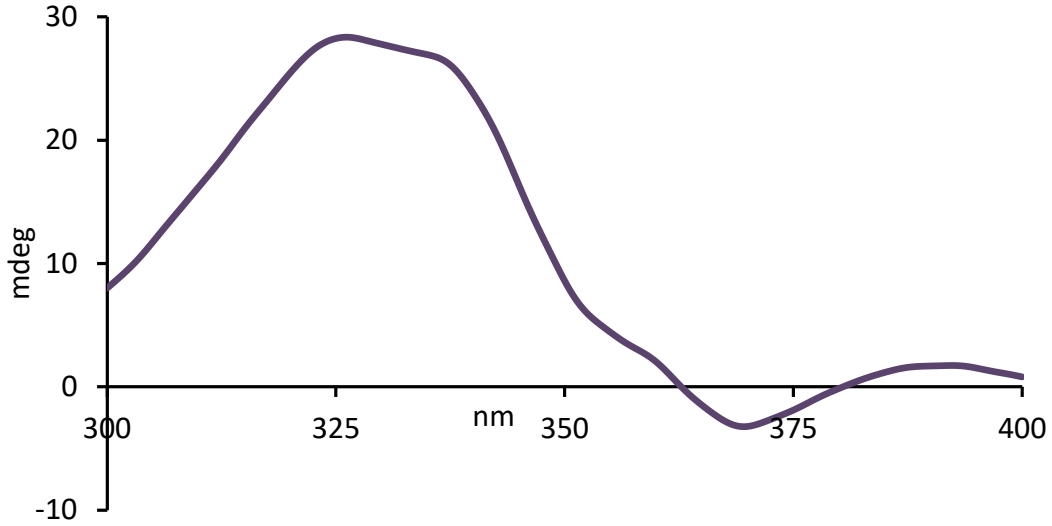

Figure S60. CD analysis of a mixture containing 0.0 mM of *(R,R)*-**2**, 0.0 mM of (*R*,*S*)-**2**, 13.2 mM of (*S*,*S*)-**2**, and 26.8 mM of (*S*,*R*)-**2** (Oxidized state).

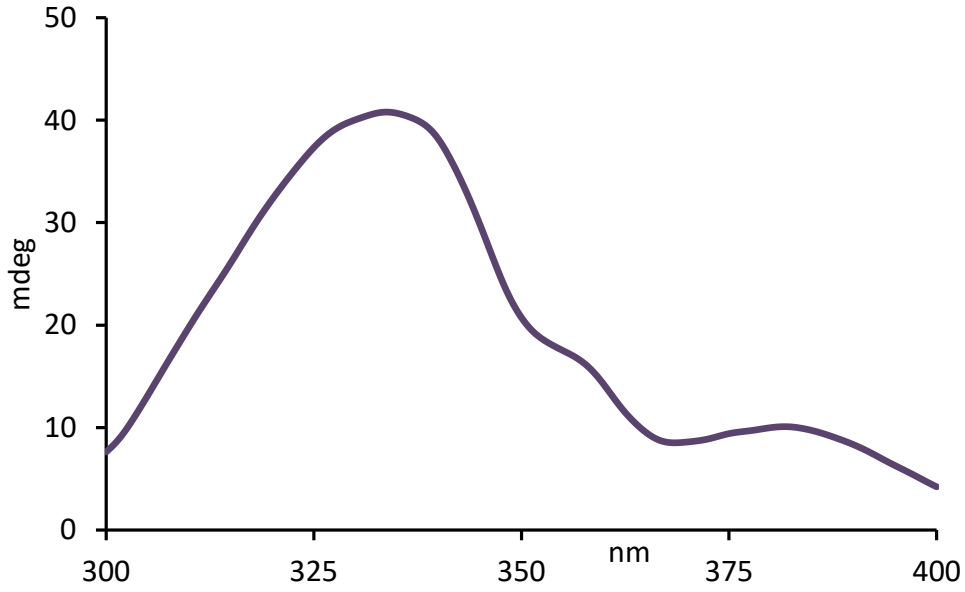

Figure S61. CD analysis of a mixture containing 0.0 mM of *(R,R)*-**2**, 26.8 mM of (*R*,*S*)-**2**, 0.0 mM of (*S*,*S*)-**2**, and 13.2 mM of (*S*,*R*)-**2** (Oxidized state).

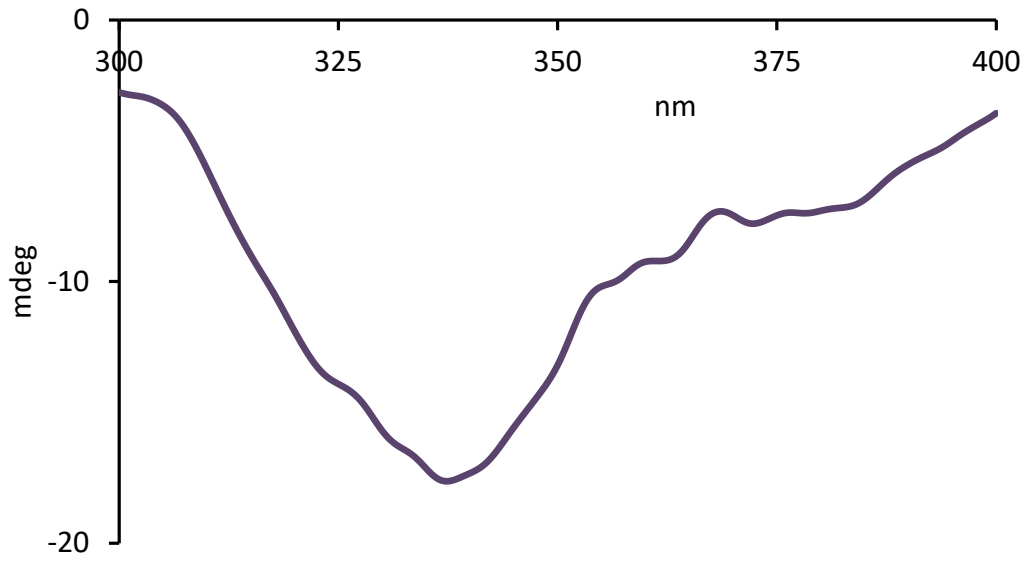

Figure S62. CD analysis of a mixture containing 0.0 mM of *(R,R)*-**2**, 9.9 mM of (*R*,*S*)-**2**, 0.0 mM of (*S*,*S*)-**2**, and 20.1 mM of (*S*,*R*)-**2** (Oxidized state).

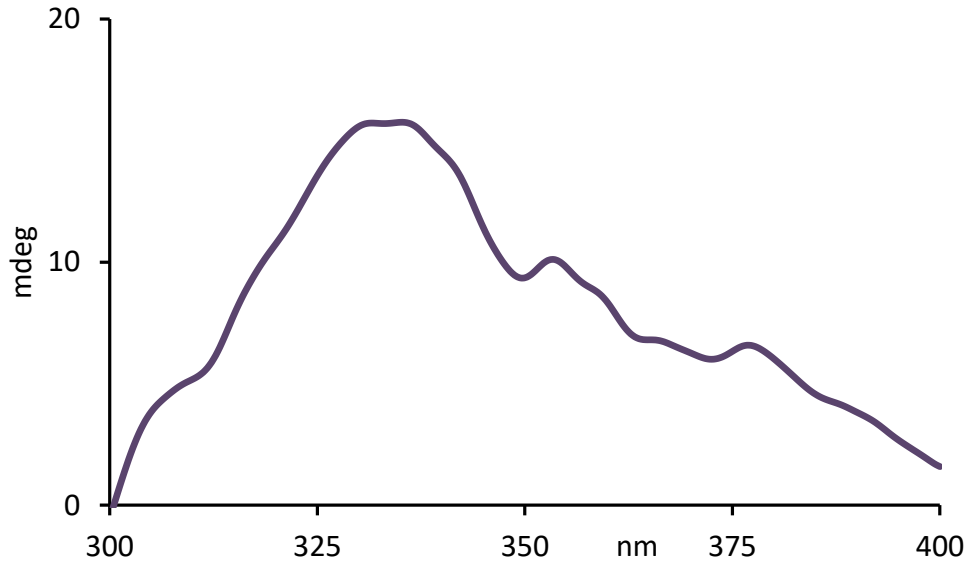

Figure S63. CD analysis of a mixture containing 13.2 mM of *(R,R)*-**2**, 13.2 mM of (*R*,*S*)-**2**, 13.2 mM of (*S*,*S*)-**2**, and 0.0 mM of (*S*,*R*)-**2** (Oxidized state).

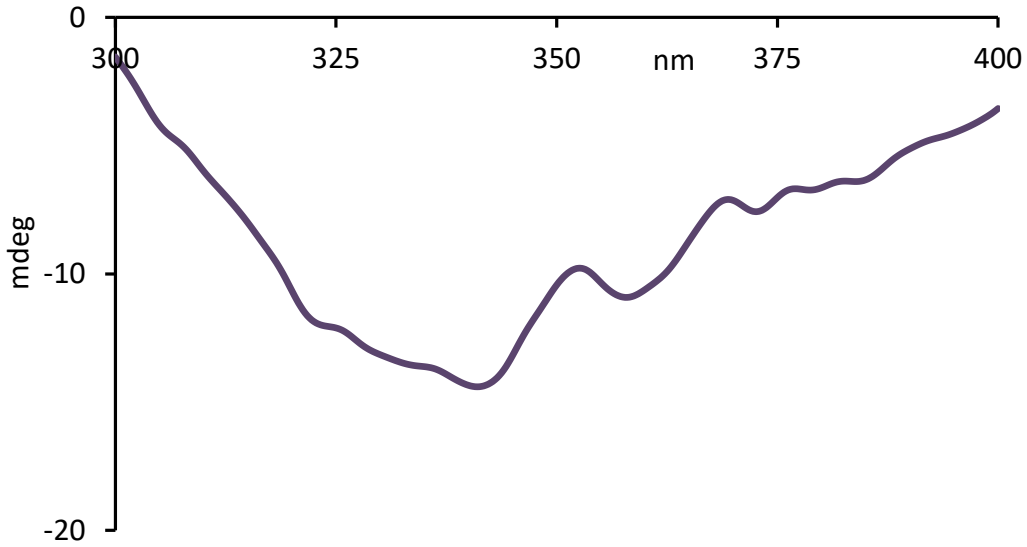

Figure S64. CD analysis of a mixture containing 0.0 mM of *(R,R)*-**2**, 13.2 mM of (*R*,*S*)-**2**, 13.2 mM of (*S*,*S*)-**2**, and 13.2 mM of (*S*,*R*)-**2** (Oxidized state).

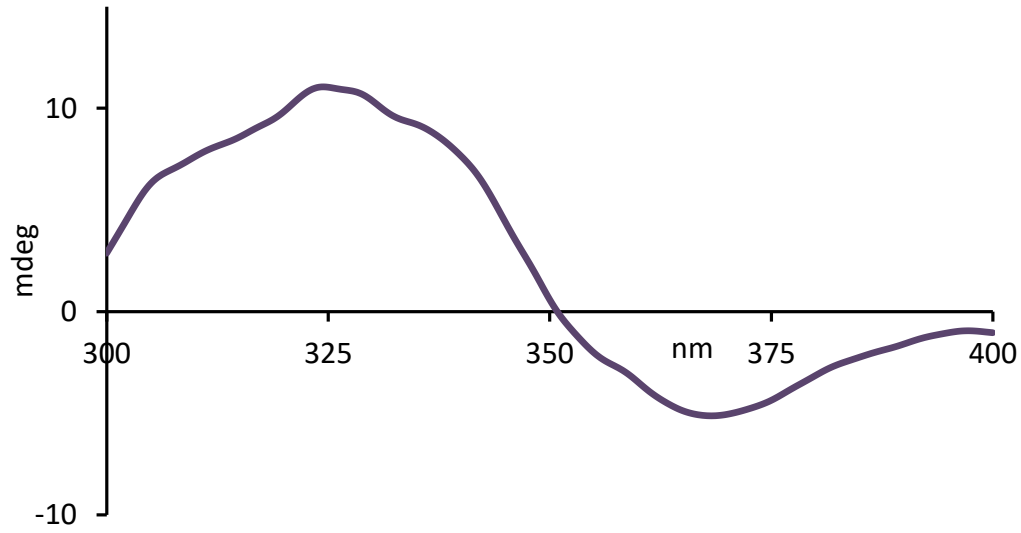

Figure S65. CD analysis of a mixture containing 11.0 mM of *(R,R)*-**2**, 0.0 mM of (*R*,*S*)-**2**, 9.0 mM of (*S*,*S*)-**2**, and 20.0 mM of (*S*,*R*)-**2** (Oxidized state).

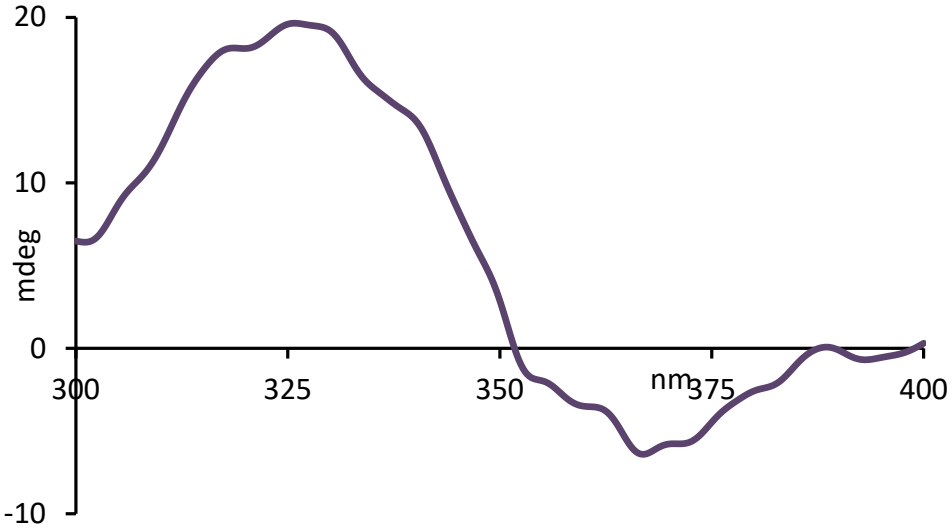

Figure S66. CD analysis of a mixture containing 21.4 mM of *(R,R)*-**2**, 9.2 mM of (*R*,*S*)-**2**, 0.0 mM of (*S*,*S*)-**2**, and 0.0 mM of (*S*,*R*)-**2** (Oxidized state).

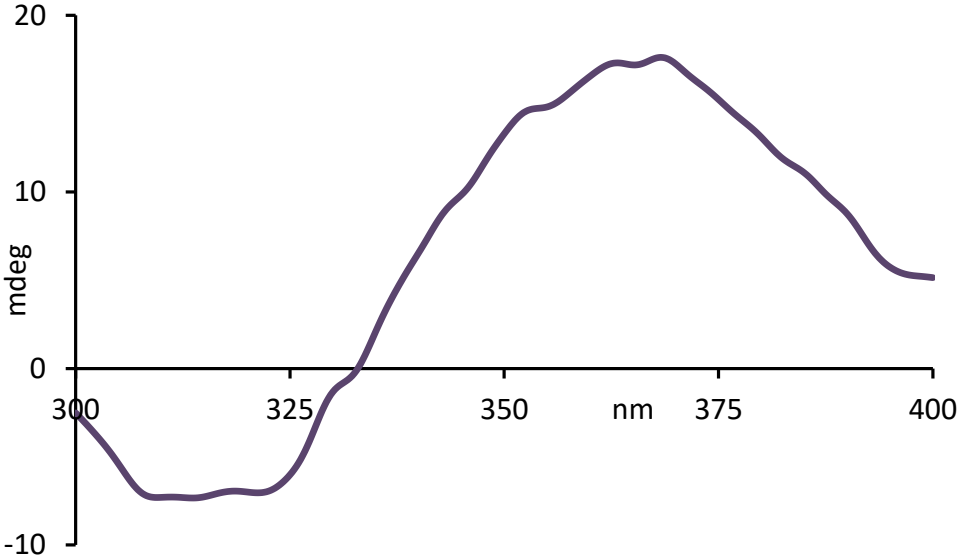

Figure S67. CD analysis of a mixture containing 0.0 mM of *(R,R)*-**2**, 0.0 mM of (*R*,*S*)-**2**, 22.1 mM of (*S*,*S*)-**2**, and 7.4 mM of (*S*,*R*)-**2** (Oxidized state).

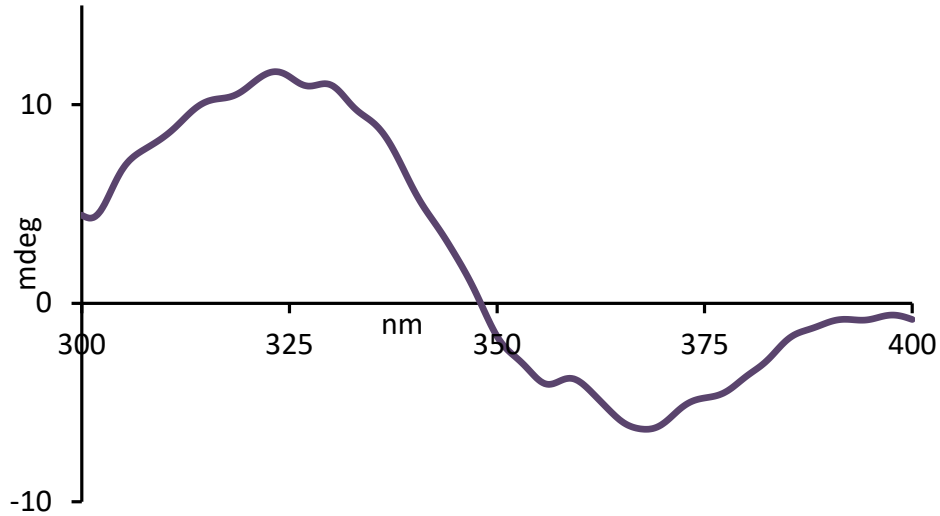

Figure S68. CD analysis of a mixture containing 26.0 mM of *(R,R)*-**2**, 0.0 mM of (*R*,*S*)-**2**, 0.0 mM of (*S*,*S*)-**2**, and 14.0 mM of (*S*,*R*)-**2** (Oxidized state).

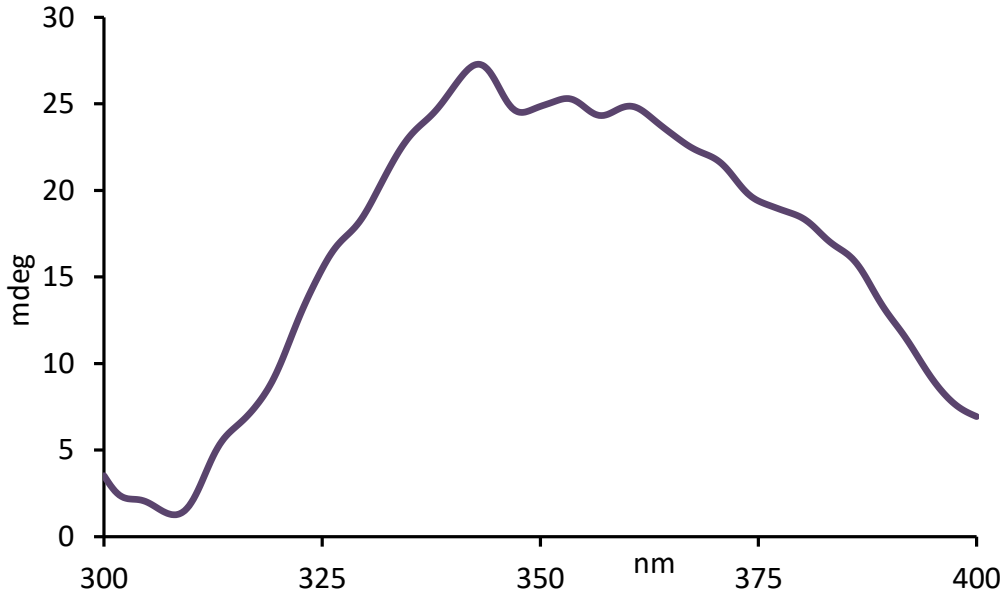

Figure S69. CD analysis of a mixture containing 0.0 mM of *(R,R)*-**2**, 9.0 mM of (*R*,*S*)-**2**, 20.1 mM of (*S*,*S*)-**2**, and 11.1 mM of (*S*,*R*)-**2** (Oxidized state).

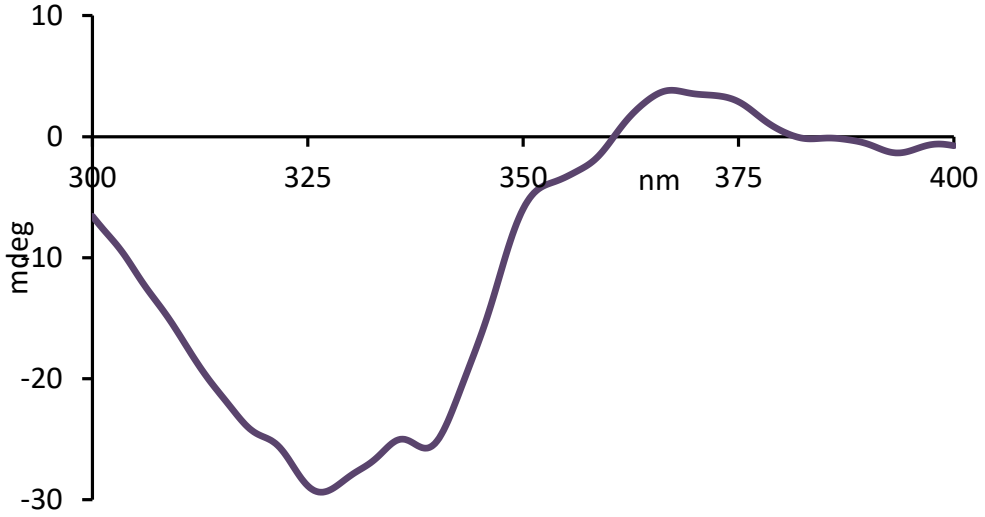

Figure S70. CD analysis of a mixture containing 19.9 mM of *(R,R)*-**2**, 0.0 mM of (*R*,*S*)-**2**, 0.0 mM of (*S*,*S*)-**2**, and 29.8 mM of (*S*,*R*)-**2** (Oxidized state).

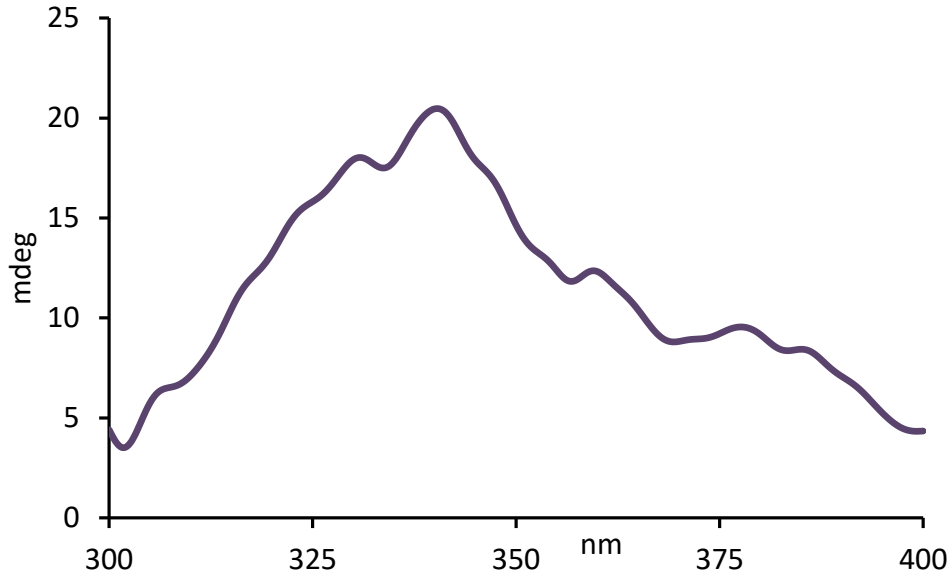

Figure S71. CD analysis of a mixture containing 0.0 mM of *(R,R)*-**2**, 8.4 mM of (*R*,*S*)-**2**, 15.3 mM of (*S*,*S*)-**2**, and 6.9 mM of (*S*,*R*)-**2** (Oxidized state).

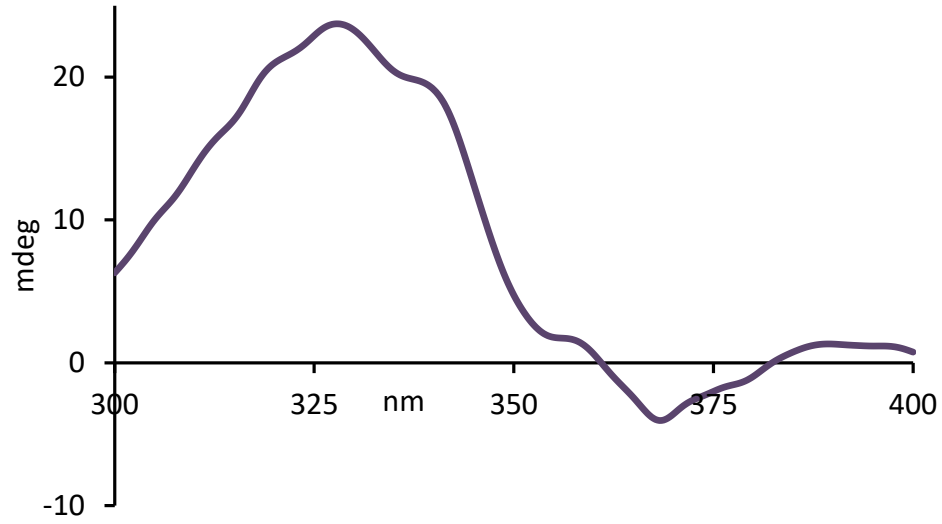

Figure S72. CD analysis of a mixture containing 15.2 mM of *(R,R)*-**2**, 6.8 mM of (*R*,*S*)-**2**, 0.0 mM of (*S*,*S*)-**2**, and 8.4 mM of (*S*,*R*)-**2** (Oxidized state).

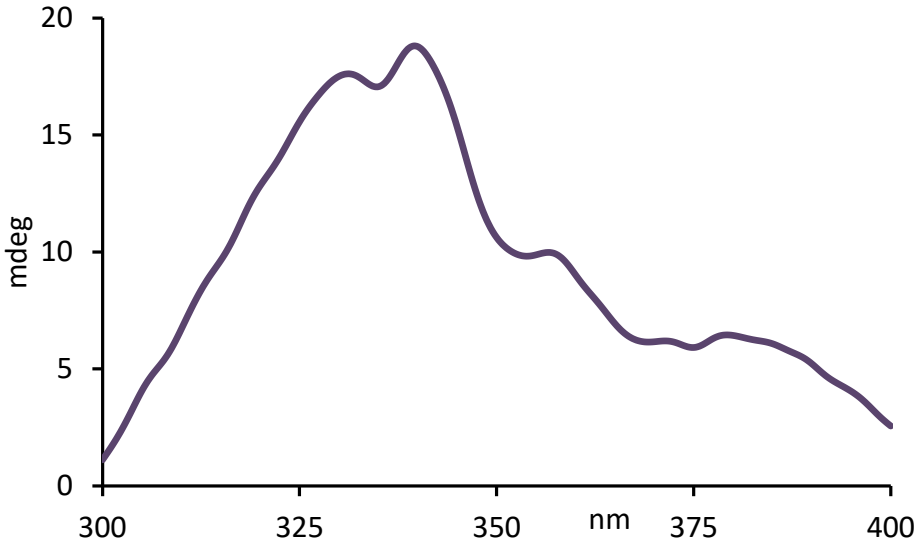

Figure S73. CD analysis of a mixture containing 6.7 mM of *(R,R)*-**2**, 0.0 mM of (*R*,*S*)-**2**, 8.2 mM of (*S*,*S*)-**2**, and 14.9 mM of (*S*,*R*)-**2** (Oxidized state).

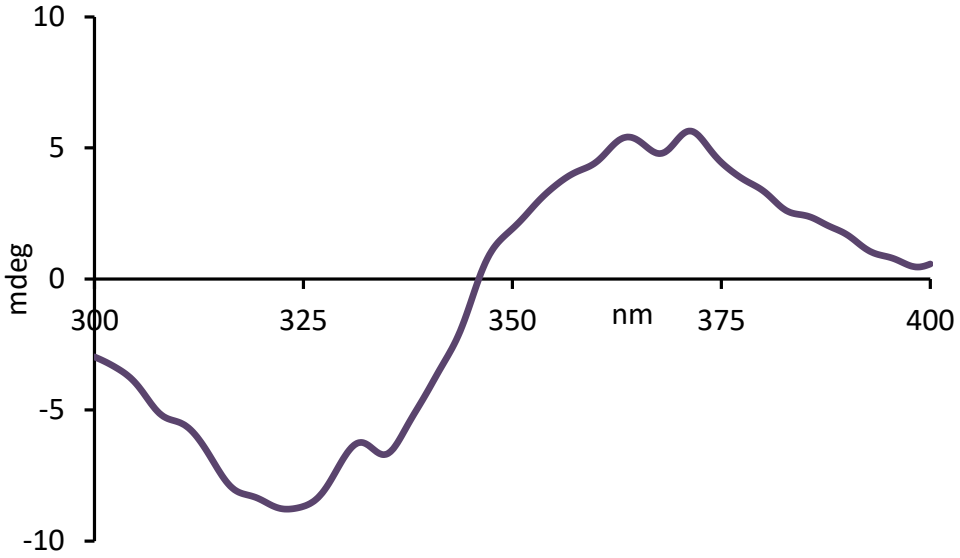

Figure S74. CD analysis of a mixture containing 8.3 mM of *(R,R)*-**2**, 0.0 mM of (*R*,*S*)-**2**, 6.8 mM of (*S*,*S*)-**2**, and 15.1 mM of (*S*,*R*)-**2** (Oxidized state).

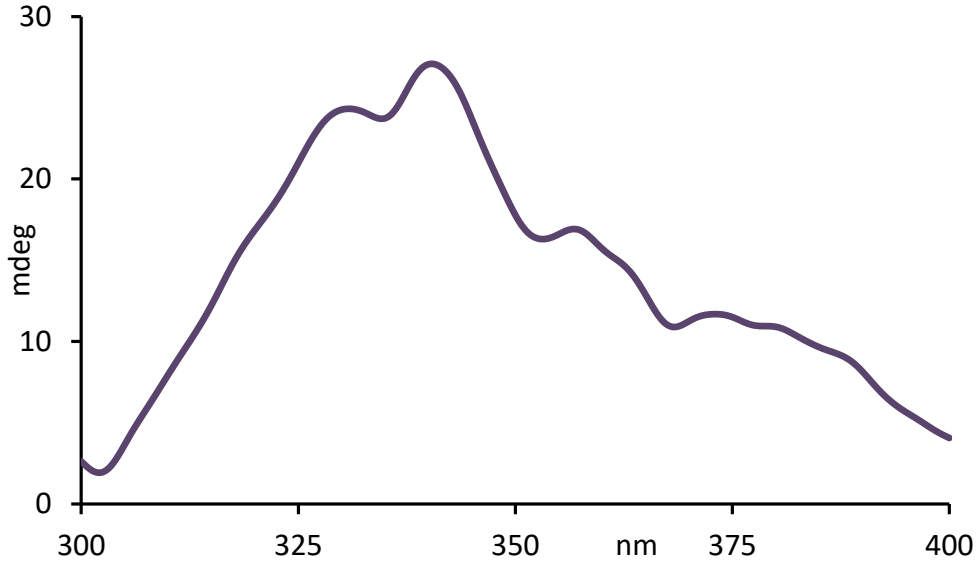

Figure S75. CD analysis of a mixture containing 9.9 mM of *(R,R)*-**2**, 0.0 mM of (*R*,*S*)-**2**, 20.1 mM of (*S*,*S*)-**2**, and 0.0 mM of (*S*,*R*)-**2** (Reduced state).

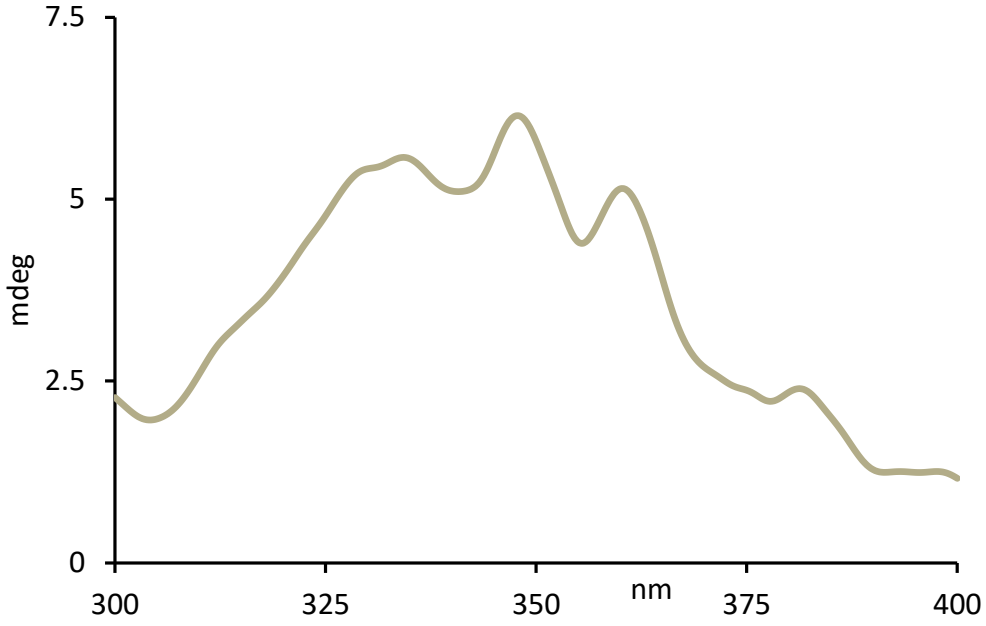

Figure S76. CD analysis of a mixture containing 33.5 mM of *(R,R)*-**2**, 0.0 mM of (*R*,*S*)-**2**, 16.5 mM of (*S*,*S*)-**2**, and 0.0 mM of (*S*,*R*)-**2** (Reduced state).

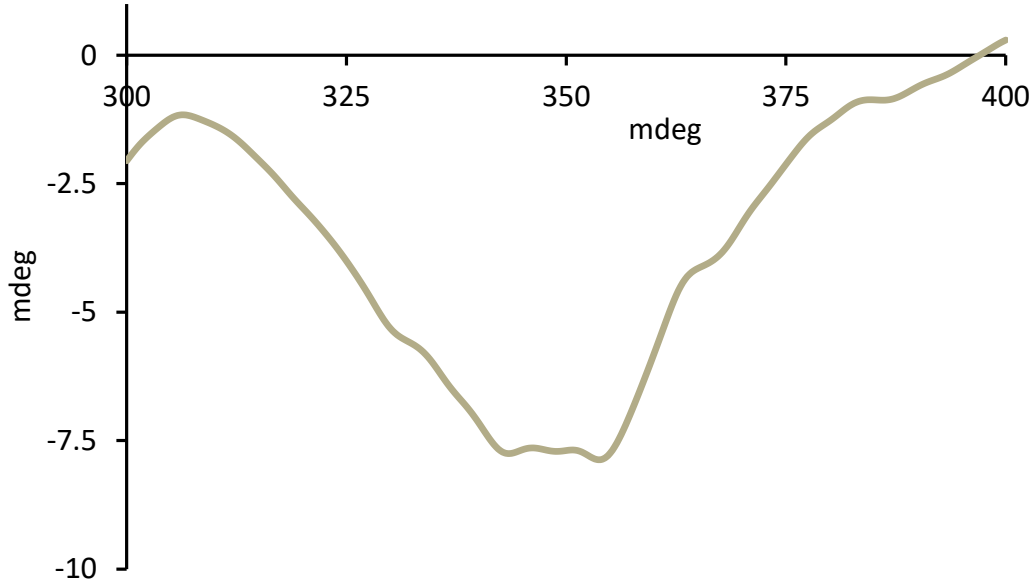

Figure S77. CD analysis of a mixture containing 9.9 mM of *(R,R)*-**2**, 20.1 mM of (*R*,*S*)-**2**, 0.0 mM of (*S*,*S*)-**2**, and 0.0 mM of (*S*,*R*)-**2** (Reduced state).

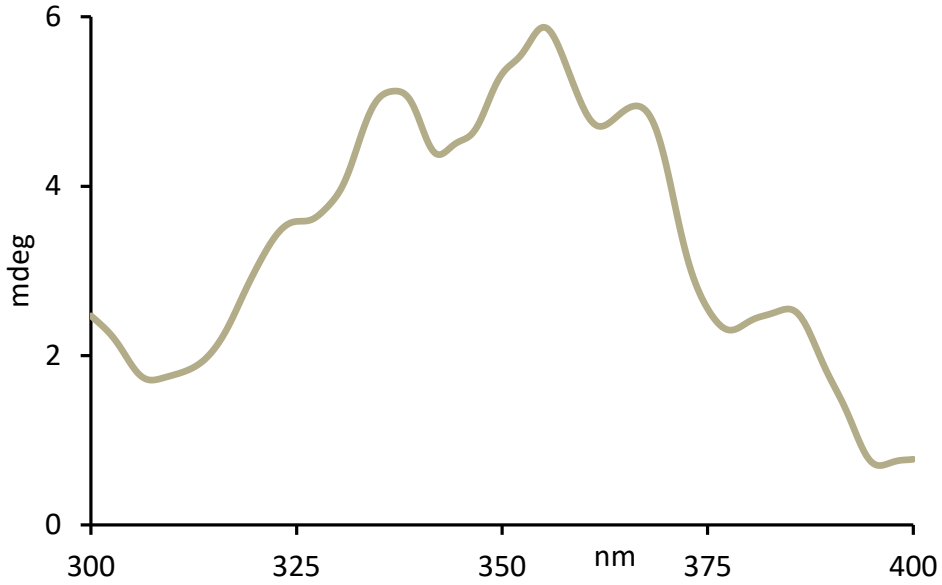

Figure S78. CD analysis of a mixture containing 26.8 mM of *(R,R)*-**2**, 0.0 mM of (*R*,*S*)-**2**, 0.0 mM of (*S*,*S*)-**2**, and 13.2 mM of (*S*,*R*)-**2** (Reduced state).

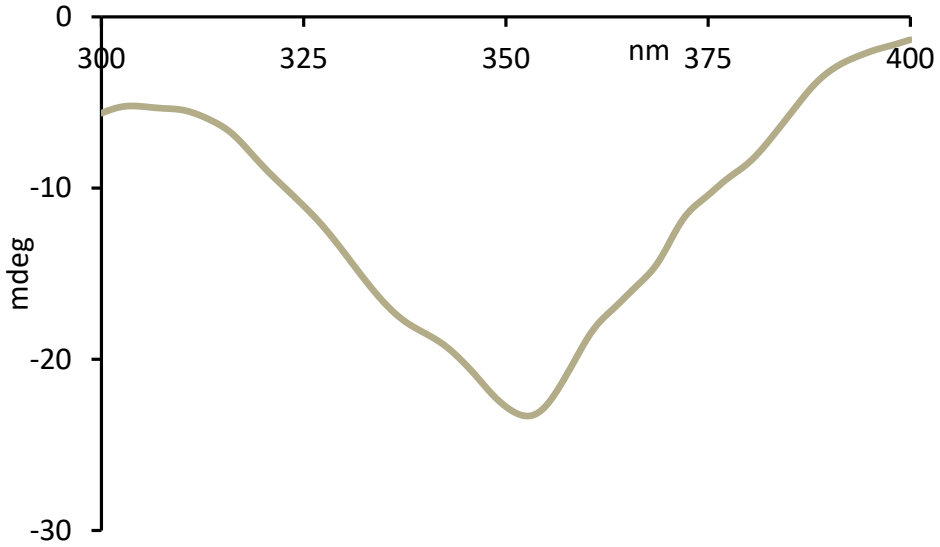

Figure S79. CD analysis of a mixture containing 13.2 mM of *(R,R)*-**2**, 0.0 mM of (*R*,*S*)-**2**, 0.0 mM of (*S*,*S*)-**2**, and 26.8 mM of (*S*,*R*)-**2** (Reduced state).

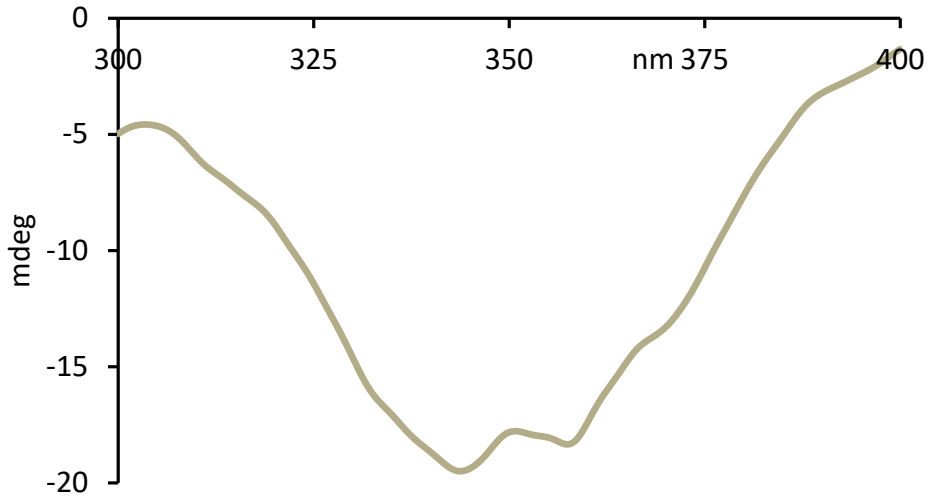

Figure S80. CD analysis of a mixture containing 0.0 mM of *(R,R)*-**2**, 9.9 mM of (*R*,*S*)-**2**, 20.1 mM of (*S*,*S*)-**2**, and 0.0 mM of (*S*,*R*)-**2** (Reduced state).

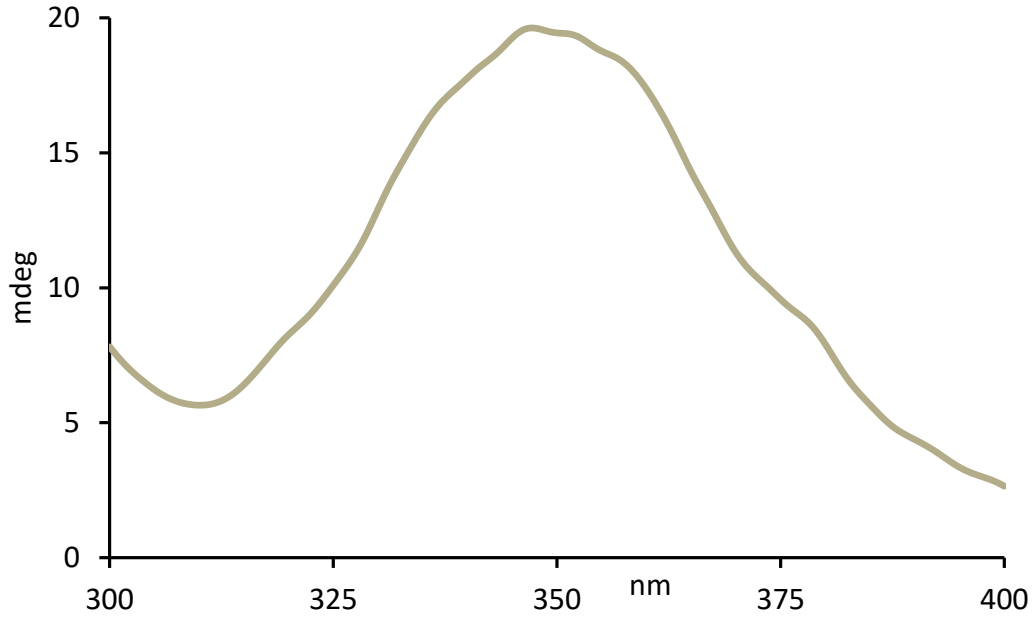

Figure S81. CD analysis of a mixture containing 0.0 mM of *(R,R)*-**2**, 26.8 mM of (*R*,*S*)-**2**, 13.2 mM of (*S*,*S*)-**2**, and 0.0 mM of (*S*,*R*)-**2** (Reduced state).

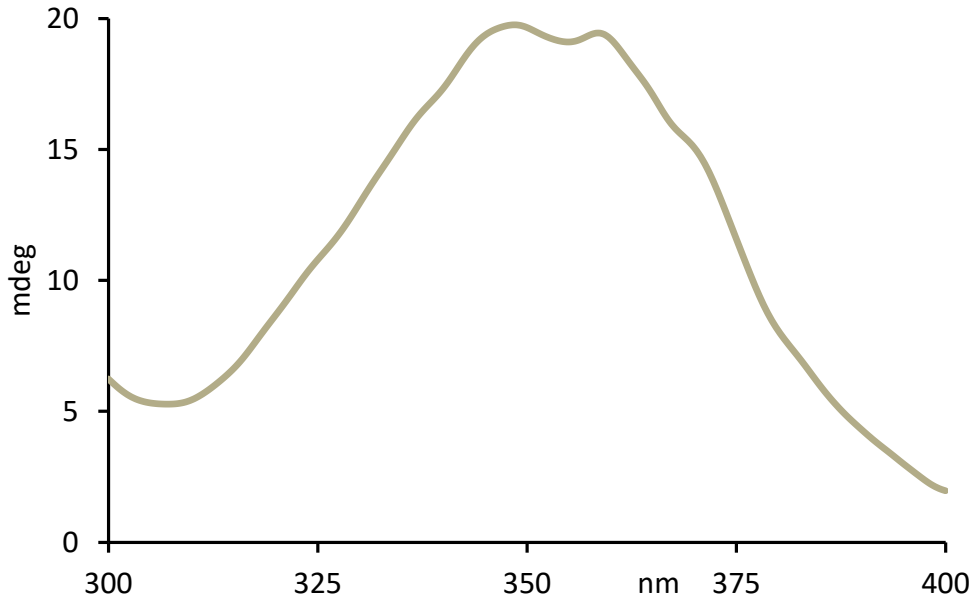

Figure S82. CD analysis of a mixture containing 0.0 mM of *(R,R)*-**2**, 0.0 mM of (*R*,*S*)-**2**, 20.1 mM of (*S*,*S*)-**2**, and 9.9 mM of (*S*,*R*)-**2** (Reduced state).

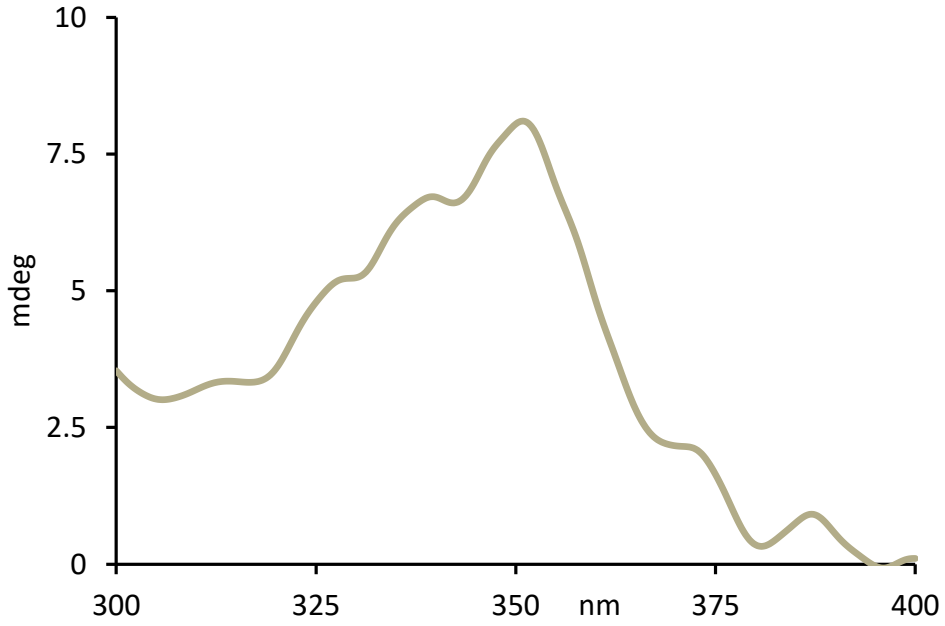

Figure S83. CD analysis of a mixture containing 0.0 mM of *(R,R)*-**2**, 0.0 mM of (*R*,*S*)-**2**, 13.2 mM of (*S*,*S*)-**2**, and 26.8 mM of (*S*,*R*)-**2** (Reduced state).

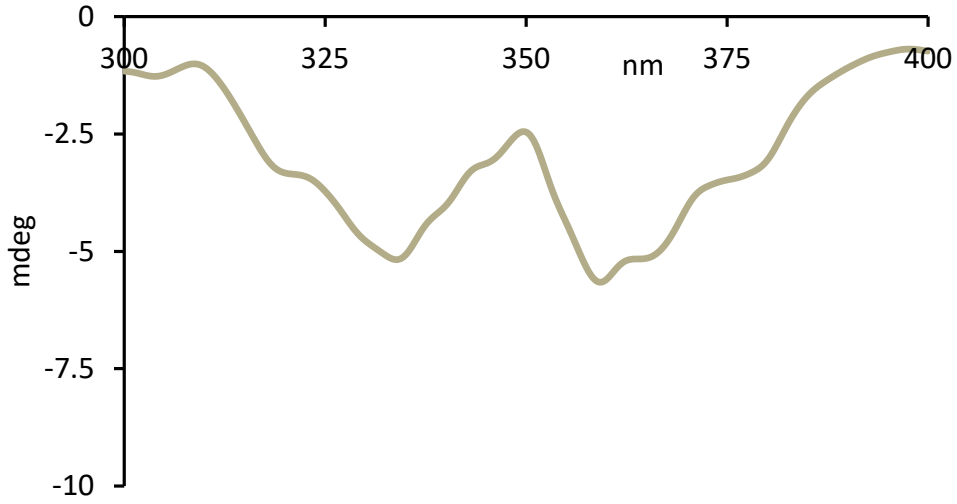

Figure S84. CD analysis of a mixture containing 0.0 mM of *(R,R)*-**2**, 26.8 mM of (*R*,*S*)-**2**, 0.0 mM of (*S*,*S*)-**2**, and 13.2 mM of (*S*,*R*)-**2** (Reduced state).

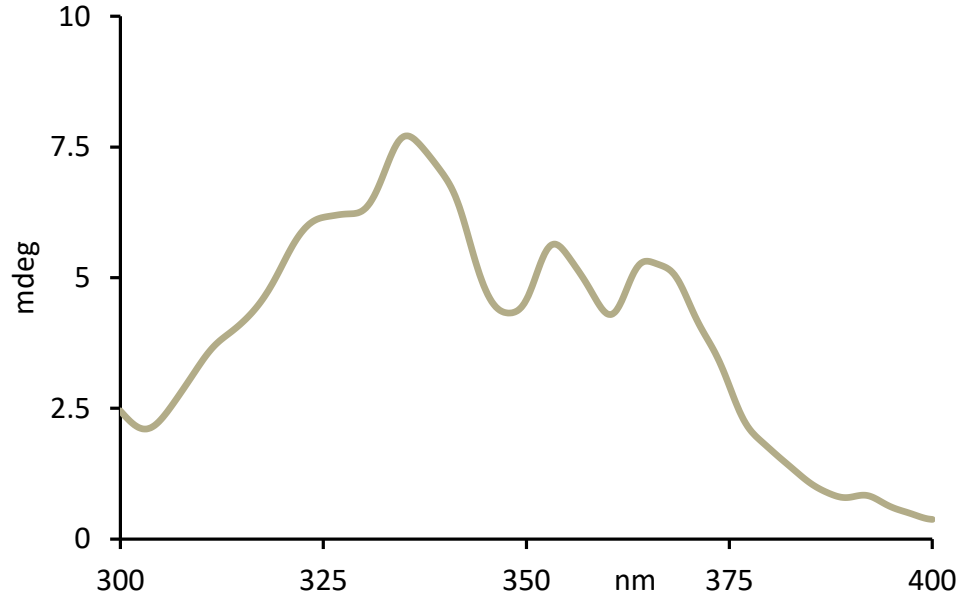

Figure S85. CD analysis of a mixture containing 0.0 mM of *(R,R)*-**2**, 9.9 mM of (*R*,*S*)-**2**, 0.0 mM of (*S*,*S*)-**2**, and 20.1 mM of (*S*,*R*)-**2** (Reduced state).

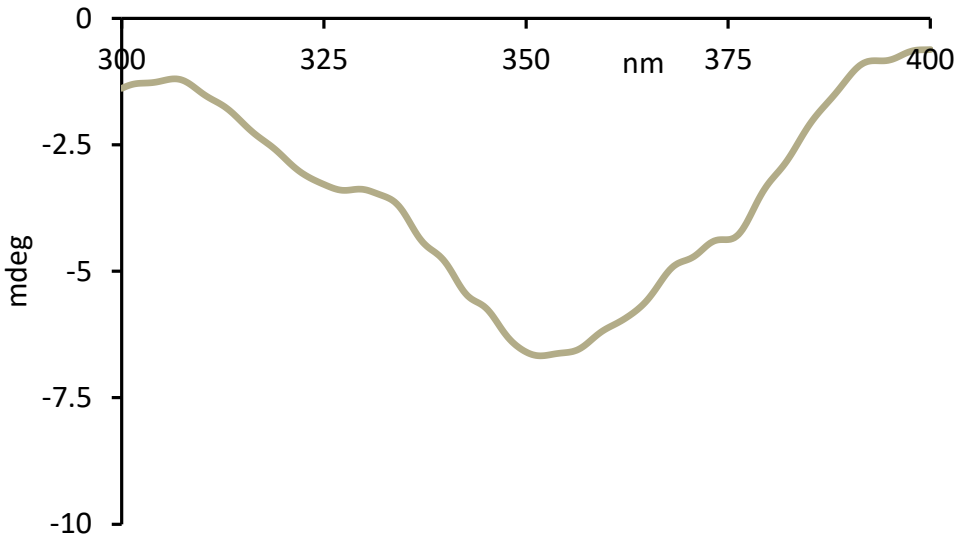

Figure S86. CD analysis of a mixture containing 13.2 mM of *(R,R)*-**2**, 13.2 mM of (*R*,*S*)-**2**, 13.2 mM of (*S*,*S*)-**2**, and 0.0 mM of (*S*,*R*)-**2** (Reduced state).

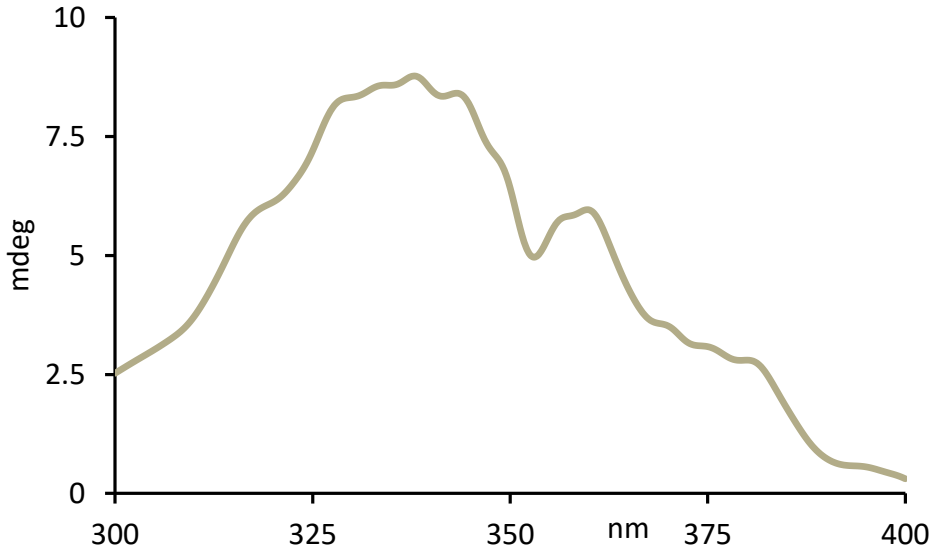

Figure S87. CD analysis of a mixture containing 16.5 mM of *(R,R)*-**2**, 0.0 mM of (*R*,*S*)-**2**, 16.5 mM of (*S*,*S*)-**2**, and 16.5 mM of (*S*,*R*)-**2** (Reduced state).

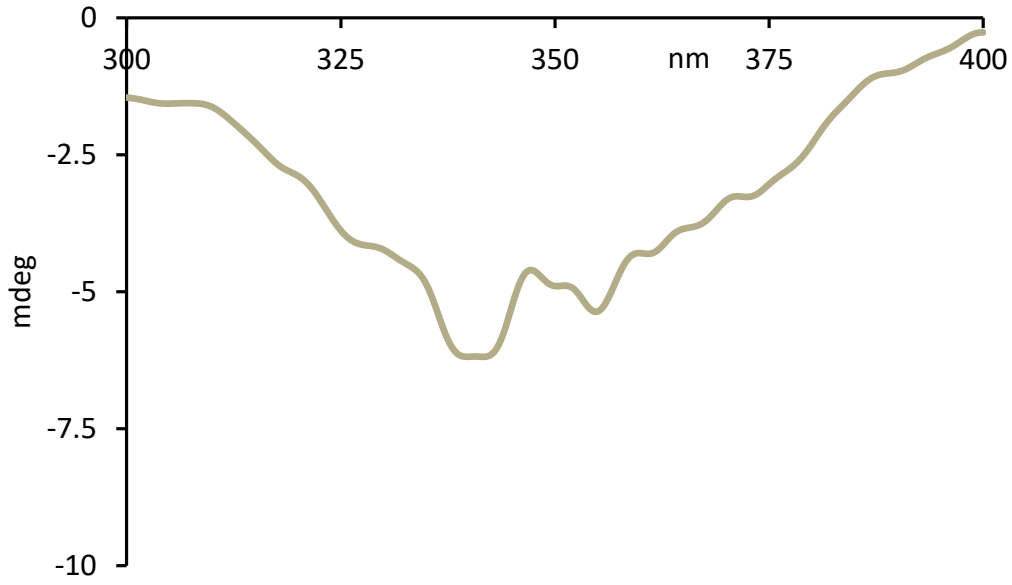

Figure S88. CD analysis of a mixture containing 9.9 mM of *(R,R)*-**2**, 9.9 mM of (*R*,*S*)-**2**, 0.0 mM of (*S*,*S*)-**2**, and 9.9 mM of (*S*,*R*)-**2** (Reduced state).

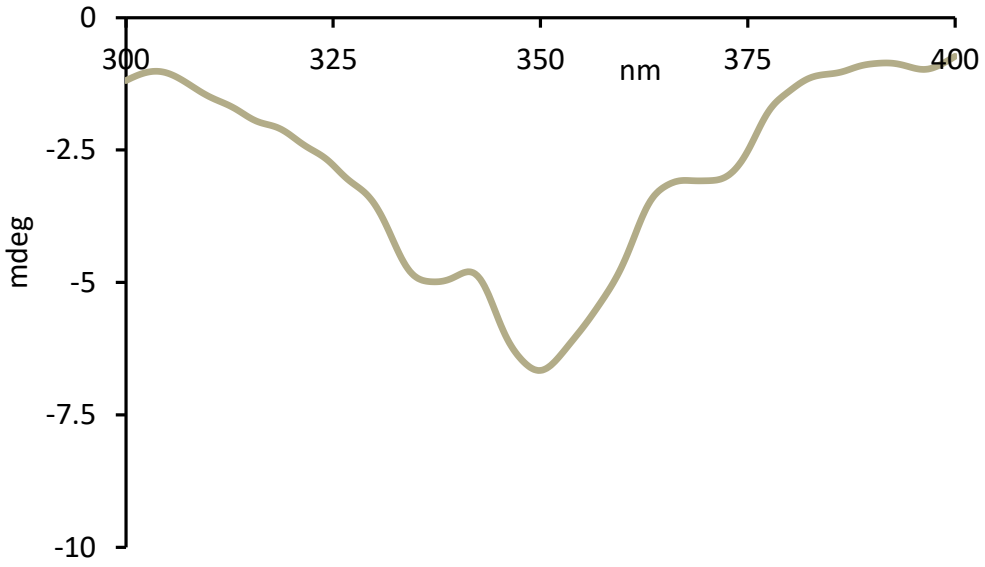

Figure S89. CD analysis of a mixture containing 0.0 mM of *(R,R)*-**2**, 13.2 mM of (*R*,*S*)-**2**, 13.2 mM of (*S*,*S*)-**2**, and 13.2 mM of (*S*,*R*)-**2** (Reduced state).

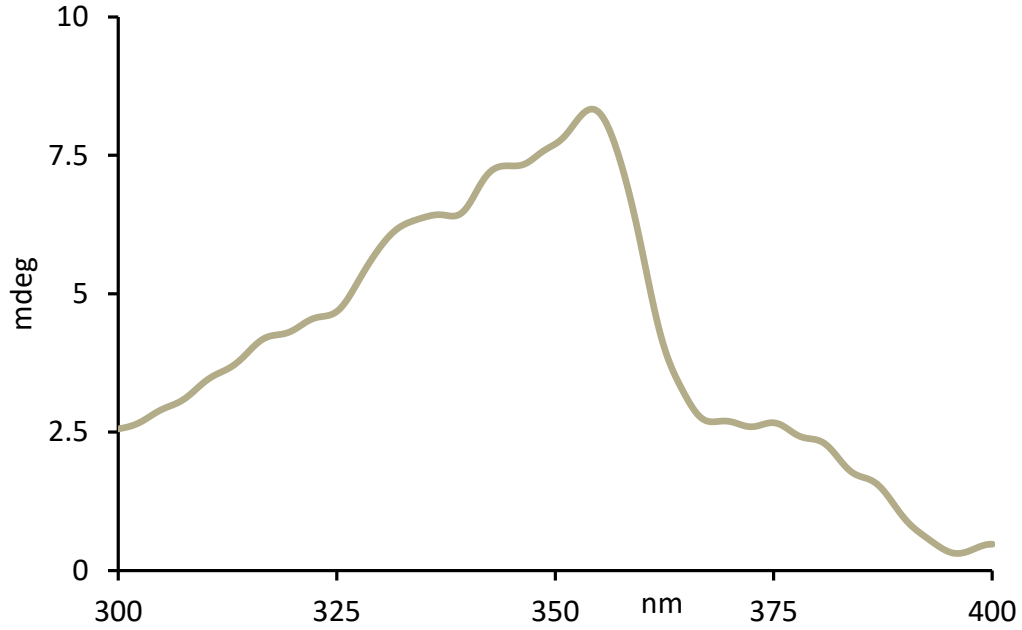

Figure S90. CD analysis of a mixture containing 11.0 mM of *(R,R)*-**2**, 0.0 mM of (*R*,*S*)-**2**, 9.0 mM of (*S*,*S*)-**2**, and 20.0 mM of (*S*,*R*)-**2** (Oxidized state).

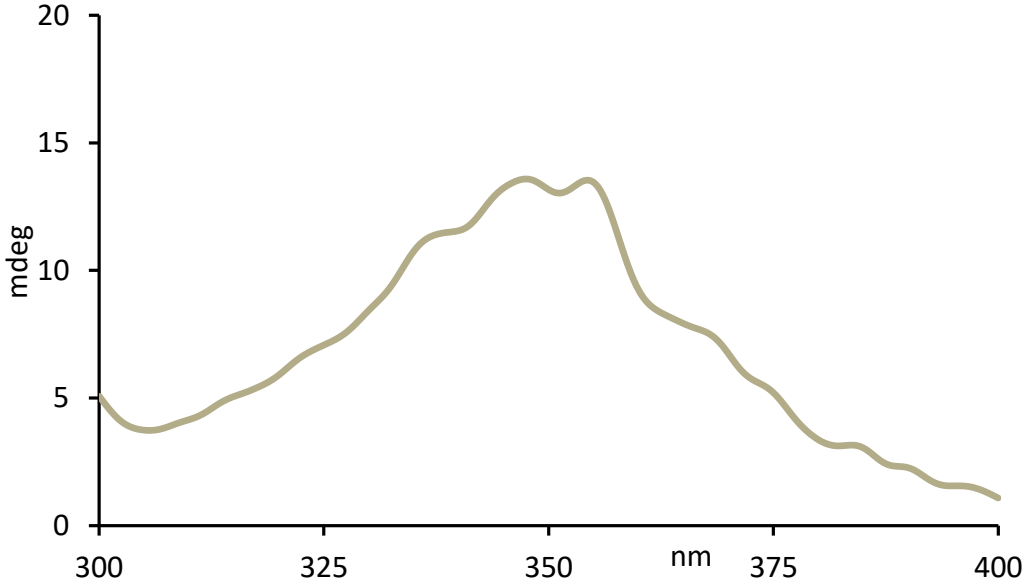

Figure S91. CD analysis of a mixture containing 21.4 mM of *(R,R)*-**2**, 9.2 mM of (*R*,*S*)-**2**, 0.0 mM of (*S*,*S*)-**2**, and 0.0 mM of (*S*,*R*)-**2** (Reduced state).

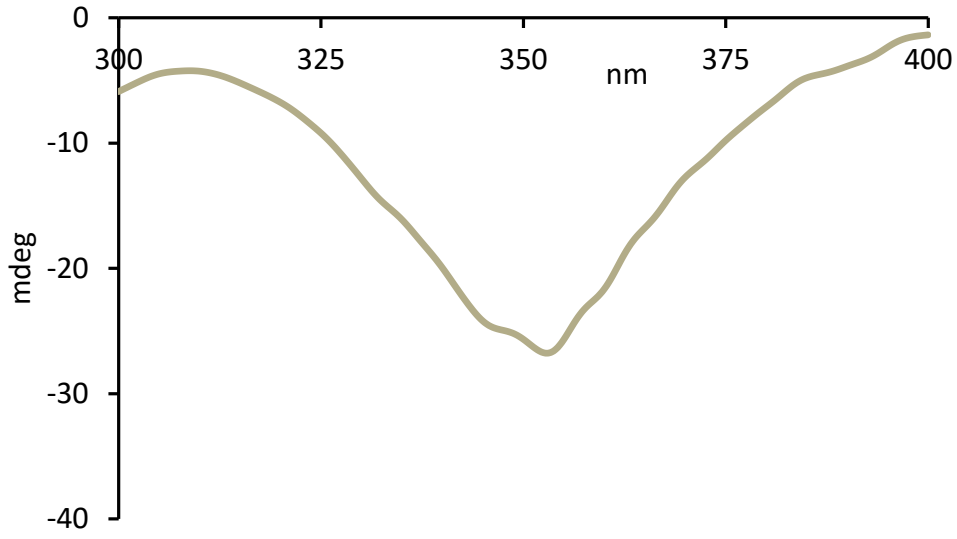

Figure S92. CD analysis of a mixture containing 0.0 mM of *(R,R)*-**2**, 0.0 mM of (*R*,*S*)-**2**, 22.1 mM of (*S*,*S*)-**2**, and 7.4 mM of (*S*,*R*)-**2** (Reduced state).

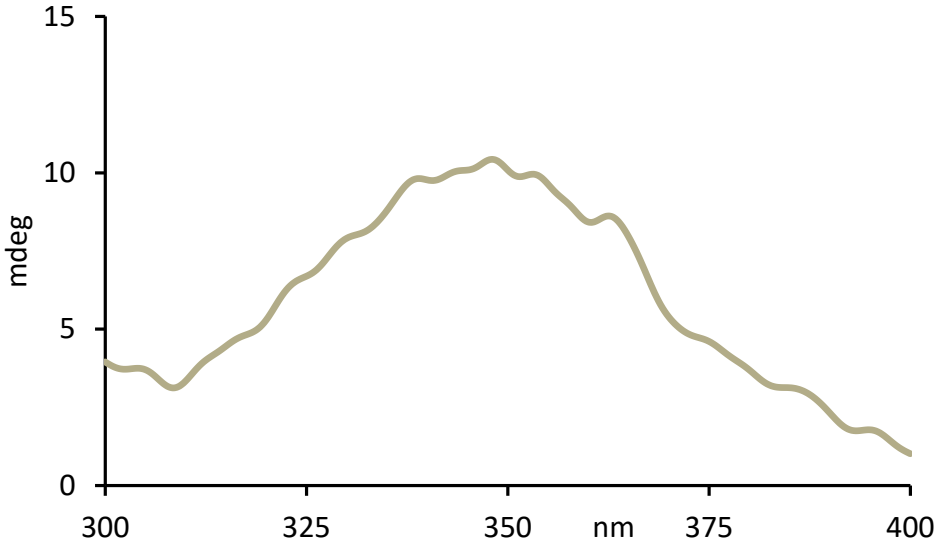

Figure S93. CD analysis of a mixture containing 26.0 mM of *(R,R)*-**2**, 0.0 mM of (*R*,*S*)-**2**, 0.0 mM of (*S*,*S*)-**2**, and 14.0 mM of (*S*,*R*)-**2** (Reduced state).

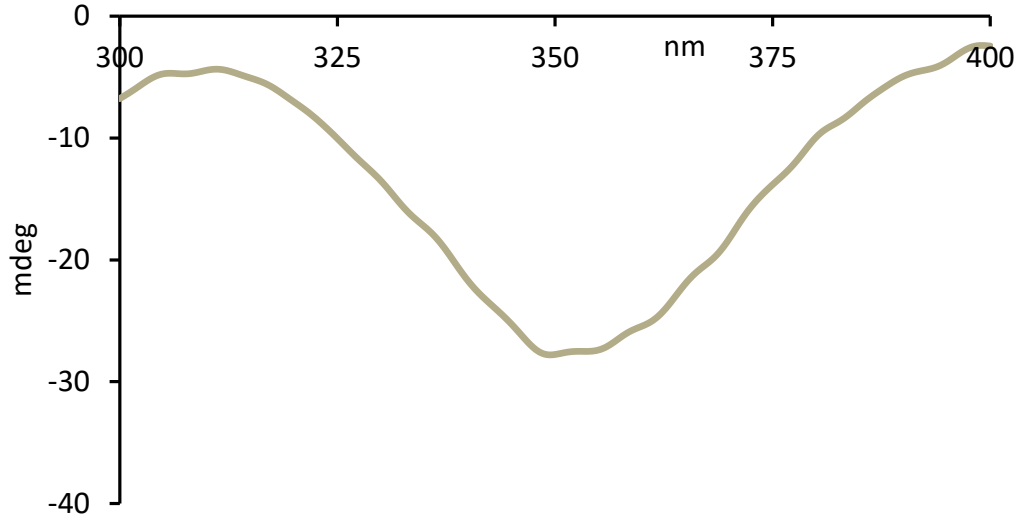

Figure S94. CD analysis of a mixture containing 0.0 mM of *(R,R)*-**2**, 9.0 mM of (*R*,*S*)-**2**, 20.1 mM of (*S*,*S*)-**2**, and 11.1 mM of (*S*,*R*)-**2** (Reduced state).

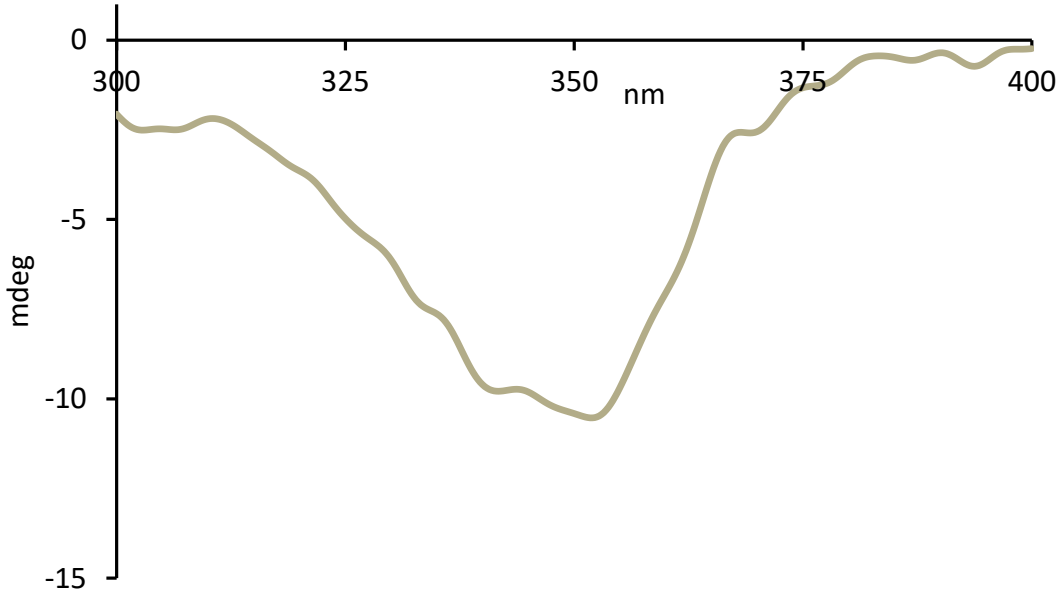

Figure S95. CD analysis of a mixture containing 19.9 mM of *(R,R)*-**2**, 0.0 mM of (*R*,*S*)-**2**, 0.0 mM of (*S*,*S*)-**2**, and 29.8 mM of (*S*,*R*)-**2** (Reduced state).

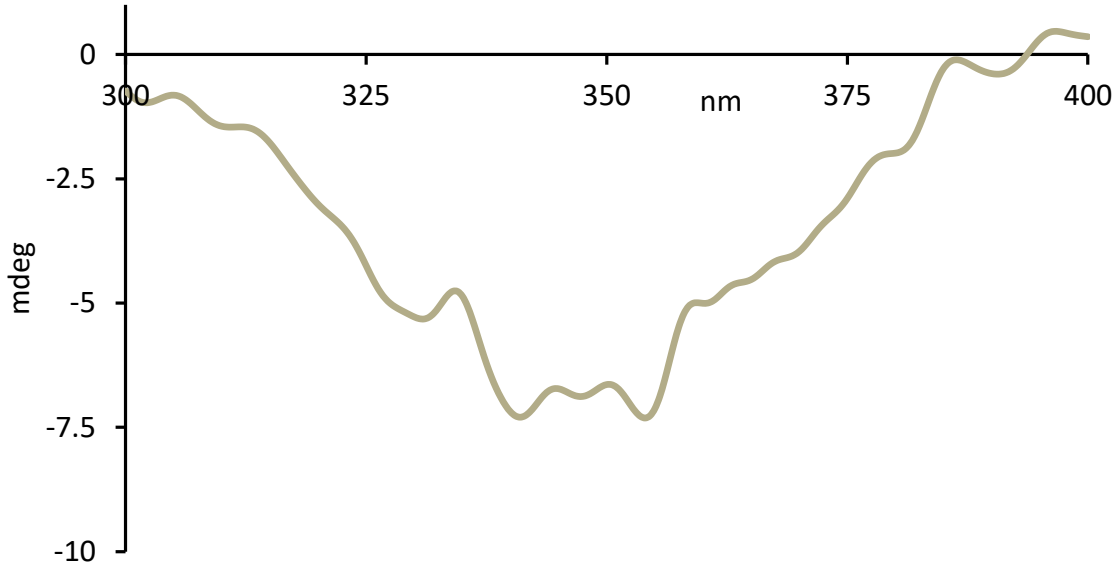

Figure S96. CD analysis of a mixture containing 0.0 mM of *(R,R)*-**2**, 8.4 mM of (*R*,*S*)-**2**, 15.3 mM of (*S*,*S*)-**2**, and 6.9 mM of (*S*,*R*)-**2** (Reduced state).

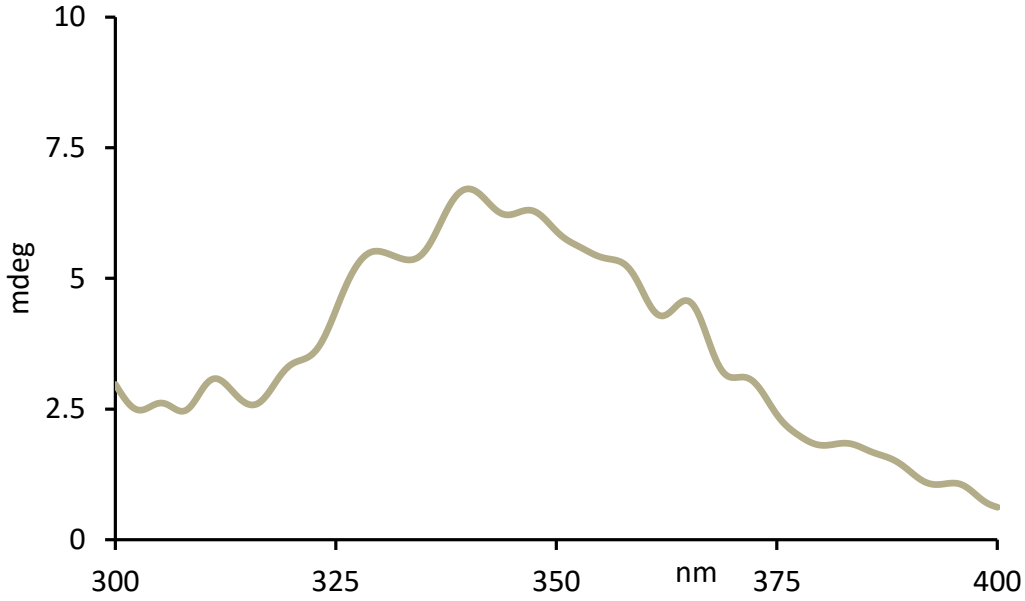

Figure S97. CD analysis of a mixture containing 15.2 mM of *(R,R)*-**2**, 6.8 mM of (*R*,*S*)-**2**, 0.0 mM of (*S*,*S*)-**2**, and 8.4 mM of (*S*,*R*)-**2** (Reduced state).

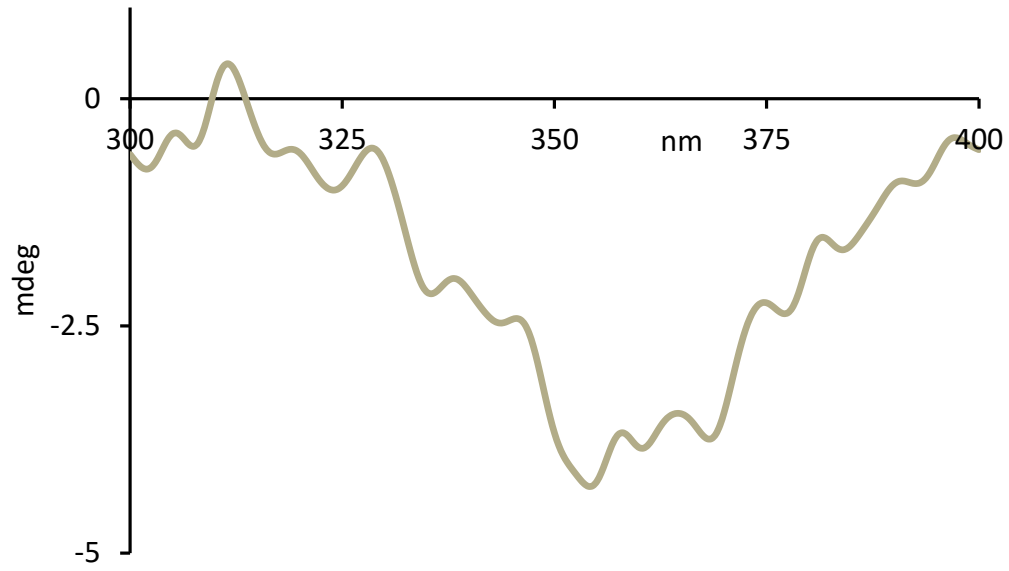

Figure S98. CD analysis of a mixture containing 6.7 mM of *(R,R)*-**2**, 0.0 mM of (*R*,*S*)-**2**, 8.2 mM of (*S*,*S*)-**2**, and 14.9 mM of (*S*,*R*)-**2** (Reduced state).

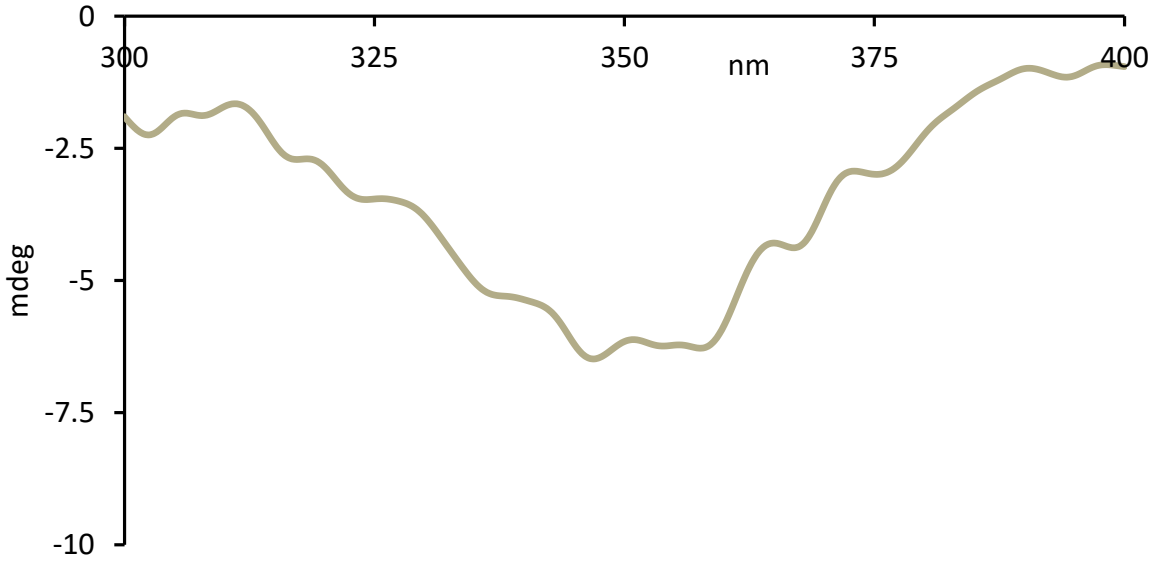

Figure S99. CD analysis of a mixture containing 8.3 mM of *(R,R)*-**2**, 0.0 mM of (*R*,*S*)-**2**, 6.8 mM of (*S*,*S*)-**2**, and 15.1 mM of (*S*,*R*)-**2** (Reduced state).

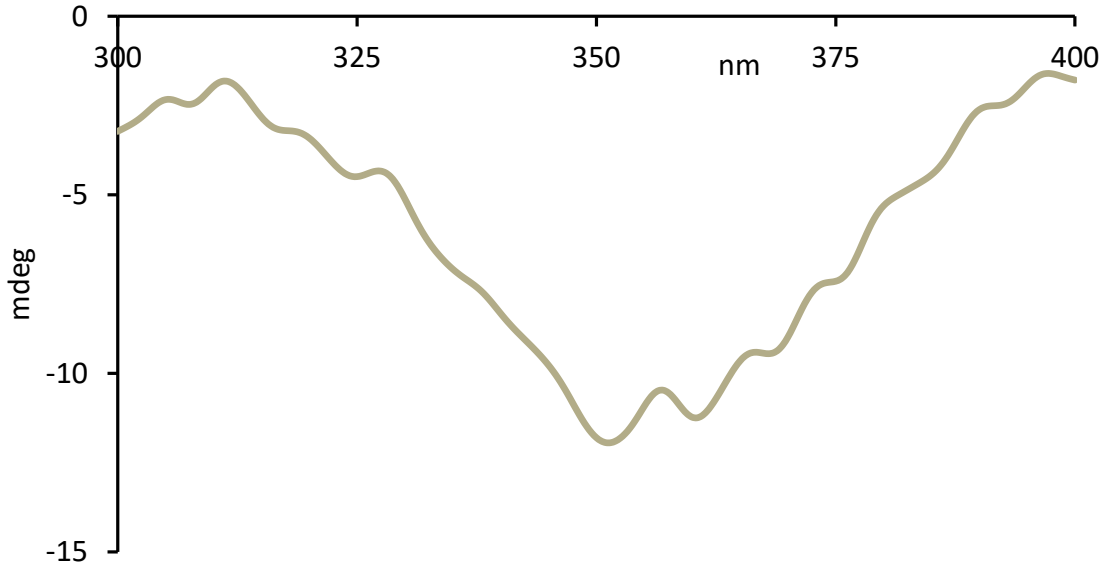

8.2. UV sensing results

Table S6. Average of 5 single UV measurements of the oxidized and reduced states of samples containing only two or three stereoisomers.

Sample number	UV absorption of oxidized state at 351 nm	UV absorption of reduced state at 370 nm
1	0.67332	0.61252
2	0.69824	0.75297
3	0.56943	0.61280
4	0.66530	0.68990
5	0.61018	0.67425
6	0.62419	0.62882
7	0.60776	0.67590
8	0.62152	0.60867
9	0.60327	0.66822
10	0.51599	0.62489
11	0.65892	0.69201
12	0.63257	0.68338
13	0.62645	0.61986
14	0.63404	0.61310
15	0.65672	0.68306
16	0.63272	0.68460
17	0.65493	0.74792
18	0.59470	0.61891
19	0.59426	0.61527
20	0.59498	0.61747

8.3. Linear regression analysis of the total concentration

The total concentration can be calculated with the same equation given in Chapter 6.3. The results are shown below.

Table S7. Actual vs. Predicted concentration (mM) of the total concentration.

Sample number	Actual concentration (mM)	Predicted concentration (mM)
1	30.0	29.3
2	50.0	50.4
3	30.0	29.3
4	40.0	40.9
5	40.0	38.6
6	30.0	31.7
7	40.0	38.8
8	30.0	28.7
9	40.0	37.7
10	40.0	39.7
11	40.0	39.9
12	30.0	30.4
13	30.0	29.4
14	40.0	39.9
15	40.0	40.1
16	50.0	49.6
17	30.0	30.5
18	30.0	30.3
19	30.0	29.7
20	30.0	30.0

8.4. Linear regression analysis of diastereomeric excess

The diastereomeric excess was determined by multiple linear regression (MLR) using the total concentration (M) and the UV absorption of oxidized state at 351 nm as the independent variables. The *de* can be calculated with the following equation:

de= 1270.7186 x absorbance (oxidized state at UV 351 nm) – 4822.672 x total concentration (M) – 611.756

The results for samples containing only two or three stereoisomers are shown in the table below.

Table S8. Actual vs. predicted *de*.

Sample number	Actual diastereomeric excess	Predicted diastereomeric excess
1	100.0	102.1
2	34.0	32.5
3	-34.0	-30.0
4	34.0	35.9
5	-34.0	-22.5
6	34.0	28.1
7	-34.0	-27.1
8	34.0	39.1
9	-34.0	-27.0
10	-100.0	-106.5
11	-33.3	-42.8
12	0.0	-0.8
13	40.0	37.2
14	50.0	51.7
15	30.0	29.8
16	0.0	-1.6
17	-20.0	-19.2
18	0.0	-2.7
19	0.0	-0.3
20	0.0	-0.9

8.5. Chemometric analysis of the individual stereoisomer concentrations

The results from the linear regression of the total concentration, the UV absorption of the oxidized state at 351 nm, and the CD spectra of the oxidized and the reduced states were used to quantify the individual stereoisomer concentration in mM using partial least squares (PLS). Scikit learn library, a free Python library for machine learning, was used for all pre-processing (scaling) and data analysis using PLS.

Table S9. Actual versus predicted concentrations.

	Sample #	(*R*,*R*)-2 (mM)	(*S*,*S*)-2 (mM)	(*R*,*S*)-2 (mM)	(*S*,*R*)-2 (mM)
1	Actual	9.9	20.1	0.0	0.0
	Predicted	9.2	23.1	0.4	0.0
2	Actual	33.5	0.0	16.5	0.0
	Predicted	32.1	0.0	16.1	2.5
3	Actual	9.9	0.0	20.1	0.0
	Predicted	10.2	0.0	22.8	0.5
4	Actual	26.8	0.0	0.0	13.2
	Predicted	28.2	0.0	0.4	13.8
5	Actual	13.2	0.0	0.0	26.8
	Predicted	15.7	0.0	0.0	27.1
6	Actual	0.0	20.1	9.9	0.0
	Predicted	0.0	23.3	11.3	0.0
7	Actual	0.0	13.2	26.8	0.0
	Predicted	1.1	16.4	25.1	0.0
8	Actual	0.0	20.1	0.0	9.9
	Predicted	0.0	19.7	0.2	11.5
9	Actual	0.0	13.2	0.0	26.8
	Predicted	0.0	14.4	0.1	26.5
10	Actual	0.0	0.0	9.9	20.1
	Predicted	0.0	1.0	9.1	21.4
11	Actual	13.2	13.2	13.2	0.0
	Predicted	13.6	12.4	13.7	0.0
12	Actual	11.0	9.0	0.0	20.0
	Predicted	10.4	9.3	0.1	20.0
13	Actual	21.4	0.0	9.2	0.0
	Predicted	24.0	0.0	8.3	0.0
14	Actual	0.0	22.1	0.0	7.4
	Predicted	0.0	23.2	0.0	7.6
15	Actual	26.0	0.0	0.0	14.0
	Predicted	25.5	0.7	0.4	13.5
16	Actual	0.0	20.1	9.0	11.1
	Predicted	0.0	20.3	9.2	10.8
17	Actual	19.9	0.0	0.0	29.8
	Predicted	20.3	2.3	0.0	28.2
18	Actual	15.2	0.0	6.8	8.4
	Predicted	15.7	0.0	7.0	8.6
19	Actual	6.7	8.2	0.0	14.9
	Predicted	7.7	7.8	0.0	16.1
20	Actual	8.3	6.8	0.0	15.1
	Predicted	8.8	5.0	0.0	16.9